Advancing Micro Optical Elements for Optoelectronic Technologies

A dissertation submitted by

Zachary E. Kranefeld

In partial fulfillment of the requirements for the degree of

Doctor of Philosophy

in

Electrical Engineering: Materials Science and Engineering

Tufts University

August 2025

© 2025, Zachary E. Kranefeld

Adviser: Thomas Vandervelde

Abstract

Innovations in optoelectronic technology are accelerating due to the advancement of micro-optical elements. Utilizing techniques for nanofabrication, micro-diffractive optical elements and metamaterials are making an impact on this technology by improving capabilities and unlocking new avenues for design. In this work, design, modelling, fabrication, and characterization of these optical elements was executed thoroughly. Infrared photodetectors and TPVs were two specific technologies investigated.

Acknowledgements

Prof. Thomas Vandervelde – Thank you for selecting me as a member of your team and for providing all the resources that were essential in reaching this point. Through my time at Tufts, I've felt that our relationship has evolved from advisor/advisee to a pair of intellectuals solving the problems of the world, and as friends. I believe this is a rare experience among graduate students and I am truly grateful for it.

Christina Behr-Kranefeld – The decision to pursue my PhD came at a strange time in my life. I was employed full-time at MITLL and the world was experiencing the COVID-19 pandemic. We were recently engaged and I had several forks in the road of my career fast approaching. With the difficulties you were facing in your own career at the time and the uncertainty of the future, my decision weighed more heavily. You decided to change your career path and pursue one in higher education, which led to your position at Tufts University. This appointment came shortly after my decision to enroll at Tufts which seemed like the stars had aligned. From my first day at Tufts, your support enabled me to focus on the road ahead. You sustained my desire to continue this pursuit and made it achievable. I hope that you share in my feelings of accomplishment.

The Group87 team at MITLL – Thank you for allowing such flexibility in my schedule to continue my employment a MITLL and providing invaluable resources throughout my research to reach success. My experience in the group led me to this point and maintaining a strong connection during this pursuit will prove to be as valuable as the degree itself.

Table of Contents

Abstract ... i

Acknowledgements ... ii

Introduction and Motivation ... 2

Background ... 7

Photons and Photonic Interaction ... 7

Semiconductors ... 11

TPV Technology ... 13

Materials and Methods ... 17

Fabrication Methods ... 17

Characterization Methods ... 23

Results ... 29

TPV Design Toolbox and Visualizer ... 30

Iridium Selective Emitter Metasurface ... 40

Metasurface Design ... 40

Metasurface Fabrication ... 46

Characterization Testbed for Selective Emitters ... 56

Monolithically Integrated Photodetector ... 60

Microlens Characterization ... 60

Multilayer Diffractive Lens Fabrication ... 69

Conclusions ... 76

Future Work ... 79

Appendices ... 81

List of Acronyms 81

SOPs and Fabrication Notes 83

Iridium Metasurface Fabrication: *83*

AFM Scanning Procedure: *87*

HiTemps Testbed Operation: *89*

Calibrating HiTemps Testbed: *91*

MLA Microscope Operation: *94*

MDL Fabrication: *96*

Code 98

TPV Design Toolbox and Visualizer *98*

JSON File Generator *115*

Microlens Focus Analyzer *115*

Bibliography 116

Advancing Micro Optical Elements for Optoelectronic Technologies

Introduction and Motivation

I've always had an inventive mind. My parents often remind me of the elaborate stories I would tell them as a child during road trips about how I am actually an alien and I work in the woods over there; pointing to an unrecognizable section of forest beside the road. My inventive mind led me towards an engineer's career path, but my fascination with the spectacles of light kept me in the discipline of physics. The culmination of these fields, on the bleeding edge of science and engineering, is where I find myself now – optoelectronic devices. It seemed fitting that my research should be multidisciplinary and position me to be the most effective innovator I can be. To compliment my degrees and certificates in physics and engineering, as well as my career experience with semiconductors and photonics, I am in pursuit of a dual Ph.D. in Electrical and Computer Engineering & Materials Science Engineering (ECE/MSE).

I worked on many projects during my PhD and throughout them all, my contributions fell heavily into these three phases of the technology development cycle: design, fabrication, and characterization. I've elected to describe three projects where I was the primary contributor. Each one focuses more strongly on one of these phases in particular, but they can all be classified as projects that aim to innovate optical/photonic elements of semiconductor devices, specifically optoelectronic devices. Design, to me, is "invention with a purpose" and this is the discipline where I truly thrive – design engineering. Design of semiconductor devices has many facets, all of which are terminal paths of study in their own rite. Most commonly, the design process for these devices is heavily reliant on modelling. This modelling requires more than just computer literacy or familiarity with a specific software. An understanding of the physics behind the model is needed

to filter out non-physical results. Additionally, a healthy knowledge of coding is often beneficial. This allows the designer to utilize all aspects of such software or create their own when lacking necessary features, as was the case for the first project described. Fabrication and characterization are pillars of semiconductor device manufacturing. Fabrication happens almost exclusively in a cleanroom environment. For those unfamiliar with cleanrooms, they are structures that very precisely control the air quality to a degree which the number of particles in any cubic meter volume can be counted. This is required because device feature sizes can be the same as a particle of dust. A single flake of dust can be enough to ruin any one of the hundred steps it takes to produce these devices. It is often said cleanrooms are "cleaner" than operating rooms. This may be true for the quantity of dust particulates, but I don't recommend eating anything off of the tables. Fabricating semiconductor devices requires the use extremely hazardous chemicals, where only several drops to exposed skin or a single breath of gas can be fatal. More critically than controlling the air quality, cleanrooms must control the safety of the occupants.

Characterization can be treated as independent, but no fabrication could be successful without utilizing characterization techniques in tandem throughout the fab process. For this reason, characterization tools are often found in cleanrooms also. The primary characteristics being measured during fabrication are usually the device's physical structure, or its material composition, while post-fabrication measurements often aim to characterize behavior be that: electrically, optically, thermally, or otherwise. The research projects described had goals of creating something new, as is often the case in this type of research. As such, characterization of the final device would require tools which did not exist. Not only was design, fabrication, and

characterization implemented in making these devices, but design, assembly, and characterization of new tools was performed to then measure what was made. In the work described henceforth, I oversaw the modelling, fabrication, and characterization of each research project, including the design, assembly, and qualification of the equipment required to perform some of the characterization. For devices of this nature, no one person can do every task themselves. I recognize and appreciate all the contributions from my team members, as well as the researchers who came before.

The project which showcases the design phase is the TPV Design Toolbox and Visualizer. The inspiration for this project came after attending the TPV-15 world conference. My impression from the community was that there is a major rift between those whose focus on improving PV cell conversion efficiency and those who are looking at system efficiency for real-world applications of TPV technology. Each group of the community treated their design process very differently, even though they were ultimately interested in the same thing. I decided to create a simulation tool that would help merge the community and settle some lingering disputes I had discussed with other attendees. One of which was when using a selective emitter (SE), is a delta function or a step function emission "better"? To properly answer that, you have to define the TPV system as a whole, and investigate the impact of the SE independently without ignoring the cascading effects this choice has throughout the system. In determining how the tool must work to answer this question, we realized an opportunity to provide the TPV community with something that did not previously exist. Our tool would be able to connect electrical conversion efficiency simulations with known semiconductor phenomena that are derived from the material properties

of the semiconductor itself. Until this point, efficiency calculations were exclusively performed with "ideal" semiconductor behavior. This behavior would treat photonic interaction as consistent across large ranges of the optical spectrum. Most publications referring to the non-idealities of these materials, were not focused on its impact to performance, but rather tried to define the physics behind the phenomena. By combining these aspects in our simulation tool, we could begin to enlighten TPV community members on how different research efforts are relevant to everyone.

The second and third projects both contain healthy amounts of fabrication and characterization work. The second project was chosen to showcase fabrication because the by-in-large time spent was in fabrication process development. This project's goals changed over time as I realized the previous goals were becoming harder and harder to achieve. The original goal was to develop a selective emitter metasurface for a TPV application, but the final goal was to show that metasurfaces could be fabricated in refractory metals. Originally pitched to me as "low hanging fruit", it was thought to be a modest endeavor to simply publish etching rates for processing techniques of iridium. I decided to up the ante and if processing was to be done, then processing an actual device with real-world application relevance should be where we start. Iridium etch rates were included in the final report, but the nuances of making a functional device turned out to be a much more intriguing challenge. Although this project yielded far more failures than successes, so much valuable information was learned. The final goal of the project reflects how publishing is overly focused on successful results, however, it also put the lessons of these many failures in perspective to show that "failing forward" is still considered success in science and engineering.

The third project that showcases characterization is the monolithic APD-MDL array. In this project, we aimed to fabricate a microlens array on the opposite side if the same substrate as the APD array, creating a monolithic photodetector. While this poses significant fabrication challenges, there was already previous work done on this project towards this particular goal. My involvement began with developing a custom microscope that would enable us to characterize the microlens arrays being fabricated. Since the lenses were designed to come to a focus inside the substrate, and back focal lengths in the reverse orientation were only tens of microns. No standard optical microscope would be suitable for these measurements. In addition, the microlenses needed to be imaged in the visible spectrum for the operator, but the lenses themselves were designed to focus infrared light. The ability of the microscope to switch between these optical bands, manipulate the sample to sub-micron accuracy, and image both a physical lens and its focused beam made it a one-of-a-kind characterization tool. I also performed the fabrication of the monolithic devices, but the fabrication process development for the MDLs and the APDs had already been qualified by others on the project.

Background

Photons and Photonic Interaction

Light can be explained as electromagnetic waves with various frequencies propagating through space. These waves carry energy which is quantized into massless particles, called photons. Light-materials interaction can be conceptualized with two general mindsets: the photon interacts with atoms in the material, exchanging momentum, or the wave interacts with the material, creating interference that reshapes the wave as it propagates. Light will exhibit both of these behaviors depending on the observations being made. This concept in physics is known as the wave-particle duality and has been a driving force of innovation in the modern physics era. Understanding which aspects of a material dominate this interaction, how they can be measured, and how they can be altered is of great interest to the scientific community and has led to countless discoveries with global impact. The most precise measurements known to man are only achievable by observing the changes after photonic interaction. Common nomenclature uses the Greek letter lambda "λ" to represent the wavelength of a photon. The relationship between the energy of a photon and wavelength is given by the following equation, where h is Plank's constant and c is the speed of light.

$$E_{photon} = {}^{hc}/_{\lambda}$$

Today, we define the material property that alters its photonic interaction as the index of refraction, $\tilde{n}$.

$$\tilde{n} = n + ik$$

This is a complex number that can be used to solve wave equations which describe the electromagnetic wave before and after material interaction. The real component of this complex number is known as the refractive index and is denoted by *n*. In general terms, it quantifies the amount a material will impede a wave of light as it passes through the material. The refractive index for the vacuum of space is defined as one, with all known elements and materials having a value greater than one. Snell's Law, a commonly known physics equation, is an example that shows how the refractive index can be used to described the change in angle a beam of light will undergo when moving between two materials with different indices. The equation for Snell's Law:

$$n_1 \sin \theta_1 = n_2 \sin \theta_2$$

only relies on the refractive index and the incident angle of the light towards the interface. The imaginary component of the index of refraction is known as the extinction coefficient, denoted by *k*. It describes the amount of energy transferred between the light and the material. If a material has an extinction coefficient of zero for a certain wavelength of light, then the material takes zero energy from the propagating wave, and is therefore perfectly transparent to that light. Another commonly known law in physics, Beer's Law, describes how the intensity of light is lost in a material as a function of the material's thickness, *d*. The equation for Beer's Law:

$$I_{out} = I_{in} e^{-d\left(4\pi k/\lambda\right)}$$

has been expanded here from its compact form to show that the relationship only relies on the extinction coefficient, material thickness, and the associated wavelength of light. The complex index of refraction of a material is typically a strong function of wavelength, but often not one that

can be easily defined mathematically. Modern optical device modelling software relies heavily on being able to access tabulated data for these values, referred to as look-up tables, and empirically solve wave equations at discrete wavelengths. The graphic below shows these concepts represented visually to aid the reader in understanding how we approach photonic interaction in the mindset of propagating waves.

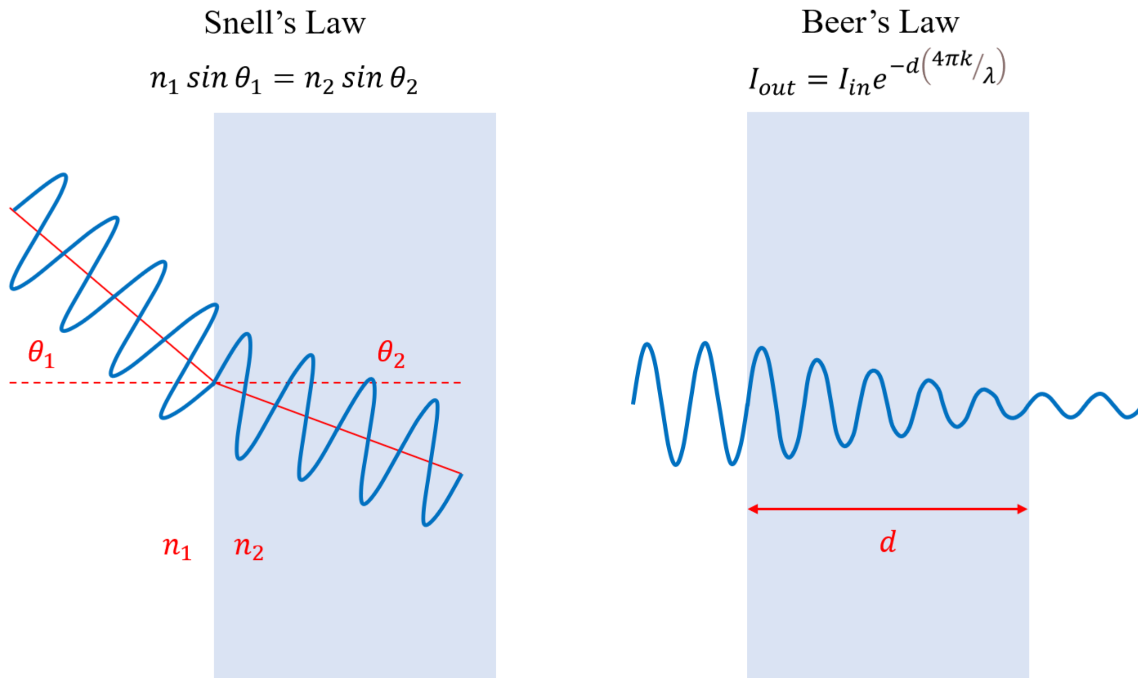

Figure 1. Depiction of light interacting with material described by Snell's Law and Beer's Law.

There is another aspect of light that must also be understood to grasp how modern photonic devices operate, and that is phase. Phase is the time-dependent component of a propagating wave. When a wave moves through a material, the wavelength does not change, but the speed at which the wave moves does. Materials with higher refractive indices slow the propagation more. It is the synchronization of phase that causes interference, which is the only known way light can interact with itself. Two propagating waves which are in-phase will add, doubling the intensity of the light.

When waves are perfectly out of phase with one another, they will negate and the light ceases to exist in that space. These interactions are defined as constructive and destructive interference respectively. Lenses take advantage of this interference by gradually altering the phase profile across a plane perpendicular to the wave's propagation, which leads to focusing. The standard lens, as everyone is familiar, is made of glass and has at least one curved side. This interface between glass and air causes the wave to change speed, introducing a phase shift between the air and the glass. The curved portion of the glass delays this phase shift across the plane normal to propagation, referred to as a phase profile. Any lenses with the same phase profile will focus light equally, regardless of their physical shape. One classical example that proves this is the Fresnel lens. The Fresnel lens design simply takes the portion of the glass curve which contributes to the phase profile and discards the rest. By placing the contributions back together in a flat arrangement, the lens is physically very different but focuses light in the same place. The graphic below depicts the fundamentals of a Fresnel lens.

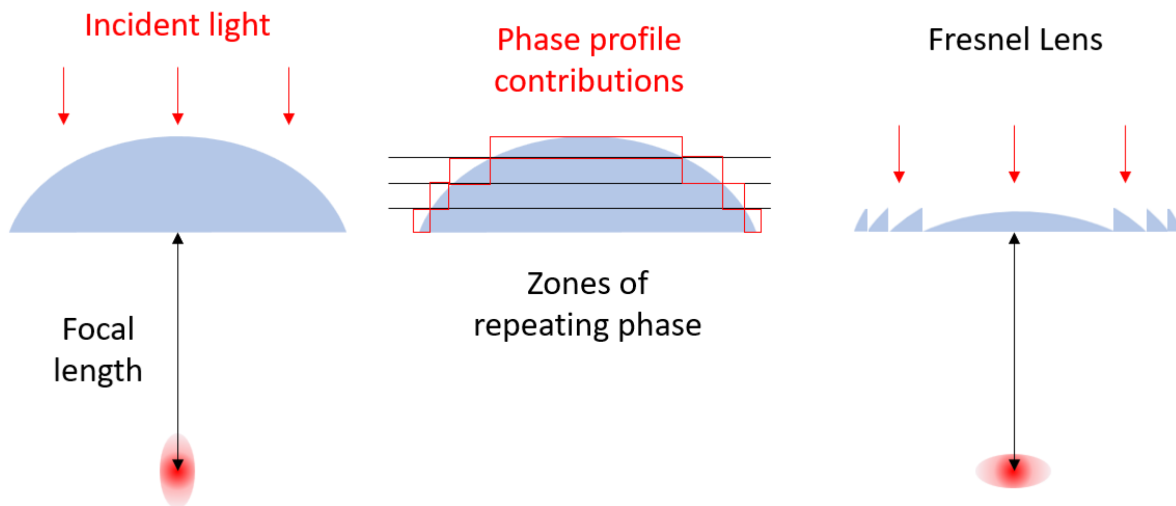

Figure 2. Depiction that compares a traditional lens to a Fresnel lens that share the same phase profile.

With advanced material engineering, we can now produce materials with precisely known refractive indices and structure them to produce a precise phase profile resulting in the desired outcome for their photonic interaction. Such examples of this are seen all around us in consumer products that most people interact with on a daily basis: the screen you are likely reading this document on manipulates the properties of liquid crystals to change the color or polarization of the light that each transmits, the sunglasses one wears that allow lower frequency light to pass through to the eye but reflect higher frequency light away with a thin film coating, or the mirror in your bathroom that provides a view into another dimension where a clone of you mimics your every move, except that their left is your right. These three examples showcase various ways that material can alter light, but the inverse is also true. Why is it that the pavement is warmer in the daytime and cooler at night? The focus of this work explores photonic interaction with a specific type of material - semiconductors.

Semiconductors

Semiconductor is a classification of material that describes how electrons move from atom to atom within the material. Conductor describes a material in which the electrons move freely. Insulator describes a material in which the electrons are trapped to their respective atoms and are not easily liberated. Semiconductor describes the in-between. In a semiconductor, the at-rest energy state has the electrons attached to their respective atoms, but when provided with just enough stimuli, such as the energy of a photon, the electron is liberated from the atom and is free to move through the material until it is arrested once more. Since the atom's energy levels are quantized, there exists only specific energy states available for the electron to occupy. Summing

all the atoms in the material provides a statistical spread of energies that electrons could have called energy bands. These bands do not cover the full spectrum of energy and these gaps between energy bands is what is referred to as the bandgap of the material. It is the nature of this bandgap that makes semiconductors such a powerful force in the advancement of technology.

This gap in energy can often be tailored to a specific value through a process called doping. To dope a semiconductor means the material is impregnated with a calibrated number of defects, through the presence of foreign atomic species. This will effectively expand or shrink the bandgap based on whether the foreign atom provides more or less electrons than the native species, called donor or acceptor species respectively. There are several techniques for doping a semiconductor such as controlling the composition of gas phase materials during growth or by implanting the dopant atoms into lithographically defined areas of an existing semiconductor. When two regions of a semiconductor with different doping are in close proximity, the bandgap boundaries are forced to bend to create a continuum of energy states between regions. The effect of band bending is what differentiates semiconductor materials from semiconductor devices. Doping a semiconductor will change its electrical properties by altering the quantity of free electrons and their ability to move through the material - which is often the intention. However, doing so also changes the optical properties of the semiconductor which can allow the material to become absorbing or transparent to wavelengths it previously was not.

When a semiconductor absorbs a photon, the photon's energy is transferred to an electron, promoting it to a higher energy level. If the energy of the photon is not enough to promote the electron to a new state above the bandgap, then the photon will not be absorbed, and the material

is effectively transparent to that light. Semiconductors can also emit photons via the reverse process – an excited electron relaxes to an unoccupied state at a lower energy level and gives its energy back by emitting a photon with an exact energy equal to the difference in energy states. The electron promotion process is exploited to create photonic devices such as solar cells or cameras where the light absorbed drives electrons that are swept out of the material by way of a pn-junction. The relaxation process is used to create LEDs and lasers where electrical current pumped into the device produces a constant supply of high-energy electrons which can relax and produce photons with consistent energy equal to that of the bandgap. These optical sensors and sources, in addition to many other semiconductor-based electronic elements, can be found on almost every consumer electronics product which is a testament to the impact level semiconductors have on our society. We refer to semiconductor devices whose primary function is related to absorbing or emitting light as photonic devices.

TPV Technology

There are many technologies that rely on photonic devices. One such technology which was one of the focuses of this work is thermophotovoltaic (TPV) technology. The goal of any TPV system is to absorb thermal energy from some source and convert it to electricity through the photovoltaic effect. The backbone of TPV is the photovoltaic cell, which converts light into electricity. This technology is the same in many regards to solar cell technology. The key difference between solar panels and cells designed for TPV is the bandgap, where TPV cells typically have much smaller bandgaps. This is because both the distribution of photon energies and number of photons available from terrestrial sources are much lower than those emitted from

stars like our Sun. Typical TPV applications include steady-power generation and waste heat reclamation. TPV technology has great potential in the global energy sector but has yet to make real impact due to the many challenges related to efficiency of these systems.

Although TPV cell researchers have published record-breaking conversion efficiencies above what has been achieved by solar cell technology, the efficiency of the entire TPV system is only a fraction of that. The primary struggle for TPV technology is that the pillars of system efficiency are fundamentally at odds. System efficiency is determined by total electrical energy out divided by the total thermal energy in. The distribution of energy from thermal sources in units of photon energy is defined as blackbody radiation. The equations which describe blackbody radiation are show below where Q denotes the number of photons per second and E denotes the total energy per area per wavelength.

$$Q(\lambda) = \frac{2\pi c}{\lambda^4}\left(\frac{1}{e^{\left(hc/_{\lambda kT}\right)} - 1}\right)\left[\frac{photons}{sm^2m}\right], \quad E(\lambda) = Q * E_{photon}\left[\frac{W}{m^2m}\right]$$

In these equations, h and c are the same as previously defined but k now represents Boltzmann's constant instead of the extinction coefficient. T is the temperature of the source in units of Kelvin and λ in meters. As previously described, photons with lower energy than the bandgap cannot be absorbed by the cell, thus this entire range of thermal energy provides zero contribution to electrical output. Furthermore, electrical output is limited by the bandgap of the cell. It is a rough, but acceptable approximation to say that the voltage applied to the load from a photovoltaic cell is half of the bandgap. With voltage being fixed, the only improvement to electrical output must be made by increasing current, which is directly related to how many photons are absorbed. Photons

with excess energy above the bandgap do not provide any additional electrical contributions than those with exact energy. TPV cell conversion efficiency can be very high when only considering photons very near the bandgap but it drops off rapidly outside of this narrow range.

The current solution to address these issues is the implementation of a selective emitter. A selective emitter (SE) is an optical element that has a tailored emissivity profile. The term blackbody refers to a material that absorbs and emits all wavelengths perfectly. By definition, this means a blackbody source has a uniform emissivity profile everywhere with value one. Natural materials do not have uniform emissivity profiles, nor does any peak value typically reach perfect unity. The objective of the SE is to redistribute the absorbed thermal energy into a desired optical spectrum which can be more efficiently converted by the TPV cell. State-of-the-art designs for selective emitters involve engineered emissivity profiles rather than relying on emissivity peaks that exist in natural materials. This can be done in a variety of ways but fundamentally the engineered material will use optical interference to suppress undesired wavelengths and boost those just above the bandgap of the TPV cell. Without a SE, TPV system efficiency would be tragically low, but even with it, optimal values barely exceed a few percent.

The major losses in efficiency stem from the wide distribution of thermal energy, the effective conversion efficiency over this range, and the transfer of energy between stages of the system. Hotter sources provide more photons but also shift the distribution to higher energies which cannot be converted as efficiently. Smaller bandgaps absorb more photons but produce a smaller electrical output for the same number of photons absorbed. Balancing this trade space to optimize efficiency must be the principal concern if TPV technology is to be considered useful for

the desired application. This necessitates TPV systems being specifically designed for target applications but this also leads to difficulties when comparing one system to another or determining which solutions are most effective for the technology as a whole. TPV-related research cannot simply investigate components independent of the system. Innovations to this technology must be made when considering each component's impact to the system as a whole.

Materials and Methods

Creating semiconductor devices is an elaborate process which consumes precious metals and rare earth elements, as well as highly toxic gases and other potentially fatal chemistry. These processes involve, and frankly require, machinery which can make efficient use of small volumes to produce nanoscopic structures while simultaneously keeping the tool operator safe from harm. Because dust and other airborne particles are at the same scale as the features of the devices, special facilities called cleanrooms are constructed to house the equipment required to perform this work. The air quality, among many other things, is very tightly controlled such that only a small but countable number of particles remain in any given volume of air. In general, these processes are referred to as nanofabrication techniques and the machinery called nanofabrication tools. This can be a misleading descriptor since many tools in a cleanroom are actually limited to the microscale, not the nanoscale, and the substrates used to prepare these devices are several inches in diameter. Because typical semiconductor devices are on such a small scale, other sophisticated machinery has been invented to measure them during the fabrication process. These tools are referred to as metrology tools – metrology being “the study of measurement” from Greek roots. In my tenure of research, I’ve become quite familiar with these tools and techniques. By no means is the following list exhaustive, but the materials and methods described henceforth were vital in producing the following results of this work.

Fabrication Methods

Sputtering is a term used to describe the process of bombarding atoms with others creating liberated atoms. The source atoms being launched are typically large or heavy, such as argon, to

increase the number of liberated atoms per collision. Sputtering can refer to the removal of atoms from a surface, but it is also often used to describe the deposition process of those removed atoms onto another surface as well. Most commonly, a solid volume of a single periodic element, such as a metal, or other material is sputtered away and the liberated atoms are deposited onto the desired surface. The atomic species used to sputter metal is often argon. Argon is in the gas phase at typical processing temperatures and the atomic radius of the atom is very large compared to most others. For these reasons, argon is not likely to be deposited onto the surface, or rather, trapped within pockets of the surface. The quality of sputtered metal films that coat a sample's surface is strongly dependent on chamber pressure and sample temperature during deposition as well as the underlying surface's roughness and permeability. When the sputtered atoms find their way back to the sample from which they were liberated, this is called back sputtering. For flat samples, back sputtering is not observed since the rate of removal and the rate of redeposition are uniform everywhere. Only the difference in these rates is observed. When the surface is patterned, back sputtered atoms will redeposit along the sidewalls of the pattern, altering the shape.

Lithography is the name for a process in which a pattern is transferred from one surface to another though a special type of material known as photoresist (PR). There are six major steps to any lithography process but finer resolution and clean-up steps are often used to increase pattern fidelity. The major steps are spin, bake, expose, develop, process, and removal. There are many recipes for PR and sub-types but are always categorized into two types: positive and negative. In all variations of lithography, the PR is poured/sprayed onto the sample's surface and a spin coater is used to produce a uniform thickness everywhere. Then the PR is pretreated by heating it, called

“prebaking”, to become more solid than liquid. Next is the exposure where energy is applied to the PR to induce a reaction. This energy can be from ultraviolet lamps, lasers, or an electron beam. The energy is distributed in the desired pattern onto the PR and the energy density must be calibrated, also called the dosage. The pattern can be formed by producing a shadow of the light, or by steering the electron/laser beam to trace the pattern. The positive or negative type of PR dictates whether you want to trace the pattern directly or it’s negative. For negative PR, the area exposed will be strengthened and much harder to remove while positive PR is weakened by the dose and that area will be removed more easily. Removing the weaker parts of the PR while leaving to rest in tact is called the develop step, like traditional darkroom photograph developing. The develop process is very fickle and the bane of existence for most fabrication engineers – especially graduate students. If the develop goes poorly, the entire process must be started anew. Success is strongly dependent on the thickness and evenness of the deposited PR, the bake time and temperature, the exposure dosage, and the chemical composition of the developer. Once the pattern is successfully developed into the PR, the sample can be processed. Processing can refer to anything but the common options would be etching the underlying material or depositing another material into the patterned spaces. Finally, the remaining PR must be removed. A more aggressive chemical is needed for removal than was required for the develop process, however, some PR can use the same chemical at higher concentrations or longer soaking times to be fully removed. All of this describes lithography in its most basic form. Depending on the processing goals, lithography can become very complex with multiple PRs and intermediate processing steps not described above.

Reactive ion etching (RIE) and inductively coupled plasma (ICP) are often seen together, but not exclusively. Inside a gas chamber, at controlled pressure, a strong electrical potential is produced which ionizes the gases present, creating a plasma. The plasma is often generated by an induction coil, thus the term ICP. The elements within the plasma are often selected such that they are chemically reactive with the sample material, which is also present inside the plasma. For example, carbon tetrafluoride (CF_4) is a gas but when turned into a plasma, the fluorine ions become highly reactive with most other elements. In order to have etching occur, there must a chemical compound formed by one of the plasma species, a.k.a. etchant, and the sample elements. Additionally, this compound must have a boiling temperature that is low enough to be present in the gas phase. If these requirements are met, then the compound is called a volatile and the reaction rate will determine the etch rate. This interaction of creating volatiles and pumping them out of the chamber is called RIE. If one would introduce a strong electric field in the gas chamber as well, the ions of the plasma would then be accelerated along the field. These accelerated atoms are sent towards the sample surface, crashing into it with significant momentum. This can enhance the etch rate significantly because of atomic bombardment effects. This reaction is similar to billiards where after the break, some of the balls are sent flying back towards the shooter. The atoms are etched at a much higher rate because they are both being "knocked loose" and chemically dissolved. Some etch rates in ICP tools have been reported as much greater than the sum of the

rates of chemical reaction and bombardment independently. The graphic below depicts how lithography and RIE are used to pattern a material.

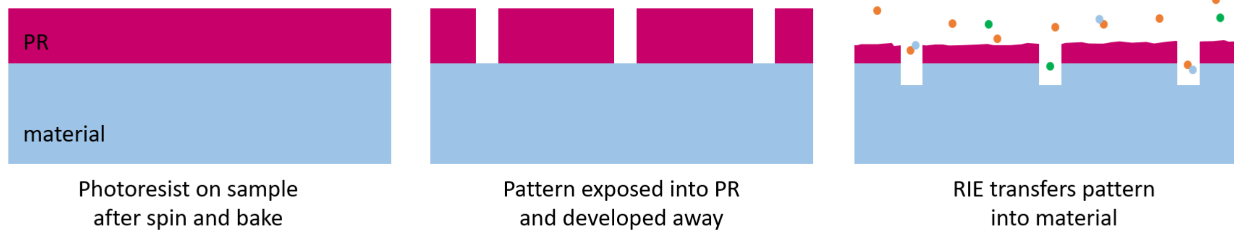

Figure 3. Depiction of lithography and RIE processing.

Metal lift-off is a specific variation of the lithography process which involves patterning a metal onto a sample. It is most frequently used for gold processing because gold does not react with any RIE chemistries so it cannot be dry etched. There is only one known acid etch chemistry composition which can etch gold, trade name Aqua Regia, but since it is a liquid etch process, pattern resolution is often poorly maintained and the lift-off process is implemented instead. The differences between standard lithography and lift-off require that the topology of the developed PR must contain an overhang and have sufficient height ratio of the metal layer being deposited. If the sidewalls of the developed PR were vertical, the metal would cover them and when the PR is removed, the metal will be peeled away with it. The overhang is necessary to create broken segments in the conformal metal coating so the parts connected to the sample will stay there when the PR is removed. This overhang can be created by using a slightly different type of PR called lift-off resist (LOR) underneath the standard PR. The exposed LOR will dissolve out faster than the PR during the develop process leaving behind a void. Other techniques can be used to produce an overhang without using LOR. One alternative method implemented in this work involved using a vapor prime oven to reverse the image exposed. In a positive resist, a photoacid is generated in

the exposed areas which weakens the polymer bonds. Rather than using a developer to remove the exposed areas, the sample is exposed to ammonia gas in a vapor prime oven and the exposed area chemical bonds are now strengthened beyond their original. Next, flood illuminating the remaining PR will weaken the previously unexposed areas and this will be developed away. The image is reversed in this process, and in doing so, a lip is formed at the top edge of the PR, creating the required overhang for a successful lift-off.

Chemical vapor deposition (CVD) is a method for coating a surface in a material, typically a dielectric material. For materials which cannot be stabilized in a gas phase, sputtering or evaporation must be used. Variations on CVD called metal-oxide, MOCVD, or plasma enhanced, PECVD, are more commonly seen in industry for growing specialized materials when molecular beam epitaxy (MBE) is not preferred. CVD requires a gaseous precursor which contains one or more of the elements desired for the coating. For example, silane gas (SiH_4) contains silicon and when mixed with nitrogen gas (N_2), silicon nitride (Si_3N_4), a solid material, can be encouraged to grow on the sample surface. In fact, it grows on all surfaces, including the walls of the deposition chamber which requires frequent cleaning cycles to prevent build-up. The temperatures required for CVD are well above room temperature, however, they are still significantly lower than those required for MBE which is an advantage for many semiconductor devices.

Characterization Methods

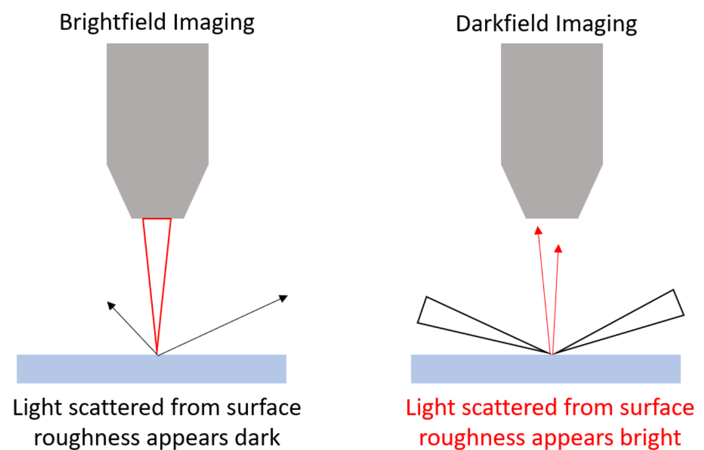

Figure 4. Depiction of brightfield and darkfield microscopy.

Microscopy is a concept that the general audience is expected to be familiar with – examining something very small. However, some microscopic techniques are worth defining here. Brightfield imaging is done with transparent samples by way of the light transmitting through the sample, directly into the microscope objective. For opaque samples, the light source is folded into the optical path and exits from the objective, directly above the sample, and what reflects mostly straight back is collected. Sample roughness that would bounce light outside of the collection area, a.k.a. aperture, appears dark or shadowed. Darkfield imaging is where the light source is hitting the sample at oblique angles and the direct reflection is not normally collected. In this case, sample roughness bounces light into the objective's aperture and appears bright. Brightfield imaging is the most commonly seen technique, in general, and was implemented during typical inspections throughout the nanofabrication processes. Brightfield imaging was also implemented in the design of the custom beam viewing microscope described in the results chapter that follows.

Optical profilometry is a technique that utilizes the interference of light to make determinations of the separation of reflecting surfaces. A structure containing a Michelson interferometer is moved relative to a sample, typically in very small, precise motions enabled by

piezo-electric positioners. The interference patterned formed on a camera is imaged and the motion of the fringes formed by the variable distance leg are recorded relative to motion. An algorithm can then deduce the spatial separation of surfaces within the field of view by the impact they play on the fringe pattern. This technique has extremely fine height resolution, as precise as 0.1 angstroms, however, the lateral resolution is dependent on the magnification and wavelength of the system which often falls short of the equivalent resolution in a standard microscope with equal parameters. Additionally, optically transparent materials will shift the fringe pattern nonlinearly, or produce a duplicate pattern which cannot be corrected for without accurately knowing either the refractive index or thickness of the transparent material. Still, this technique provides one of the most precise physical measurements that can be performed non-destructively.

Stylus profilometry can be performed by a common tool seen in the cleanroom, Dektak by Bruker Technologies. This is a tool where a very thin and sharp probe is dragged across the sample surface and the force exerted on the cantilevered side is recorded and translated into a height reference. This technique depends greatly on the sample roughness, speed of the dragging motion, and overall flatness of the sample area being recorded. The measurements are strictly relative but can be performed quickly and multiple collections can be averaged for increased accuracy. In nanofabrication, this technique is often used to determine etch or deposition rates in a “quick and dirty” fashion. In processes where the rates must be known with very high confidence, alternative techniques are implemented.

Atomic force microscopy (AFM) is a unique type of stylus profilometry where some key differences give AFM a substantial improvement to accuracy and resolution. The first key difference is that a laser is reflected off of the top of the cantilever and the deflection of the laser spot on a camera is what is converted to differences in height. Another key difference is that the probe is electrically charged. In tapping mode, and alternating current is used and tuned to a resonant frequency of the probe. Whether in tapping mode or standard, this charge produces an electrical attraction between the atoms at the tip of the probe and the atoms in the sample. When in close proximity, the atomic attraction is enough to deflect the delicate probe without having the probe and sample in physical contact; thus, the name "atomic force". AFM is exceptionally useful in measuring sample topology on the nanoscale. The lateral resolution in AFM is only determined by the scanning speed. Stage motors implemented in AFM tools are often of the highest quality and can achieve nanometer lateral resolutions.

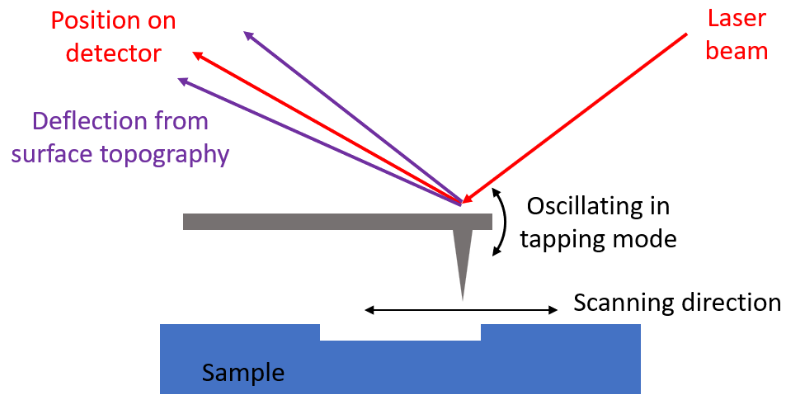

Figure 5. Depiction of atomic force microscopy fundamentals.

Scanning electron microscopy (SEM) is widely implemented in fabrication of semiconductor devices and many other microscopic sciences. SEM images are commonly recognized as the glamour shot used in publications because the user has the ability to image a subject with any magnification and at incredible resolution. There are many types of images that

can be produced in SEM but the general concept of the technique can be described as a very finely focused beam of electrons which is rastered over and area while sensors that capture electrons are recording hits. The electrons recorded can be liberated from the sample, reflections from the beam, transmitted into the sample and then exit after a few bounces, or some combination of these phenomenon. Measuring the momentum of the recorded electron helps identify the phenomenon of its origin and then filtering by type of origin or location is what leads to the many imaging modes of SEM.

Current-voltage (I-V) sweep is a common electrical testing method to determine the resistance of materials, but it can also be used to determine capacitance and other electrical properties when using a variation of probing configurations. The simplest, and that which was implemented in this work, involves using two probes. The probes are aligned under a microscope and placed in contact with the sample. The two probes are not in contact with one another and therefore the circuit must be completed by flowing through the sample between probe tips. By sweeping a range of voltages, and measuring the current that flows through the circuit at each voltage, electrical properties are deduced. When testing diodes, the voltage supplied can be either positive (forward-bias) or negative (reverse-bias). Some diodes, such as avalanche diodes, will experience a breakdown voltage where the current will become infinite. The slope of the I-V plot, and curvature of the area near breakdown, inform the engineer about resistance, leakage current, and avalanche gain.

Variable angle spectroscopic ellipsometry (VASE) is a very powerful technique which exploits the fact that index of refraction is a function of wavelength. By measuring an oblique

reflection, the strength of the reflection also becomes a function of polarization and phase. A sample is illuminated by a light source where the wavelength is swept through a range and the intensity of the reflection is recorded. By repeating this sweep at several angles, the response will vary at each wavelength as the criteria for interference has now changed. The wavelength sweep for each angle is compiled as a data set and compared against a numerically calculated reference model. The model is altered until the calculated data is fit very closely to the measured data. Once this is complete. The model represents the real sample structure to a very high accuracy. This technique is so sensitive that surface roughness and underlying layers below the top surface must be accounted for in the model. You cannot learn both the layer thickness and the material index from this technique simultaneously. You must know one and solve for the other, however, much work has been done to characterize the index of refraction for many common materials with very high accuracy and these are often considered what is "known" in the model. If the material properties are what is to be solved for, then the layer(s) thickness must be independently characterized with an alternative technique.

Photoluminescence (PL) is a phenomenon in which a material will store energy by absorbing high-energy photons and release that energy via emission of other photons. In semiconductors, the emitted photons can have a range of energies, but the primary population comes from electrons which have relaxed to the conduction band then combine with a hole across the bandgap. By measuring the wavelength and intensity of the emitted photons, the semiconductor bands and defects can be better understood. This can also be done as a function of temperature, which semiconductor device performance is often very dependent upon. If one were to time stamp

the arriving photons, relative to the pump photon being absorbed, the carrier lifetimes of electrons and holes could also be measured. This is called time-resolved photoluminescence (TRPL) but the extremely fast electrical equipment required makes this technique rarely implemented. Most often, the source of photons, a.k.a. pump, is a visible or ultraviolet laser. The source photon wavelengths are very narrowly distributed and sufficiently far enough away from the wavelengths of interest so they can be filtered out of the signal.

Results

The following sections will describe each project in full, in the order previously listed. The three projects described henceforth are: a design toolbox and visualization tool used to design or analyze thermophotovoltaic (TPV) technology systems, an optical metasurface fabricated into the refractory metal iridium, and a monolithically integrated photodetector utilizing a multilayer diffractive lens (MDL).

The TPV Design Toolbox is intended to be used as a modelling aid in the design process and displays a visual representation of TPV system efficiency across multiple dimensions of the system parameters. This was strictly a software project, unlike the other two projects, but designing a tool which is meant to be used for design, requires a carefully thought-out design of its own. The optical metasurface was a fabrication-focused effort, but a characterization tool was also built. Iridium is a very stubborn material to work with and the bulk of the research performed aimed to discover suitable fabrication methods for making optical devices with this material. The third project also involved both fabrication work and characterization, but the characterization tool was built and qualified will be highlighted. Although this project involved a decent amount of fabrication, the characterization of the lenses, both independently and after monolithic integration, required a sophisticated piece of equipment which needed to be built. A microscope was designed which could inspect and characterize all variety of microlens arrays by both imaging the surfaces and mapping how each one focuses light through its substrate. To qualify this microscope, it performed characterization of several variety of microlens arrays, some commercial and others fabricated in-house.

TPV Design Toolbox and Visualizer

After attending the 15th World Conference on Thermophotovoltaic Technology, several observations stood out. The first was that much of the theory-based work seemed repetitive and all claimed that TPV technology has the potential to become a leader in the energy production sector based on growth and efficiency metrics. Secondly, there was a huge disparity between conversion efficiency demonstrations and system efficiency demonstrations. After socializing with other attendees, the reason for this disparity became apparent. TPV-cell focused researchers are aiming to optimize conversion efficiency by using very hot sources and narrow-band selective emitters (SE) while TPV-system focused researchers are aiming to minimize thermal losses with moderate source temperatures, and using wide-band selective emitters. I argued that the optimal SE profile would be one that is neither of these, but rather one that is matched to the system parameters. TPV technology can be applied to a wide variety of applications, such as decarbonization, waste heat recovery, and steady-state electric generation. Each of these applications mandate the TPV system to operate in very different parameter space and therefore the optimal SE would be different for each. The reason for omitting high energy photons in a narrow-band SE is to reduce thermalization losses – boosting conversion efficiency. The reason for including those photons in a wide-band SE is because the source is more energy-dense at shorter wavelengths. Getting as much energy converted as possible from this region of the spectrum will boost system efficiency. However, the number of photons available for each wavelength will greatly vary given the source temperature. In addition, the cell conversion efficiency will vary with the number of photon-generated carriers present. Therefore, the optimal SE must be dynamically based on the system application parameters.

To test this theory, as well as provide the TPV community with a useful design/analysis tool, I developed the TPV Design Toolbox and Visualizer software in MATLAB. To set this tool apart from other theory works, it would include calculations dependent upon material properties for the semiconductors used. This detail is commonly omitted by assumptions made in similar works, such as the famous detailed balance by Shockley and Quiesser. Including effects based on material property impacts the efficiency result in two major ways. First, rather than calculating efficiency as a function of arbitrary bandgap, the bandgap values are directly calculated based on the material chosen and the system parameter bounds. This limits the output to a range achievable with realistic doping and alloy compositions. Secondly, the carrier recombination mechanisms are far from equal between materials. Including this in the calculation provides a more accurate estimation for cell conversion efficiency and, of course, overall efficiency. This tool should also be able to provide a method for comparing TPV designs to one another even if they were designed with very different application parameters – an asset that the TPV community is currently lacking which could be contributing to the rift between community members.

The Design Toolbox simulates a TPV system as a block diagram with energy flowing from one block to the next. The system is modelled with four blocks: Source, Filter, Cell, and Electricity. To avoid confusion from repeated word usage, SOURCE, FILTER, CELL, and ELEC will be used

when referring to the data contained within the respective blocks of the Design Toolbox. Figure 6 shows the depiction of the TPV system block diagram with energy flowing between blocks.

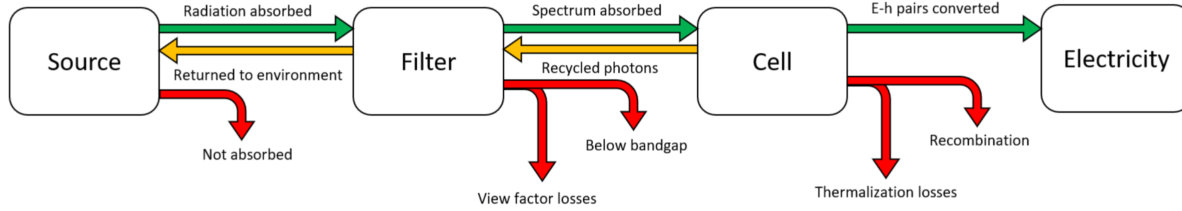

Figure 6. Block diagram of energy flow through a simplified TPV system which define the data products of the TPV Design Toolbox and Visualizer.

The first prompt allows the user to define SOURCE values and units as a range in temperature and spectrum. This input is then used to calculate the blackbody radiation present within this two-dimensional range. The radiation is calculated both in Watts and photons per second, E_{in} and Q_{in} respectively. E is used when determining system efficiency since it is more useful to represent this in units of power. Q is used to determine photon-generated carriers which influences recombination rates, diffusion lengths, and ultimately photocurrent. A realistic TPV application would not have a perfect blackbody radiation curve as the spectral input, but rather this multiplied by the emissivity profile for a graybody or otherwise known emitter profile. To simulate this, the FILTER prompt is presented for the user to scale down the blackbody source to a more application-specific one. At this step, SOURCE is fully defined. The equations used to calculate the blackbody spectrum are shown here.

$$Q_{in}(\lambda, T) = \frac{2\pi c}{\lambda^4 * 10^9}\left(\frac{1}{e^{hc/\lambda kT} - 1}\right)\left[\frac{phot}{sm^2nm}\right], \quad E_{in}(\lambda, T) = Q_{in} * E_{photon}\left[\frac{W}{m^2nm}\right]$$

The filter block allows the user to apply spectral filtering to the spectrum before it is absorbed by the cell block. This is where the user will define the SE. Although the filter block is

next in the series of energy flow, it is more useful to the designer to define CELL immediately after SOURCE. The SOURCE visualization informs the designer as to where the energy resides in the parameter space and this information should influence the user when choosing cell material. The CELL visualization will then influence the user in designing the SE emissivity profile, such as selecting the cutoff wavelength. For this reason, FILTER is finalized after defining CELL. The CELL prompts in the Design Toolbox allow the user to define: cell material for each layer in a p-i-n (or n-i-p) junction as well as the substrate, performance of optical coatings such as anti-reflective front surface and backside reflector, thickness of each layer, operating temperature range, emitter-to-cell geometry, and electrical fill factor. The most "value-added" feature provided by the Design Toolbox comes into play when selecting the cell material. Each cell material is defined in a pre-configured JSON file, with a custom file extension "*.matl.json". A JSON file is simply a formatted text file that lists a variable name, followed by the value(s) for that variable. Variables are comma separated with the name preceding a colon and values are contained within square brackets. These JSON files we have pre-configured contain look-up tables for temperature-dependent refractive index, electron and hole effective masses and mobilities, and coefficients for solving equations such as temperature-dependent bandgap (Varshni) and Auger recombination rate. The format is simple and universal, enabling users to take our material database files and use them in other software as well as easily collect data from other sources and create new material files to be used in the Design Toolbox. The code running in the background interpolates the exact values of refractive index needed for the user-defined temperature and spectrum by performing a plane fit from the nearest two points in temperature and wavelength that exist in the look-up tables. For each wavelength, the temperature-dependent index of refraction is used to calculate the

transmittance through each layer of CELL and the reflectance at each material interface. Absorption is then easily determined by the subtracting reflectance and transmittance from unity. Absorption is calculated at differential slices through the material to more accurately determine the location and quantity of photon-generated carriers in the device. The equations to determine photon absorption are shown here.

$$R(\lambda) = \left(\frac{n_i - n_j}{n_i + n_j}\right), \qquad T(\lambda, x) = (1 - R)e^{-(4\pi k x/\lambda)}, \qquad A(\lambda, x) = 1 - R - \sum_x T$$

In the equation for absorption, the summation of transmittance denotes the sum of each incident and reflected beam at that position in the material. For example, if there is a material index mismatch between the layers, the top layer will contain: the first transmitted beam in, a reflected beam from the top-intrinsic interface, a reflected beam from the intrinsic-bottom interface, and a reflected beam from the bottom-substrate interface. An example image of the CELL visualizer is shown in Figure 7. In this example, the material is GaAs for each layer and substrate, there is a 95% effective anti-reflective coating and 95% effective backside reflector. From left to right: the

n-layer is 100nm thick, the intrinsic layer is 1.4μm thick, and the p-layer is 500nm thick above the substrate.

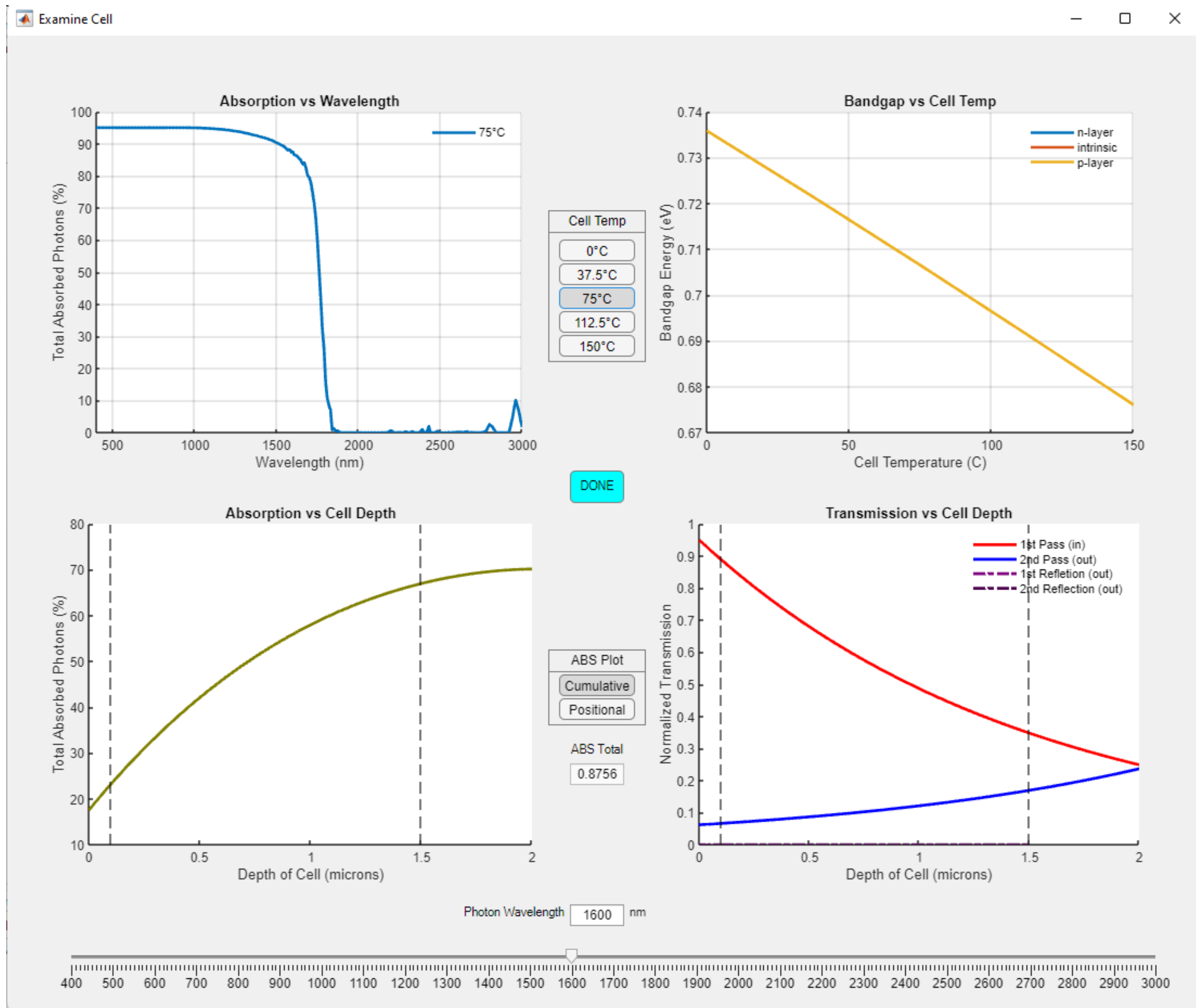

Figure 7. TPV Visualizer output for defined CELL parameters.

After defining CELL, the user can finalize FILTER. This block is called filter, but it represents more in a real TPV system. A real TPV system would have an absorber which collects heat from the source. This absorber then re-emits that energy outward in all directions. The emissivity of this component would ideally be designed differently for opposite sides. The source-facing side(s) should emit as little as possible, so that it stores the source's energy rather than

returning it to the environment. The cell-facing side should contain the selective emitter which converts that energy into an optical spectrum distribution ideal for conversion to electricity. To simplify this behavior, FILTER simply modifies SOURCE to the final output before sending energy to CELL. The filter prompt allows the user to build a variety of SE emissivity profiles and combine multiple filter steps to achieve the desired output. For all SE profiles, the user must define the cutoff wavelength, which designates where the emissivity goes to zero at all energies below the cutoff. A square profile must have a width defined. A Gaussian profile will be defined by a standard deviation (sigma) and Z-score. The center of the profile (mu) will be placed Z*sigma above the cutoff energy. There are also decaying profiles of linear, exponential, and hyperbolic shape. The linear curve will produce a triangular shape beginning at the cutoff and terminating at the end of the defined spectral range. The other decaying profiles are defined by a magnitude of curvature. Once FILTER is fully defined, the final emissivity profile is multiplied with SOURCE and scaled to the emitter area defined in CELL. Figure 8 shows the visualization of SOURCE2 (after 90% graybody is applied) next to the SE profile and the resulting SOURCE3 which represents the emitter output spectrum. The SE profile in this example was Gaussian defined by a cutoff wavelength of 1800nm, a sigma of 200nm, and a Z-score of 2.0.

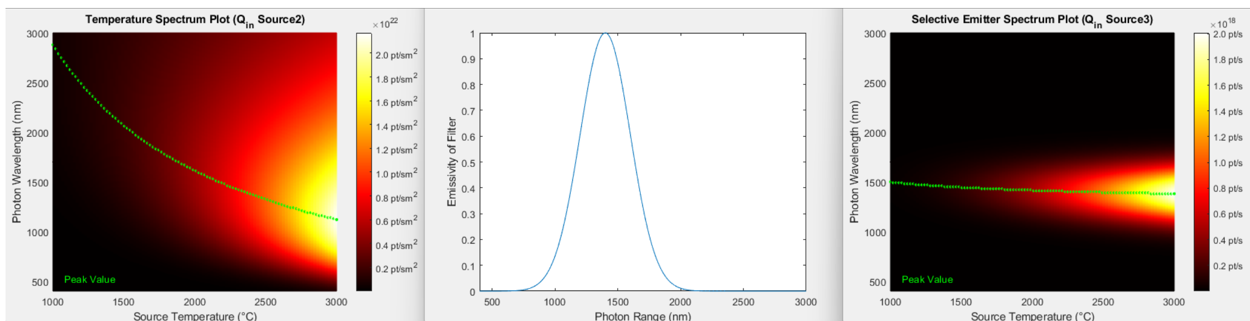

Figure 8. TPV Visualizer outputs of SOURCE (left) and FILTER (right) after SE profile (center) is applied.

The ELEC section does not contain any prompts for the user to define, as the remaining work to be done is just mathematics. The ELEC visualization provides maps for efficiency as a function of cell temperature and source temperature. With the set of equations from CELL that define where and what fraction of photons are absorbed in the cell layers and the final distribution of photons defined by FILTER, we can now calculate the position and density of photon-generated carriers, G, in the cell. With G known, a series of equations can be solved that will determine the electrical power output by the cell. The values dependent on G are the following: number of free carriers, radiative recombination lifetime, Auger recombination lifetime, electron and hole diffusion lengths, carrier extraction probability, and photocurrent. An example of the ELEC visualization is shown below for a GaSb cell using a wide-band square-profile SE.

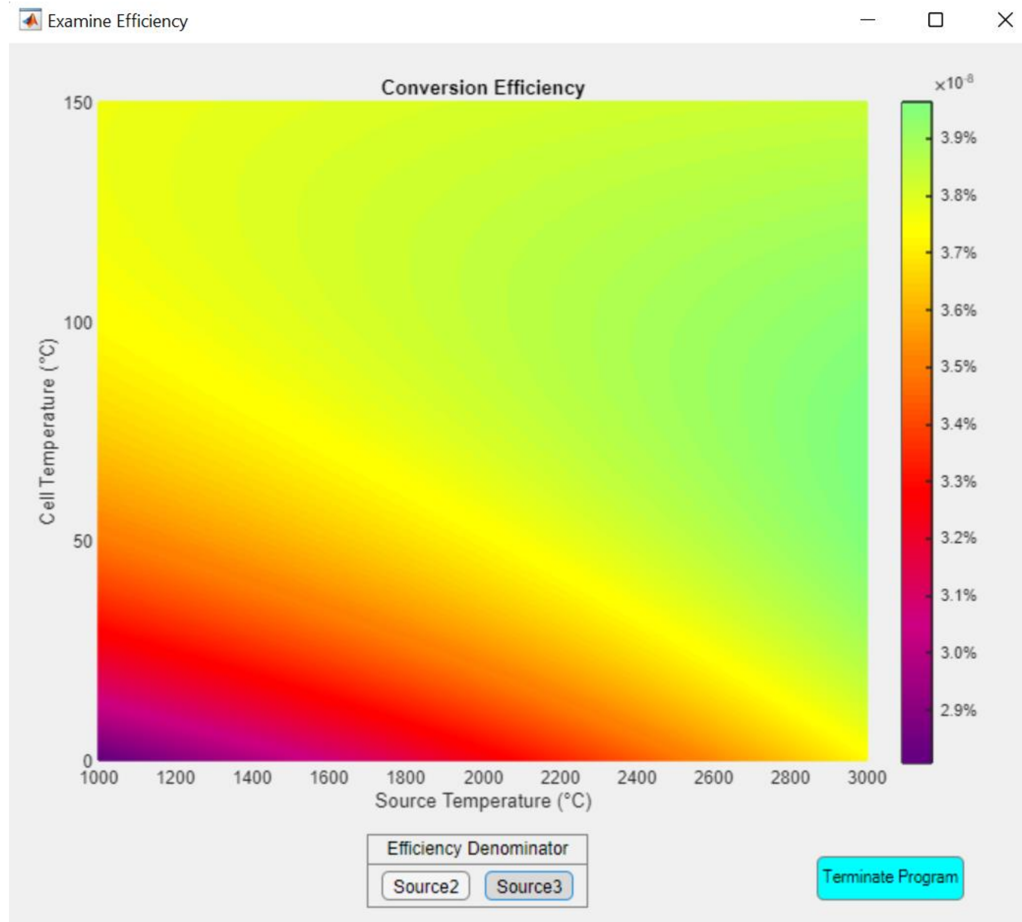

Figure 9. TPV Visualizer output for final efficiency.

If one were to run the Design Toolbox several times, changing certain choices on each iteration, a series analysis could be performed for any component of the TPV system. One series of interest to researchers would be investigating new materials. If the user were to grow a new compound semiconductor, a series of growths for alloy composition and doping would need to be performed. The material characterization performed for these growths would traditionally include mapping the index of refraction as a function of temperature and Hall effect measurements which deduces carrier mobilities. The user can easily format this data into a JSON file and run the Design Toolbox. With the feedback provided from the Visualizer, the user can then know which

composition to focus on for device fabrication – rather than repeating fabrication on each growth series and testing each device individually. This is just one example of how the TPV Design Toolbox and Visualizer can make a positive impact for TPV researchers.

Iridium Selective Emitter Metasurface

Metasurface Design

An optical metasurface is a device which has a three-dimensional structure patterned into the surface of a material. The pattern often has features at the nano-scale which is critical to the principal of how they work. Thinking of light as a wave in the electromagnetic spectrum, imagine a single wave of light approaching the surface. If the pattern features are smaller than a single wavelength, then the light "sees" a mixture of two materials, typically air and the base material for the metasurface. By carefully adjusting the ratio of air and material seen by any particular wavelength of light, the behavior of the light interaction can be precisely controlled. A periodic structure will create structured interference leading to spectral filtering or beam steering. A structure that varies radially will lead to focusing, like a lens. Changing the structure differently based on orthogonal orientations will change the interaction based on the polarization of the incident light. All of these interactions can be combined to create very specialized optical elements. Additionally, by controlling light interaction at the surface, the device need only be a thin film to operate. These are the reasons why optical metasurfaces are becoming much more popular and enabling new types of scientific experiments and equipment. However, optical metasurfaces are not without their limitations. These nano-scale features that enable the film to control light interactions, must be sharply defined and precisely spaced in order to produce the required phase shifts and interference to function. The features would lose fidelity due to edge-rounding and oxidation – two common mechanisms that lead to surface morphology changes in high-temperature environments.

There are technologies that would greatly benefit from optical metasurfaces, but are being limited by the application environment. One such example would be thermophotovoltaic (TPV) technology. High-temperature industrial processes, such as glass and metal manufacturing, have been identified as a target for energy harvesting applications that reclaim waste heat utilizing TPV cells. These mfg. processes can see furnace temperatures that range from 1200-2000 Celsius, which corresponds to peak wavelengths of about 2.0 microns to 1.3 microns from a blackbody source. Photovoltaic (PV) cells tuned to these short-wave infrared (SWIR) wavelengths are a mature technology, however, these devices could not be sufficiently close to the furnace to still operate. Instead, the device should be operating at a reasonable distance from the furnace where the radiated temperature is closer to 500 Celsius. At this temperature, the peak wavelength of a blackbody source has shifted from SWIR to mid-wave infrared (MWIR). PV cells in the MWIR regime are less mature and suffer efficiency losses outside a very narrow range of bandgap energies. One such suitable semiconductor for this application would be InAsSb, lattice matched to GaSb, which has a band gap around 0.4eV. TPV devices operating at these bandgaps often struggle with efficiency because two pillars of the system are fundamentally at odds – power density and conversion efficiency. Having a very hot source would provide the desired power density, but the photovoltaic cell cannot efficiently convert all that energy without help. The current state of the art to address this problem uses a selective emitter (SE). An ideal selective emitter has an emissivity function very close to one at desired wavelengths and very close to zero at undesired wavelengths. In the TPV system, the SE is used to harness energy from the source and convert it to an optical output which can be much more efficiently converted by the PV cell. Selective emitters can be exceptionally well designed in the infrared spectrum by utilizing

metasurfaces, however, the base material must be able to remain unchanged after prolonged exposure to an extreme environment. In order to realize a functional SE for a TPV cell in this environment, the metasurface must be resistant to oxidation and have a sufficiently high melting temperature so that plastic deformation does not occur at operating temperatures. In our work, we designed a SE metasurface for a theoretical TPV system targeted at waste heat reclamation. We designed and fabricated a SE in the MWIR from iridium.

Iridium, element 77 on the periodic table, is what's known as a refractory metal, which is a classification given only to the most robust. The properties which earn metals this classification are high melting temperatures, high hardness, chemical inertness, and high density. Iridium thin film coatings have been implemented as an ideal material for high-temperature protective coatings for many years and would be the best choice for our metasurface material. The stability of these elements in extreme environments makes them ideal candidates for certain scientific applications. Unfortunately, these material properties also present a major challenge for creating a nano-structure in the iridium film using fabrication techniques commonly seen in semiconductor manufacturing. In particular, iridium's lack of reactivity and hardness present major obstacles for lithographic pattern transfer. In this work, we present an iridium-based SE and describe the methods employed for its design and fabrication. In order to quantify the performance of our SE, a custom high-temperature emission spectroscopy testbed was developed to directly measure the emission spectrum of the SE at various temperatures ranging as high as 500°C.

In our TPV system design, the SE would convert the hot source's optical spectrum to a delta function centered just above the bandgap energy target of 0.4eV. Realistically, the delta function

is approximated by a narrow Gaussian curve. By limiting the spectrum to only photons with energy just above the bandgap, conversion losses will be minimized. The SE would need to maintain minimum spectral shift at high temperatures. Iridium was chosen as the metasurface material due to its slower oxidation rate and higher Young’s modulus than tungsten, while still boasting similar hardness and melting temperature. There are several other reasonable choices for refractory metals to attempt making a metasurface with. Already having access to the material and the know-how to create smooth, dense films was also a factor for selecting iridium.

We designed the metasurface using the software CST Microwave Studio. The software simulates the surface’s interactions with electromagnetic waves using a finite-difference time-domain (FDTD) model. A unit cell of the structure was excited with transverse electromagnetic waves to induce electric fields in opposing horizontal directions across the top of the structure. To increase the model’s accuracy, we deposited an iridium film onto a substrate and measured it with VASE. By fitting a general oscillator model to the VASE data in the software WVASE, the optical

properties for the as-deposited iridium film were found and imported into the CST model. Figure 10 shows the complex index of refraction as a function of wavelength for our iridium film.

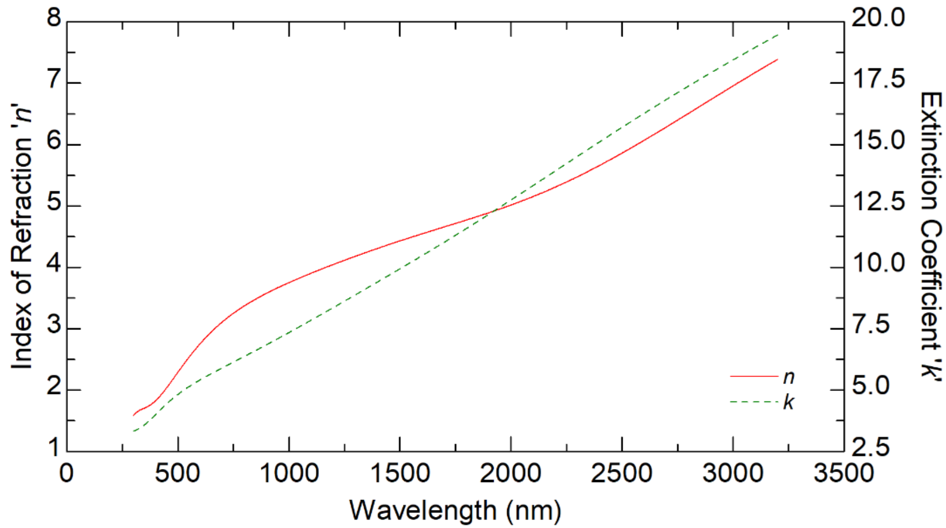

Figure 10. Complex index of refraction for as-deposited iridium determined by VASE modelling.

Once the unit cell was created, various dimensions were studied and adjusted such that the unit cell produced a peak in absorbance at the desired wavelength. Absorbance can be used as a metric to determine emissivity through Kirchhoff's Law. Our study showed that the pillar width dominates the spectral response and increasing or decreasing the pillar height was directly responsible for red- or blue-shifting the spectrum, respectively. The peak in absorbance was targeted such that the falling edge would cross the 0.4eV bandgap wavelength with an emissivity around 50%. The cell was originally designed with 90-degree sidewalls; however, fabrication techniques can rarely achieve such verticality so the wall was adjusted to 85 degrees. In hindsight, the adjustment from 90 to 85 is insignificant and still outside of modest tolerance ranges. When modeled, decreasing this angle causes the absorption curve to blue shift and broaden. A revised cell design was generated for the final device, taking a realistic sidewall profile into account.

Figure 11 shows the modelled unit cell from the CST workspace inset on a plot of absorbance versus wavelength.

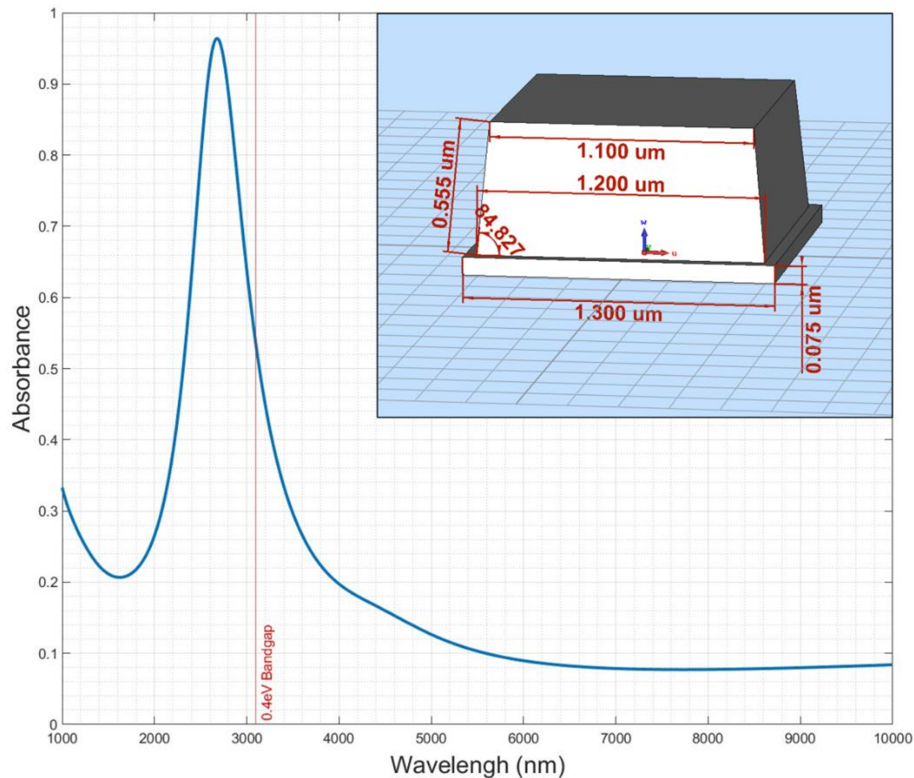

Figure 11. Absorbance versus wavelength function for an iridium metasurface unit cell (inset) modelled in CST Microwave Studio.

The base layer in the CST model, below the pillar, is also iridium. The thickness of the base layer does not affect the metasurface performance after several nanometers - beyond the skin depth. Before attempting any fabrication, there were some critical details observed stemming from this design. Firstly, the minimum feature size of the trench between pillars is 100nm which forced us to use e-beam lithography to create the pattern. Secondly, the aspect ratio of the trench is 5.5:1, which eliminates the opportunity to use the lift-off technique for metal patterning. Lift-off patterning with iridium would likely not be advised even on reasonable structures due to the metal's unwillingness to tear.

Metasurface Fabrication

Iridium films were deposited on silicon substrates with a titanium adhesion layer using magnetron beam sputtering. The film was deposited at a chamber pressure of 4.0mTorr and DC power of 160W to produce 600nm thick, fully dense films. The hard mask ultimately used to pattern the iridium was also deposited in-situ in this chamber to eliminate any surface defects between the materials. A "hard mask" is simply an intermediate material that is patterned by the photoresist mask. This then becomes the new mask to pattern to intended material below it. This is done when the selectivity between the photoresist (PR) and underlying material is unsuitable to complete the pattern transfer. Iridium is one of the hardest materials known to man and photoresists are often quite soft comparatively, about the consistency most plastics. The removal rate of the material divided by the removal rate of the mask is the ratio called selectivity. Ideally, one would select a mask material with a selectivity much greater than one. 4:1 or 3:1 would even be suitable choices for most processing steps. With iridium, the selectivity to photoresist is about 1:200. Majority of materials available still cannot even reach 1:1 selectivity with iridium. Mask selectivity is solely dependent on the processing method. For a physical removal process, the hardness of the two materials will determine the selectivity. For a chemical removal process, the reactivity will be the determining factor. Iridium was intentionally selected for this application because of its extreme resistance to both of these. Finding a suitable hard mask to process iridium was the single most challenging aspect of this project.

The primary problem to be solved is how we would etch the iridium film. PMMA was used as the photomask for e-beam lithography. A publication by Yeh et. al. [15] that also etched iridium

identified IrF_6 and IrF_3 as volatile compounds that can form when using RIE. The melting point of IrF_6 and IrF_3 were published as 44°C and 250°C respectively. The boiling point for IrF_6 was 53°C, but unknown for IrF_3. This meant that a fluorine-based etch gas could be used to dissolve the iridium, but it would require extremely high temperatures to access both volatile compounds. The work published by Yeh et. al. showed that the iridium etch rate increased significantly when the substrate was heated in excess of 300°C. Unfortunately, I would not have access to an RIE tool that is capable of such high chuck temperatures. Additionally, there is a great deal of concern that the CTE mismatch of materials would lead to delamination of the iridium from the silicon substrate or the mask material from the iridium film. Eligible RIE recipe parameters were copied from Yeh's work and some initial tests were done to etch iridium. Room-temp RIE etch rates of iridium were collected for CF_4+O_2, CHF_3+O_2, and Argon recipes at 450W forward power. The Ar only recipe uses physical sputtering to etch the film, not a chemical reaction, and was added for comparison. Initial results showed that only the CF_4+O_2 chemistry etched the iridium at a measurable rate - roughly 9.3 A/min, before completely burning through the PMMA mask. Based on these initial results, it was obvious that a hard mask would be required to reach the etch depths required by the metasurface design. The work by Yeh et. al. also showed that aluminum has a very high selectivity in CF_4+O_2, and could be used as a hard mask if patterned with a chlorine-based etch chemistry. However, since the available options for increasing the etch rate of Ir are either very high ICP powers or very high substrate temperatures, it was deemed more reasonable to use argon ion beam etching (IBE) to sputter away the Ir. In fact, the higher etch rates for Ir found by Chung et. al. [4,5] correlate more with sputtering from ion bombardment than chemical reactivity from process gas concentrations.

For reasons previously explained, material choices for a proper selectivity of the hard mask were very limited. If using RIE in a purely chemical etch process, an aluminum mask would be the best choice. However, pure aluminum is very soft compared to iridium and would be a poor choice for a hard mask if using a physical technique to etch the film. An aluminum oxide (Al_2O_3) hard mask was deemed the optimal choice because it was one of very few materials with a physical etch selectivity greater than one and the aluminum content should act as a reaction buffer to increase the chemical selectivity as well. The required mask thickness was calculated based on the measured selectivity to physical etching and the Al_2O_3 film was deposited roughly 120nm thick. We would later discover that the hard mask selectivity in a chemical process was not as good as we had hoped. Evidence suggests it barely achieved a 1:1 selectivity ratio. This was not discovered until much later in the project and since more than a year was dedicated to process development of the Al_2O_3 mask, it was not advised to return to the beginning of the fab process to make all new samples with different hard mask materials.

The first e-beam PR mask material used was PMMA. After exposure, the developing process was refined by taking AFM scans of the surface. The features were very well defined but with a mask height of about 400nm, the 4:1 aspect ratio of the trench required more process development in order to verify the AFM scans' accuracy. High aspect ratio (HAR) tips with a 10:1 ratio were used and the scanning direction was 45 degrees relative to the trenches. The scan area was 256 points across a 2-micron line at 1Hz or less. This provided the best visibility to the structure with improved confidence in the intersections. Indications of a flat bottom with constant phase on the AFM scans suggest the mask is fully developed. There were some artifacts in the AFM data which

were unable to be removed. These artifacts made the pillar tops appear indented and the trench intersections lower than the rest of the trench, matched with the 45-degree scanning angle. In later processing, the PMMA failed to provide suitable etch selectivity to pattern the Al_2O_3 hard mask and was swapped out for ZEP520A. The first pattern used for etch rate testing was not the metasurface pattern; an array of simple squares at much larger sizes was used instead for easy characterization. When writing the metasurface pattern, a fully developed film has very small isolated pillars. These pillars will become loose and float away if the film is overdeveloped. There is also a risk of blasting them off completely if sprayed with too much force when using deionized water or solvents. It is recommended to use an HMDS coating before spinning the e-beam resist to help with pillar adhesion after developing. This was the same solution that was implemented when fabricating the MDL pattern rings.

The hard mask was patterned using ICP with 25sccm of BCl_3 gas at 2.0mTorr. The chuck temperature was 30°C, with DC power set to 100W and coil power of 1000W. In addition to AFM, cross-sectional SEM (X-SEM) was also used to characterize the pattern transfer from photomask to hard mask on test samples. However, it was discovered that ion milling used to prepare the samples for X-SEM imaging would introduce variations to the PR structure which would not be present on the real samples. Nonetheless, these images were very helpful in refining the process parameters for PR mask and hard mask processing. Figure 12 shows SEM and AFM data during

the process refinement of pattering the Al_2O_3 mask. Evidence of adhesion issues previously described can also been seen in Figure 12.

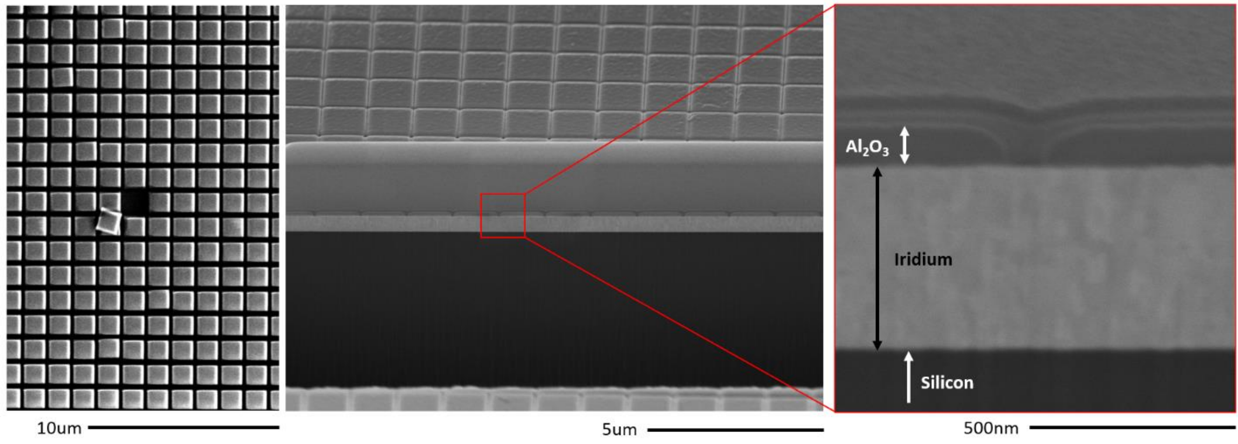

Figure 12. SEM images of metasurface patterns. A loose pillar in photoresist redeposited nearby (left) and the resulting pattern transfer after hard mask etch (center) with a zoom in of the etched away area (right).

Without the ability to use RIE at high substrate temperatures, it was determined that a physical sputtering technique would provide the highest etch rate for iridium and was the best place to start. Accessing the highest possible etch rate is important here as it reduces the overall processing time. The importance of reducing processing time and logic for this determination was the following: if the etch rate of Ir was 1nm/min in RIE, then the RIE process would need to run for 550 minutes (~10 hours) to hit the target etch depth. A plasma chamber would not be able to sustain this so the recipe would have to be broken up into two mins etching and five mins cooling, a time when the plasma is off and the sample temperature can return to normal; making the total recipe time over 32 hours. Toxic gas at CNS is only available between the hours of 7am and 10pm. To complete the pattern transfer, it would require booking the RIE tool for the three entire days. Even if the CNS administration would allow this, it is very impractical to attempt. The alternative tool to RIE which could allow much higher etching rates is the ion beam etcher (IBE). This is a sputtering

only technique that uses accelerated argon ions to etch material. A 400V acceleration Argon ion beam was used. The etch rates of the Ir and Al_2O_3 were measured at 30.46 nm/min and 4.58 nm/min respectively with a stage angle of 85 degrees. These rates were measured on simple films, containing no patterns. With these rates, the total amount of IBE cycles to hit the target etch depth should be 18. This is now a total processing time of just under two hours, far more reasonable to attempt.

The IBE recipe setting were: 18sccm of argon, 400V acceleration, chamber pressure at 10mTorr, chuck temperature of 20°C, stage angle of 85° relative to the beam, and cycles of 1 min etching, 5 min cooling. Initial etch rates suggested that about 18 cycles would reach the target etch depth but a dummy sample with the properly patterned mask was processed to refine this rate and hit the target depth precisely. When running this dummy sample for 15 cycles, a limitation was discovered which stems from the aspect ratio of the metasurface pattern. Back sputtering of the iridium alters the mask and a V-shape begins to form in the mask opening. Once the trench goes from a rectangular bottom to a closed V-shape, this is the maximum etch depth that can be achieved. This transition denotes the change from etching to physical vapor deposition (PVD). While in the PVD regime, continued processing only shallows and widens the V-shaped trench. This is caused by back sputtered atoms being redeposited along the edges of the opening. This redistribution of atoms no longer etches into the material but rather smooths the surface by filling in the patterned area. Figure 13 provides a schematic of this behavior. With a mask opening slightly under 100nm, a 550nm etch depth target is unachievable before the PVD regime takes over and the total etch depth will reverse. The etch depth after 15 cycles was measured to be only 178nm,

which correlates to an etch rate of only 12nm/min. The planar film etch rate of iridium was originally measured at 30nm/min indicating the opening is being backfilled with sputtered material during etch cycles.

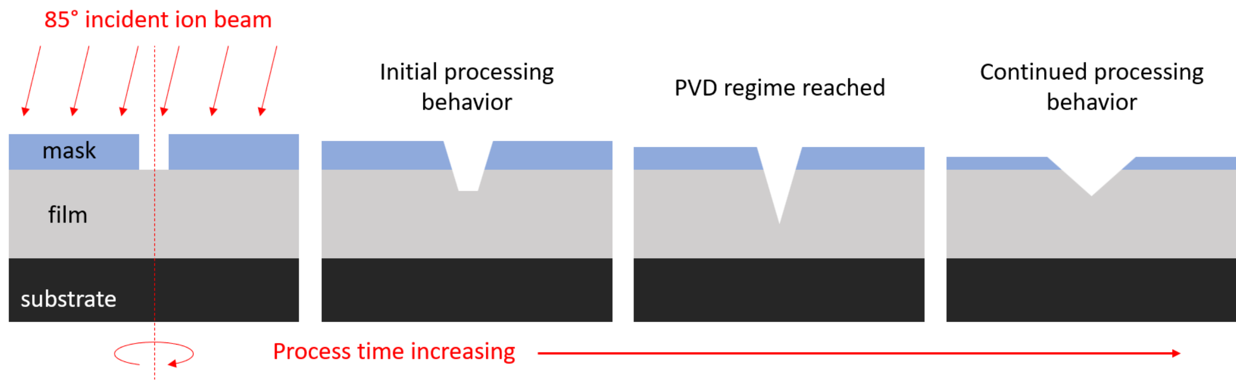

Figure 13. Cartoon depiction of the IBE process etching behavior versus time.

IBE proved to be a suitable method for processing iridium and a reasonable mask selectivity was discovered, however, our SE design was outside the range of achievable. After learning that IBE was not a suitable method to create our SE design, I explored other physical etching techniques. Focused Ion Beam (FIB) writing is the technique that is used to prepared X-SEM samples and it seemed FIB had the potential to directly scribe the trenched directly into the iridium film. The FIB source was gallium which has the potential for alloying with the iridium, though this was not observed. Initial calibrations showed that FIB could successfully cut trenches partially through the iridium film. The boundary conditions we found for the beam settings highlight two extremes, both of which were unfavorable for this process. At one end, we can increase the beam spot size so the pattern is written in a single pass with an acceleration and dwell time that cuts directly to the target depth. These patterns were dominated by back sputtering; the trench depth varied wildly and the sidewalls were not straight or even. At the other boundary, gentle beam

settings could cut clean, straight sidewalls but required several passes to make a single trench. With these beam settings, it would take several weeks of continuous writing to form a square pattern area of 0.25mm^2. For comparison, the write time for the e-beam lithography tool used was 75 minutes to write an area 25mm^2. This equates to writing 100x less patterned area in 300x more processing time. Figure 14 shows an X-SEM image of the IBE profile after 15 cycles of etching and an AFM scan of test trenches with the "fast cutting" beam settings.

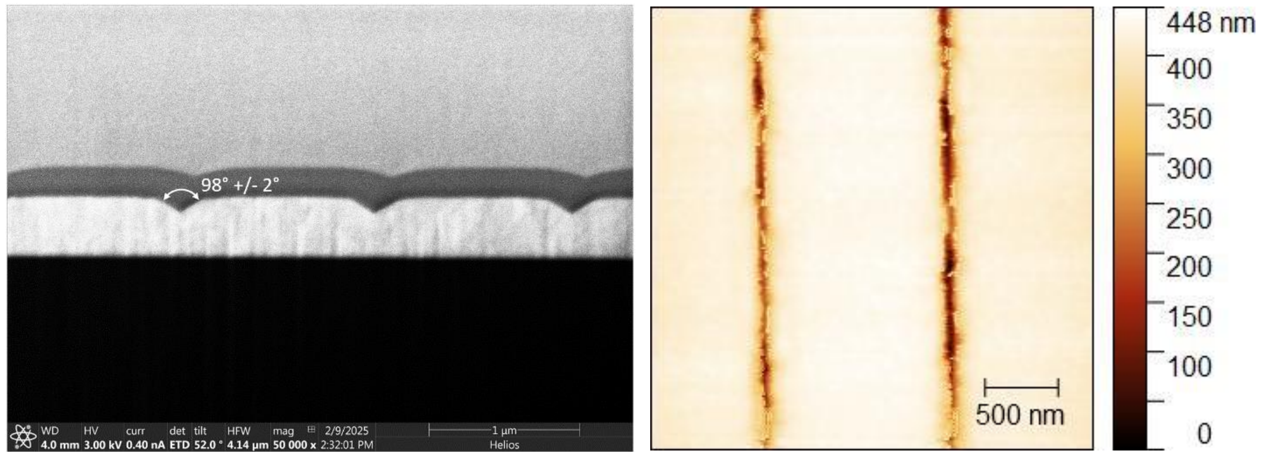

Figure 14. Cross-sectional SEM of the metasurface after IBE processing (left) and AFM data after FIB processing (right) using the "fast cutting" beam settings.

Returning to RIE with a CF_4+O_2 recipe, every available adjustment that could be made was explored to increase the etch rate. With an unknown selectivity, it was unclear if the hard mask thickness was appropriate to complete the SE processing. As we discovered, it was not even close. The reactive ion etching was performed in an Oxford PlasmaPro Cobra 300 chamber. The table in Figure 15 describes the recipes tested to determine which etch process would yield the best results. We were only permitted to increase the chuck temperature to a maximum of 80°C. This was shown to provide a minor enhancement to the etch rate. Increasing the coil power showed a reduction in etch rate as well as significant surface roughening. The most impactful enhancement to the etch

rate of iridium was the ion bombardment momentum. This agrees with our previous measurements that indicate physical etching provides faster etch rates than chemical. Using a combination of temperature and bombardment, an iridium etch rate above 50nm/min could be achieved. Select data from the table in Figure 15 is displayed in a bar chart to show the impact to etch rate of each recipe variant from the control recipe (first row).

RF Power (W)	Coil Power (W)	Temp (°C)	Cycles (etch/cool/loops)	Ir Etch Rate (nm/min)
100	1000	20	2 min / 5 min / 5	29
100	2500	20	2 min / 5 min / 5	18
100	1000	80	2 min / 5 min / 5	34
100	1000	80	30 sec / 1 min / 30	32
200	1000	20	2 min / 5 min / 5	47
200	2500	20	2 min / 5 min / 5	28

Figure 15. Bar graph of iridium etch rate by RIE recipe variant beside the associated recipe details.

RIE provided the highest overall etch rate for iridium, but it required both physical and chemical etching components working together. Finding a suitable mask selectivity for either one of these aspects independently had already proven a significant challenge. With all of these lessons learned, we believe there is still a potential for metasurfaces to be an effective technology for high temperature optical applications. Based on the limitations we measured for the processes explored in this work, an iridium SE could still be fabricated. It is likely that the design must change to accommodate smaller aspect ratios and less steep sidewall profiles. FIB could in fact yield viable SE metasurfaces for large areas if time was not a factor. However, the reality of bringing a technology to industry-scale applications cannot ignore the abuse of this critical resource. RIE processing showed the most promise of all the techniques attempted. Future attempts to follow-up on this research should investigate alternative hard mask materials for RIE etching. The etch rates

for iridium we found were certainly high enough to reach the target etch depth in a reasonable amount of processing time. The isotropic behavior at first appeared to be a concern but if the mask selectivity had been better, a reasonably steep sidewall angle could still be achieved. If the bombardment aspect of ICP etching is reduced, pure aluminum may be a reasonable choice for mask material. Additionally, aluminum nitride could also be used, but the best choice would be something that will not form any volatile compound with carbon, fluorine, or oxygen.

Alternative techniques for creating the metasurface that do not rely on removing material from a bulk film would also be worth investigation in future works. Achieving successful formation of such high aspect ratios with precise sidewall angles may require elaborate pattern transfer techniques. One such method we discussed would be to form an inverse structure, ridges rather than trenches, on a silicon substrate. Coating the ridges with a material that can be dissolved in wet chemistry would provide a mold to deposit the iridium, or any stubborn material, into. After planarizing the backside of the iridium and bonding it to a carrier wafer, one could transfer the metasurface from the mold and be left with the desired structure. In this scenario, the most difficult challenges to overcome in our work, isotropic etch conditions and sufficient mask selectivity, have been circumvented. Although we did not achieve our goal of fabricating a selective emitter for a TPV application, we have demonstrated several techniques which could produce nano-scale patterns into an iridium film. This is the basis for fabricating metasurfaces, and doing so in a refractory metal, such as iridium, enables the use of metasurfaces for high-temperature optical applications

Characterization Testbed for Selective Emitters

In preparation for a functional SE metasurface, a custom high-temperature emission spectroscopy setup was designed and built to directly measure the optical output of the sample. In order to accomplish this, a miniature furnace was fabricated to heat the sample via thermal radiation. The sample surface temperature was measured with a K-type thermocouple. The sample's emission spectrum would be measured at various temperatures. The detector's absorptivity as well as transmission losses for the collection optics would be eliminated from the data. These losses were determined by measuring a controlled high-temperature black body source and comparing to the theoretical black body spectral distribution for that temperature.

The design target for the furnace was slightly greater than 1000 degrees Celsius. Our thermocouples were only rated to 1000°C so our measurements were truncated at this point. This temperature presented a major problem for proximity to opto-mechanical stages, which would be damaged if not thermally isolated from the furnace. Using convection to heat the sample to the desired temperature would require an immense amount of engineering and deemed unreasonable to attempt. At these temperatures, the only solutions for convection involve liquid metals and that wasn't an option for our timeline and budget. Using thermal radiation to heat the sample to the desired temperature was chosen over conduction because contact resistance was expected to produce local hotspots and substrate warping which would be unwelcomed sources of error in the data. Metasurfaces are already notoriously sensitive to morphology changes so eliminating any opportunity for nonuniformity was a priority. When designing an optical system in the infrared, especially MWIR or LWIR, the options for highly transmissive materials become very limited.

This is further complicated by our testbed where the goal is to make a part of the testbed very, very hot. Lenses' behavior is dependent on the index of refraction of the material, which is both a function of the wavelength of incident light, as well as temperature of the glass. With IR suitable glasses, their index can be a strong function of these parameters resulting in alignment issues over wide temperature and spectroscopic ranges. To overcome this, reflective optics are used instead of refractive. An off-axis parabolic mirror (OAP) is a mirror that both reflects and focuses incident light, eliminating the need for a lens. The OAP does not suffer focal length shifts due to changes in temperature or wavelength, at least at a measurable scale, which makes it the perfect choice of optical element for this testbed. The OAP being used has a reflective face of gold protected by a thin dielectric layer. This layer does reduce the effectiveness of the mirror, but the protection of the surface in close proximity to a direct heat source far outweighs the performance losses. The most severe loss is around eight-micron in wavelength where the reflectance drops just below 70% for neutrally polarized light.

The mirror's reflectance, detector's absorptivity, and transmission losses from the monochromator used for spectral selection all combine to make an imperfect transfer function for our light collection capability of the testbed. To quantify this transfer function, this same optical configuration is used to measure a known optical source in the wavelength range of interest. The calibration source used is a high-temperature black body. This black body chamber is engineered such that it has an emissivity very close to one at all wavelengths. Though this is theoretically possible, it is physically impossible to create such a source. For our wavelength range of interest, we will assume the device operates as theory suggests. By measuring the emission spectrum of a

black body with our testbed equipment, we can compare the normalized response curve to the theoretical curve and deduce the transfer function of our collection optics. This information allows us to deconvolve the selective emitter's measured output so we can understand the sample's emissivity independently.

The furnace is heated by a resistive wire coil which alternating current passes through. The AC power is transformed with two variacs in series from the mains supply (110V) to single volts. Reducing the voltage with a variac increases the current by the same ratio. This high current flowing through a wire with high resistivity leads to significant energy losses in the circuit. The loss is due to ohmic heating, which we exploit to heat our sample. Because the sample is both being heated by radiation, and is also emitting radiation that we aim to measure, the sample shape must be carefully processed to provide consistent measurements. The SE metasurfaces were fabricated as 5mm-by-5mm square areas in the center of each quadrant of a 4-inch silicon wafer. After fabrication is completed, the wafer is cleaved into quarters, with a SE in the center. From there, a stencil is used to map out a 40mm-wide octagon around the SE, using the cleaved edges as a reference. The octagon is cut out of the quarter wafer using a dicing saw. This octagon is then placed over the opening of the furnace, which is roughly a circle just under 40mm in diameter. Several corners of the sample are in contact with the furnace opening edge when aligned to the opening. This prevents the sample from falling into the furnace while simultaneously reducing the area for conductive heat transfer. This shape also keeps the temperature distribution more uniform across the sample as it is more radially symmetric around the SE and radiating input source. The coil temperature was directly measured to calibrate safe operating voltages for the wire coil. Test

samples were then measured in two locations simultaneously while being heated – the center and one edge of the octagon. This allowed us to map a trendline for sample temperature relative to coil temperature. When a SE sample is being measured optically, a thermocouple cannot be placed directly on the surface to confirm its temperature. There is however, significant space on the perimeter to place the thermocouple during this optical measurement. The outer edge of the sample's temperature will be measured during optical collections and the statistics gathered on dummy samples will be used to estimate the actual SE temperature in the center of the sample.

Monolithically Integrated Photodetector

Microlens Characterization

Avalanche photodiode (APD) detectors are an emerging technology that offer single-photon-sensitive light collection and superior timing resolution to other camera technologies, as fast as several nanoseconds. MIT Lincoln Laboratory has been developing this technology for nearly two decades and have seen their components being implemented in laser communication and lidar systems at the highest level. Literally, there is one in space, beyond Mars's orbit on its way to the asteroid Psyche at the time this was written. So, like any good team of engineers, we looked at this completely functional component and said, "how can we fix it?". Perhaps we cannot make them better, but can we produce them faster? At the core of the APD detector is the focal plane, which consists of the semiconductor diode array and a microlens array (MLA) which focuses light into the tiny pixels. One leading concept for accelerating the timeline of APD production is to fabricate the entire focal plane monolithically on a single substrate. This means the photodiode would be fabricated on one side and the MLA fabricated on the opposite side of the same substrate. A multi-layer diffractive lens (MDL) array was selected for the lens design due to the simplicity of the fabrication processes required to produce it. A MDL is simply a digitized version of a Fresnel lens. The Fresnel lens design takes a curved surface and divides it into equal thickness of curvature which produce a 2-pi shift in phase of the incident wave. The sections of material below each curve, which are uniform blocks of the same material, do not contribute (or all contribute equally) to the phase profile of the lens so they can be removed. Removing the sections which do not contribute to phase changes results in an overall flat lens with a sawtooth

like structure. The slope of these teeth are exact copies of the corresponding curvature from the original, however, they can be approximated into layers that follow the same curve. A single layer would produce a binary lens element, this specific design is called a Fresnel zone plate, but when additional layers are used to better resolve the curvature of each tooth, it is referred to as a multi-layer diffractive lens. As more layers are added, the performance of the lens will increase, approaching the limit of the Fresnel design. However, producing additional steps also complicates the fabrication process and creates opportunity for errors in layer height or pattern alignment, which would significantly decrease performance. The number of layers that can be produced equals two raised to the power of the amount of process steps. It was determined that four process steps, resulting in sixteen layers, was the appropriate balance between simplicity and performance. Being able to produce MDL arrays monolithically integrated onto a substrate containing APDs provides a significant improvement to the timeline of the current technique which has the photodetector and MLA fabricated on independent substrates, diced into chips, and hybridized one-at-a-time. With this technique, the lens pixel to photodiode alignment is defined lithographically, which is an improvement in accuracy compared to current techniques, and the wafer of arrays are completed several months, even years, before the equivalent amount of chips could be assembled individually. Even though the timeline is vastly improved, there still remains the concern of performance decreases with this MDL design compared to the currently optimized MLA design. Balancing the "quantity vs quality" equation requires the researcher to know not only the end performance of the assembled focal planes, but the level of effort required to reach any number of performance goals throughout the fabrication process for each independent component.

Before describing the fabrication process and results of the monolithic photodetector, it is necessary to investigate the challenges of this effort related to characterizing the MDL and other microlens technologies it was compared to. Micro-anything topology is typically characterized using various profilometry techniques. When one is trying to characterize a micro-optical component, it is sometimes sufficient to simply import this measured surface into an optical modelling software and simulate the results the surface would produce in terms of bending light; refractive optics especially. However, there are still features on the nanoscale generated by the fabrication process that impact the component's optical performance which could not be captured by this simulation process. For diffractive optics, this issue is magnified because they rely on sub-wavelength features to produce exact phase changes, leading to a global interference across the optic. A superior method for comparing various microlens technologies would be to directly image the beam they form and characterize each component under the same beam conditions. In order to investigate new designs and compare different types of microlens technologies on a fair and consistent basis, a custom microscope was built. This microscope was designed to image the MLA surface as well as its focused beam which required solutions to the following challenges: 6-axis manipulation of the sample, sub-micron positional resolution, perpendicular travel to the optical axis, brightfield imaging, multispectral imaging, image processing, uniform irradiance over the sample area, and calibrated absolute optical power measurements. This microscope design enables the back focal length range of the sample to be mapped with sub-micron accuracy along the paraxial ray. The imaged beam spot is quantitatively analyzed in MATLAB for $1/e^2$ diameter and encircled energy, as well as qualitatively with complementary data sets. It was shown that MDL

and plano-convex refractive MLA designs made from various materials could be compared equally in a side-by-side comparison.

The microscope was designed as a series of optics and mechanical stages mounted with 60mm cage construction to a single optical rail which stands vertical from the table. Commercial-off-the-shelf (COTS) parts were used for the entire build with the exception of the mounting surfaces for MLA/MDL samples, which were fabricated in-house. The design implements a standard brightfield illumination optical pathway to image the sample surface with white light. The brightfield path consists of an LED, optional diffuser, condenser lens, iris, collimating lens, fold mirror, and beam splitter plate. The beam splitter lies in the collimated space between a microscope objective and 200mm focal length tube lens. The microscope objective is on a turret to allow various magnifications and an open position for optical path alignment. The tube lens focuses to a monochromatic CMOS camera. The camera format was chosen such that the FOV at 50x was greater than 100 microns and had greater than 20 pixels per micron resolution. The camera must respond to visible light, as well as the laser wavelength being focused by the sample, in this case 1064nm. An NIR enhanced silicon CMOS detector was selected over an InGaAs SWIR detector for cost considerations.

The MLA/MDL sample is placed on the top of a 6-axis positioner (hexapod) with a clear aperture below the sample. The base of the positioner is mounted to an XYR (in-plane linear with rotation) stage. Below the XYR stage are a series of optics connected by one-inch tubes from a mirror mount which provides tip/tilt control. A laser coupled through an optical fiber enters through the back of the mirror mount. The optical elements after the fiber are a collimator,

expander, several ND filters, and a pinhole aperture. These optics allow the laser to be considered as having uniform intensity across a known beam area so that an absolute power series could be calibrated for the beam. Figure 16 shows a SolidWorks assembly of the optical components and cartoon diagram of the optical elements.

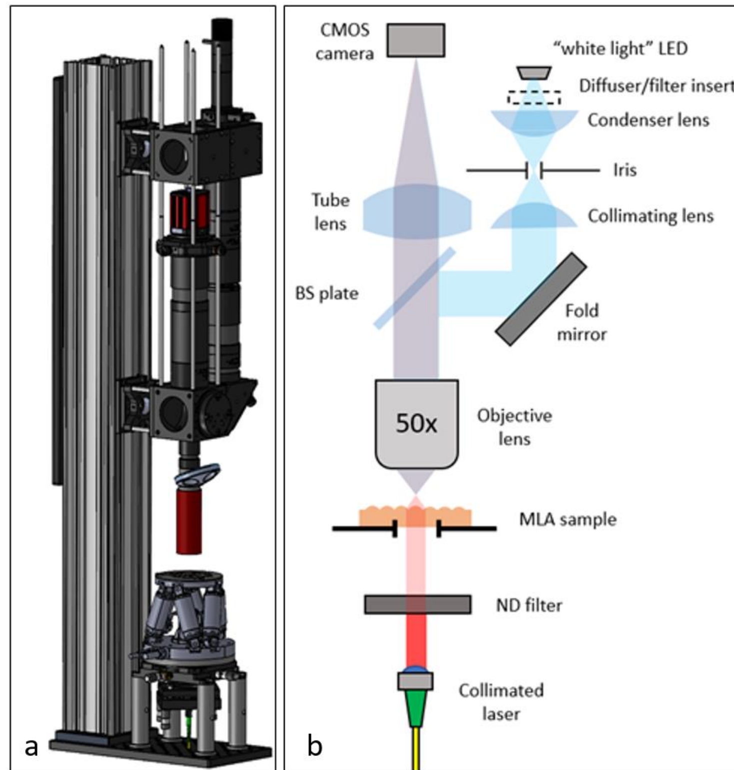

Figure 16. CAD rendering (left) and cartoon (right) for the assembly of the optical elements within the custom microscope.

Regarding the alignment of the microscope components and how each sample is aligned to this system, the following description is provided. The laser is expanded and collimated to infinity in a preconfigured sub-assembly before mounting to the base stage. The laser is pointed up through the clear aperture of the sample stage and into the microscope so that the laser beam is directly imaged. With no sample or microscope objective present in the optical path, the beam strikes the tube lens and a focused spot is formed on the camera. The tip/tilt of the beam is adjusted and

rotated until the beam does not move on the camera with rotation. This denotes the parallel path to the paraxial ray a.k.a. “gut-ray” of the optical system. The camera is then adjusted in XY to center the beam in its FOV. The system relies on a fixed plane that the optical column stands perpendicular to. From this plane, the laser stage is mounted below, free to move in five axes (no Z motion), and the sample is mounted above, free to move is six axes. The laser that passes through MLA/MDL samples is aligned to the system optical path and held constant, independent of the sample’s presence or stage’s position.

With the sample in place, two alignment techniques are used to normalize the sample stage to the system’s optical axis using brightfield illumination. The first involves using a white-light Michelson interferometer objective to image the sample surface. Once the fringe pattern generated is null, the sample is normalized. A cruder, but effective, method is to use a high magnification objective with a very short depth of focus and track the sample in/out of focus over a long lateral traverse. Our 50x objective has a depth of focus of one micron. The hexapod has a maximum XY linear motion of 32mm. Using trigonometry, the offset angle can be determined to keep a 1-micron depth of focus on the sample surface over more than 10mm of linear travel in X and Y independently. This is equivalent to achieving better than 100-microradian planarity in tip and tilt. Once aligned, the sample can be moved to any position on its aligned plane and the sample lens pixel that lies over the pre-aligned laser is imaged. The in-plane travel available from the hexapod covers greater than a one-inch diameter of the sample. The sample is then adjusted in the Z-axis to have the full range of its focused beam move through the image plane. These 100nm precise adjustments enable BFL measurements to be made while simultaneously analyzing beam images

for energy density metrics. The center of rotation of the sample stage, a.k.a. “pivot point”, can be carefully set to tip and tilt the sample lens without moving from the image plane for angle of incidence beam characterization. Figure 17 provides an example of the operator’s view during the sample alignment process with descriptive text for the steps of the data collection process.

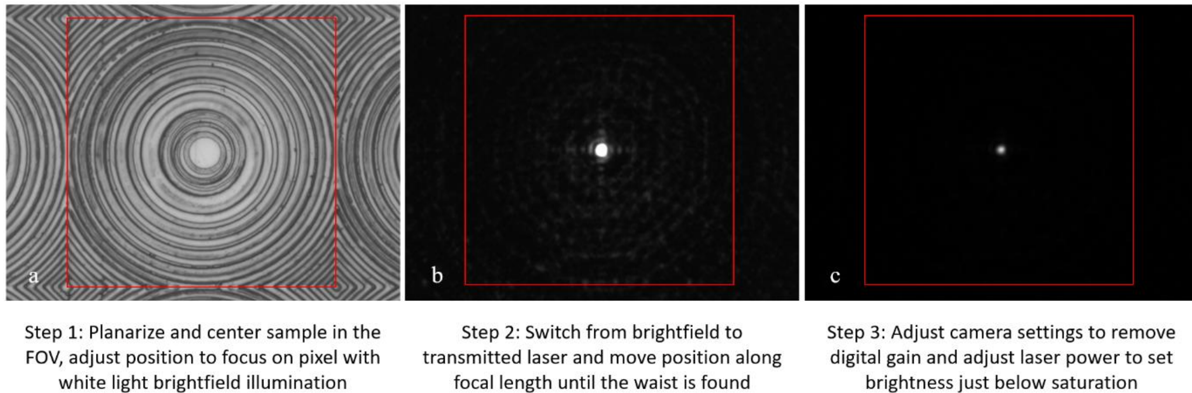

Figure 17. Data collection steps with written details for custom microscope operation.

Using the camera viewing software provided by the manufacturer, the gain settings of the detector can be adjusted to see the defocused laser beam more easily. This can be observed in Figure 17b where the unintended diffractive pattern from fabrication imperfections can be seen around the main spot, but disappear in Figure 17c once the main spot’s brightness is brought below the saturation limit of the detector. It is important to keep gain settings equivalent when making comparisons between two MLA designs. If more or less light is required to produce a bright and unsaturated image, the laser power should be adjusted with no, or at least consistent, camera gain settings. A calibrated laser power series was performed for the beam so direct comparisons between MLA designs can still be made when focusing power varies greatly. Intensity of the laser light is read out as an 8-bit value for each pixel in the image which are saved as TIFF or JPG formats. Image analysis is performed in MATLAB and begins with finding the centroid of the

beam spot. Once the single detector pixel, or pixel intersection, of the image representing the centroid is identified, integrating intensity provides an encircled/ensquared energy calculation. Then, the “gauss2” fit algorithm from MATLAB was utilized to determine beam parameters. An example data set from a commercial-off-the-shelf (COTS) MLA is shown below in Figure 18 which was used to compare various MLA designs with the MDL that was fabricated.

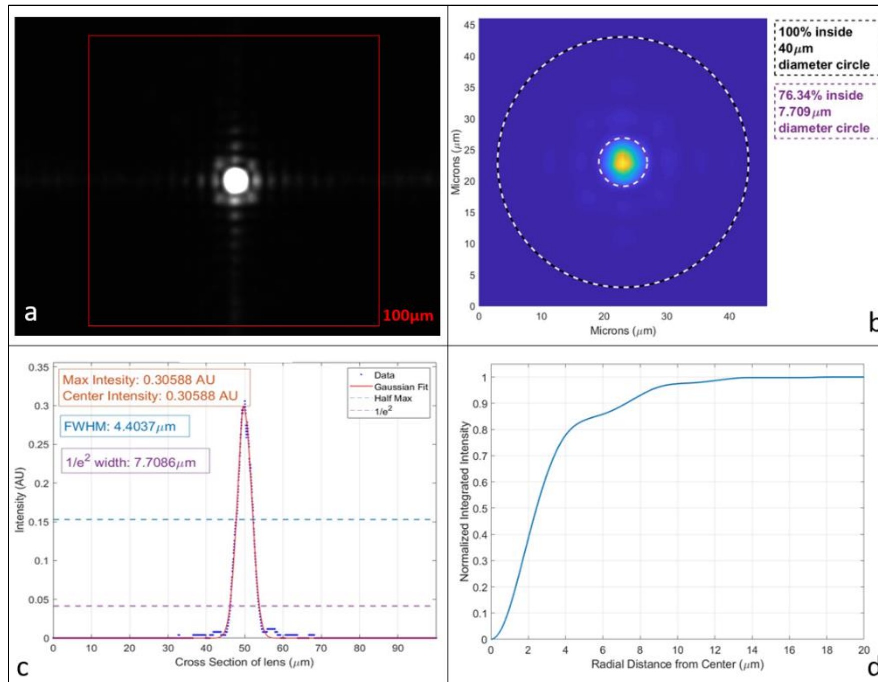

Figure 18. Microlens characterization data sets generated from images collected with the custom microscope. A saturated image of the focused infrared light (a) beside a colormap of an unsaturated copy (b). A horizontal data slice through the peak intensity (c) beside the measured encircled energy curve (d).

These foci images can be qualitatively analyzed when paired with complimentary data sets, such as optical profilometry height maps, to better inform the designer of the realistic non-idealities of the lens after fabrication. Optical models can then be updated with more accurate data to make better predictions when implementing the detector into a camera or a larger optical system. Figure 19 provides an example of a complimentary data set where each 100-micron square pitch sample

is compared side-by-side. In particular, the residual surface of Sample B shows some striping from the lithographic writing process, seen in Figure 19-ii, which suggests a cause for the dominant bright vertical lines on the focus image, Figure 19-iii. These bright lines are very likely diffractive patterns created from the superimposed stripes on the lens's curvature. In a proprietary data set, it was also observed that more severe striping in the residual surface coincided with focal spots that had large astigmatism.

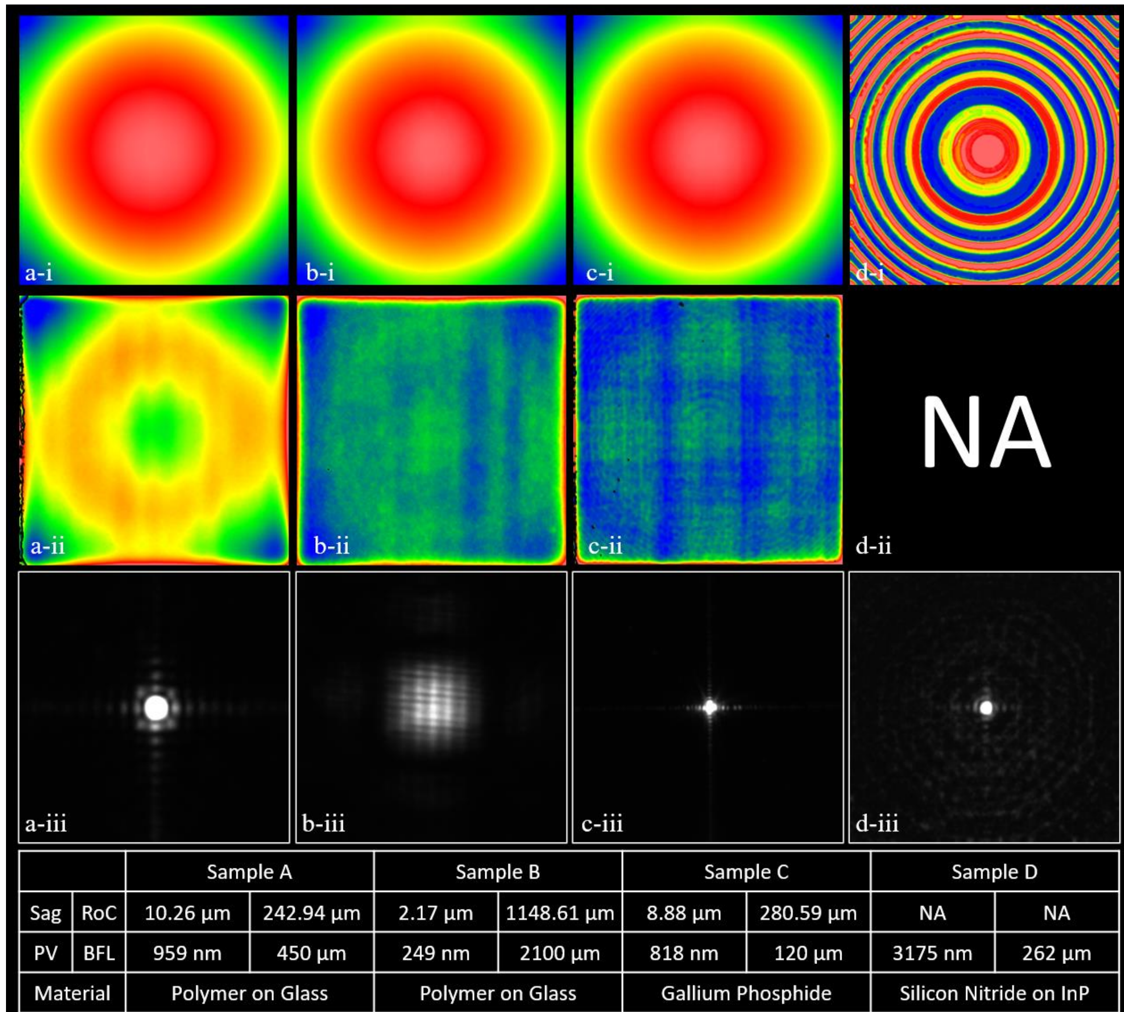

		Sample A		Sample B		Sample C		Sample D	
Sag	RoC	10.26 µm	242.94 µm	2.17 µm	1148.61 µm	8.88 µm	280.59 µm	NA	NA
PV	BFL	959 nm	450 µm	249 nm	2100 µm	818 nm	120 µm	3175 nm	262 µm
Material		Polymer on Glass		Polymer on Glass		Gallium Phosphide		Silicon Nitride on InP	

Figure 19. A qualitative comparison of 100-micron square-pitch microlens arrays. The 3D profile (row 1) with the best-fit spherical surface removed (row 2) beside their respective foci (row 3) and optical prescriptions (table).

Multilayer Diffractive Lens Fabrication

The MDL fabrication was performed as a lens-only fabrication before it would be attempted on substrates that contained high-value APD arrays. The mask layers to form the MDL appear as rings of decreasing width at further radii from the center of the lens pixel. On the first etch mask, these are the smallest of the features in the design and those at the edges were deleted because they fall below the resolution of the lithography tool used to write them (Heidelberg MLA-150). It was known that this would negatively impact the lens performance, but the simulation to know exactly how much impact it would have, was not performed. An attempt was made to simulate the performance of an as-fabricated MDL using Lumerical FDTD. However, each iteration of the simulation required more than 10 hours running on the MIT supercomputing cluster so thorough investigations were not performed. The impact of removing these small features and any defects which occurred during fab in layer height, ring alignment, or nonuniformity would be lumped together in the final performance analysis metric. These first MDL lenses were used to qualify the lens characterization microscope and data from this fab run is shown in Figure 17 and Figure 19 above. The mask also contained a variation in focal length across each column of the array for the MDL design. This provided us the ability to observe the impact of defocus in the diffractive lens on the active area of the APD, and also informed the accuracy of the calculations used to determine the overall focal length for the monolithic design. Figure 20 highlights the process steps of how the four mask layers are stacked to produce 16 steps along the curve. It can also be seen in the figure that the rings of layer 1 stop before reaching the edge of the lens pixel, which were below the minimum feature size of the lithography tool. This impacts the outer lens

curves by resolving only half as many steps, and not reaching the correct final depth at the base of the curve, evident in the proceeding layers.

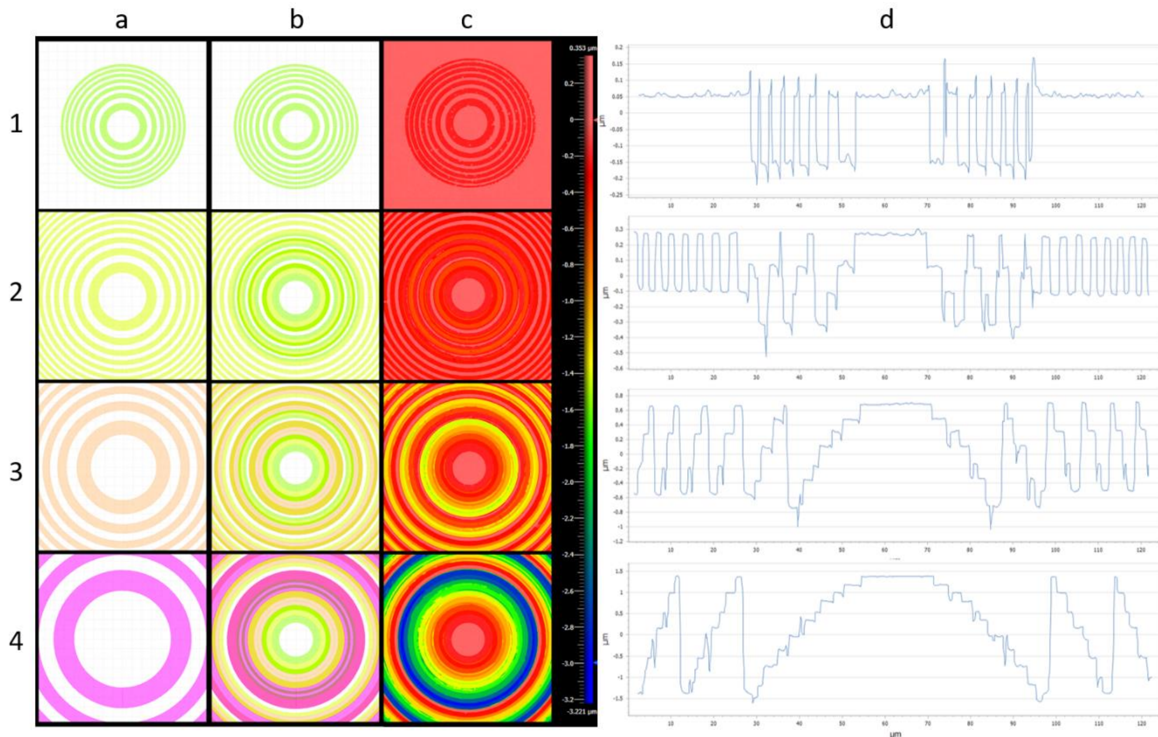

Figure 20. Four lithography steps (rows) where GDS patterns (column a) combine (column b) to produce the MDL structure. The 3D profile (column c) is measured after each process step with a diagonal slice shown (column d).

As indicated in Figure 19, the MDL material was silicon nitride (Si_3N_4) deposited onto the indium phosphide (InP) substrate. The Si_3N_4 material was deposited thicker than the minimum required height feature of the MDL design. Material was removed with RIE to form the lens pattern and since not all the material was removed, there remained a thick layer of Si_3N_4 between arrays on the wafer surface. Early trials of this MDL were fabricated on blank substrates (no APDs) and diced into chips to be characterized. After dicing, many of the arrays had chipped and delaminated from the InP. It was then determined that the remaining areas of Si_3N_4 which covered the wafer but did not contribute to the lens, must be removed before dicing. Two approaches were conceived to remove the unnecessary material: add the additional feature to each layer of the existing mask

set so that the material is removed during each process step of forming the lens, or create a new layer which only contains the dicing areas and add additional RIE steps to remove these areas of material after the lenses are fully formed. It was determined that the latter involved more risk to the wafer and the former would provide additional areas outside the lens array to be used for process tracking metrology, which would be beneficial. Ultimately, both were performed to ensure all of the Si_3N_4 would be removed between the arrays.

Two approaches were also considered for the overall fabrication of the monolithic device, APD-first or MDL-first. The ideal situation would be a hybrid process where selected processing steps would be completed on either side of the substrate as appropriate. However, the funding and timeline for this effort could not produce APD wafers from scratch. The only components available were wafers which already had the APDs completed or a wafer from MBE growth which could have the APDs fabricated in the future. Both types of samples were processed in parallel. The first step in the process would be metal lift-off to produce alignment marks for the future MDL fabrication steps. The APD-first sample required a front-to-back alignment such that the MDL arrays would be properly aligned to the APD arrays. This alignment was unnecessary for the MDL-first sample so the pattern was centered to the wafer. The metal stack up was an existing recipe used for APD processing which consisted of Ti, Au, Pt, and Au again deposited via sputtering. The lithography steps to produce the overhang necessary for a successful lift-off used a YES oven and flood exposure as previously described. Lift-off was very successful on both samples and images were collected with a Keyence VHX3000 microscope. It was at this point; processing difficulties began and became a dominate theme throughout the duration of the fab.

While cleaning the APD-first sample, it rolled free from the Teflon wand and fell. The wafer dropped to the padded wipe directly below on the bench surface from a height of no more than two inches; but still the InP substrate broke into three segments from this minor bobble. The three segments were still connected by the passivation layer on the APD side. It was possible to keep the wafer together by resting it on a carrier for the next process step, Si_3N_4 deposition. It was determined that the segments should be intentionally separated before continued processing. The Si_3N_4 deposition was done with PECVD and both samples, as well as a few dummy samples, were coated together in a single 7-hour run. A run this long resulting in a coating as thick as we needed posed a great potential to damage the wafer due to stress in the film. Several recipes were trialed by the PECVD tool owner to come up with a low-stress film. Because the layers tested were of typical thickness, around 200nm, the rate was not defined well enough to produce an exact target for the MDL height. The 7-hour run erred on the side of "thicker is safer" but the final thickness would be unknown. It was thought that there was a potential of the Si_3N_4 layer keeping the segmented wafer connected, since the crack was not even visible to the naked eye once flattened. Alas, it was not to be and the segments remained separate. One benefit though was that there were no edge effects observed in the film thickness from the crack, only the wafer perimeter showed signs of edge effect in the film. The final Si_3N_4 film thickness was determined by spectroscopic ellipsometry. Although the fitting accuracy of the ellipsometry model was not as high as would be considered standard practice, there was a very high confidence that the film was thicker than the minimum height needed so the fab proceeded without needing to know the precise film thickness. The segments were wax mounted onto two-inch sapphire carrier wafers. The dummy wafer for

this sample was intentionally cleaved and mounted to match. The MDL-first sample and its dummy remained unmounted.

The next steps of the fabrication would be lithography and etching the Si_3N_4. This series of steps (lithography and RIE) would be repeated 4 times with the only changes being the line width and quantity of the rings, as well as the target etch depth. The first of these steps would prove to be the most difficult as it contained the smallest features. Features were deleted if they fell below the tool resolution, yet those remaining which are very close to this limit do not have a high yield. Additionally, these tiny rings of photoresist had adhesion issues and were floating off during the develop process. The MDL-first sample had these same difficulties, yet not nearly to the level of the mounted segments. Through many experiments, it was discovered that the baking of photoresist on a hotplate was the root cause for the difference in behavior. The mounted samples do not transfer heat well enough from the hotplate to the photoresist and the mounted samples would be oven baked for the remainder of fabrication. Due to the awkward shape of the segments, the resist also had uneven thickness from the spin coater which impacted many of the arrays. Yield losses were deemed unavoidable on the segments and the process continued. After two RIE steps, the MDL-first sample looked great but it was questionable if the APD-first segments would performance as expected. During post-develop inspection on the third round of lithography, the MDL-first wafer was fumbled from the edge of the microscope and dropped to the floor, shattering into countless pieces. It was at this point I deeply contemplated all of the choices I've made in my life and started searching for 10-story buildings with roof access.

There was not enough time left in the funding period to begin another the MDL-first sample from the beginning so that half of the experiment was lost. I eventually recovered from my despair and continued on with the APD-first segments. The final rounds of lithography and RIE went similar to the previous ones for the segments. At the end of each round, once the sample has been cleaned of any residual resist, the step height was measured and tracked for areas which received multiple rounds of etching. At first, this was being performed with stylus profilometry, however, the stylus struggled to resolve each step on the way up/down for multiple layers and optical profilometry proved to be much more useful and accurate. Once the MDL fabrication had been completed, the segments were removed from the carriers and the APDs were I-V tested to see if they had survived the MDL fabrication. It turned out that the APDs were overall unaffected by the processing steps, with the exception of those near the broken area which were deemed lost from the beginning. Thankfully, there were many focal length variations and even though yields were expected to be low, there still exists many arrays with a successful MDL fab. Figure 21 shows a set of three completed MDLs from three different arrays, each with significantly different focal lengths.

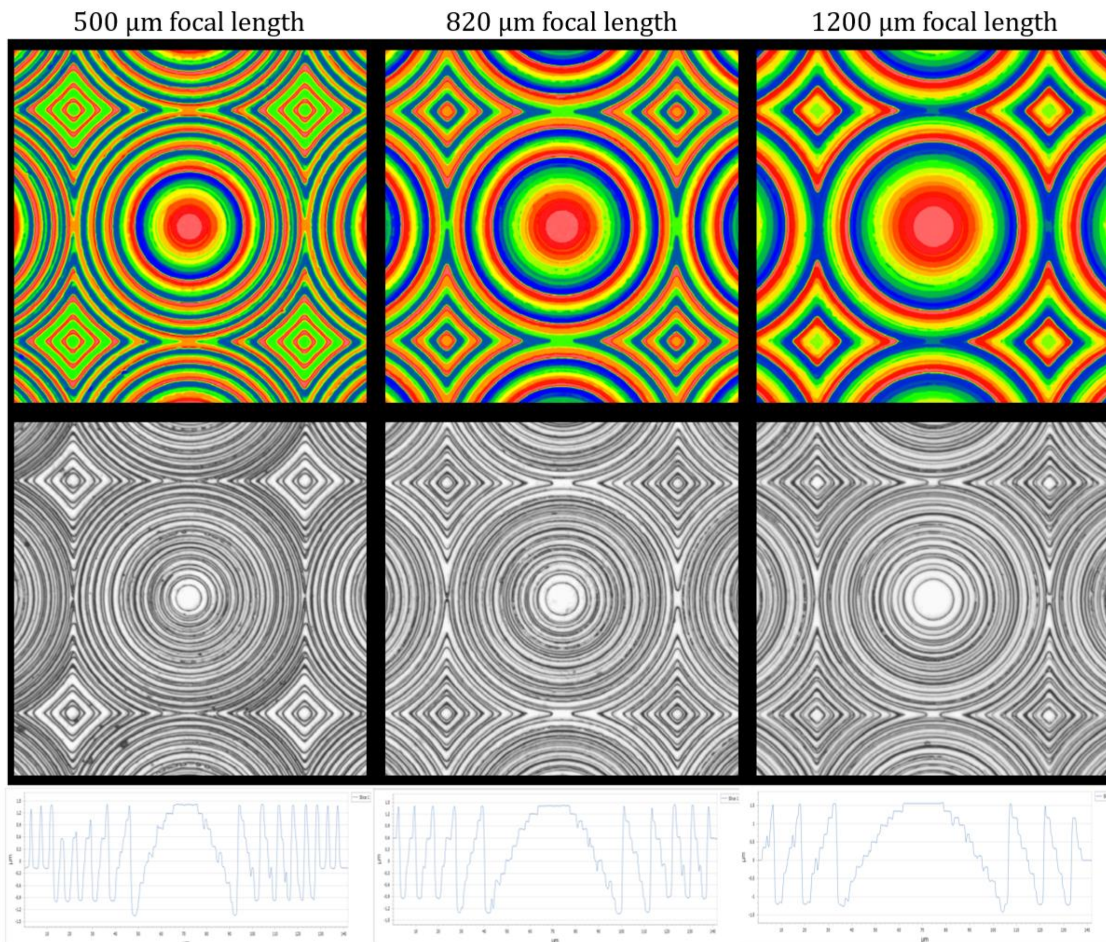

Figure 21. 3D profile scans (top row) with diagonal data slice (bottom row) and microscope images (middle row) of fabricated MDL arrays with varying focal length (columns).

We recognized that there were several areas of improvement to increase the MDL performance, but it was still valuable to understand what level of performance can be achieved with a “quick and dirty” fabrication. The areas for improvement which we believe would have the most impact are: use EBL to write all the features of the first layer so that none are lost, smoothing the steps into a curve by either thermal mass transport or grey-scale lithography, and establishing a more precise etch recipe/technique to hit the profile with high accuracy. These changes could provide improvement to a diffractive lens design, but performance could also be enhanced by attempting to fabricate a monolithic refractive lens as well.

Conclusions

Optoelectronic technology development is complex and can be a mentally and emotionally trying ordeal. Its multidisciplinary nature often means that projects require more steps, bigger teams, and longer timelines than sister technologies. Sadly, these projects rarely receive larger budgets to match these requirements. The consequence of this means that researchers, like myself, have to fill multiple roles within a team which in-turn makes us adaptable, innovative, and clever. I've previously said that the most valuable part of my education in physics was the training to learn something entirely new, and become proficient at it quickly. Without this training, the pursuit of my Ph.D. would have been arduous to say the least.

Exploring new concepts in technology development requires equal parts science and engineering. The projects I worked on during my Ph.D. research were never going to win a Nobel prize, or change the world overnight. However, they are still an important step towards innovation and scientific advancement. Learning what did not work is just as valuable as learning what did, provided it was well documented. This was the case for the iridium metasurface project. Of course, there were many potential design or fabrication paths that were not explored during that project. But the knowledge gained about why, when, or how that path led to failure can be immensely valuable when choosing the next path. Although a rare occasion, sometimes the cause of failure itself is a major discovery that can lead to many more innovations. Another note about innovation is that there is always room for improvement. In the case of the monolithic photodetector project, our goal was not to create a higher performance detector package. We knew that we were fundamentally producing a photodetector that would not quite reach the optimized performance

metrics of its predecessor. However, by producing detectors with a technique favorable to scalability, we could produce them orders of magnitude faster, which also means cheaper. This is still an improvement to the technology for many vested parties, even if it required trading away some device performance.

It is generally the case that knowledge is the more valuable result from research projects, not the devices being worked on. I find this to be true for all the projects I've been involved in, beyond the three highlighted here. There is, however, a tangible value left behind from these projects other than knowledge which is provided by the characterization aspect of these projects. The tangible items that remain from the iridium selective emitter metasurface and monolithically integrated photodetector projects are characterization testbeds. These testbeds will continue to provide value to future researchers that either continue on with these research efforts or endeavor new ones. The MLA beam characterizing microscope has already been a critical component to two different research efforts since the monolithic photodetector project performance period ended. The HiTemps testbed also provides this capability for future research at REAP Labs. These testbeds provide long-lasting value because they make exquisite use of the most valuable resource there is in research, which is time. The time spent to design, build, and qualify these tools was an expended resource on my research projects so that it does not need to be spent by anyone else. The value of these tools comes from the characterization data they provide but it is compounded by the time they save all future researchers who use them. I have a similar sentiment for the JSON file architecture that comes out of the TPV Design Toolbox, even though it is not technically tangible. My hope is that the value of these tools or testbeds does not go overlooked.

These three projects might appear to be disjointed from one another, which to some degree is true. The projects had different objectives, different determinants for success, and different audiences. However, these projects show how optoelectronic technology development is multifaceted and that individuals must contribute to many of these facets within the same project or across several projects simultaneously. The other commonality amongst these projects is that they are only a part of the whole. TPV technology requires much more than simulation or custom selective emitters, just as photodetector technology requires more than just the sensor array. To realize any of these technologies as useful products, teams of people collaborating across many disciplines are required. My accomplishments were not achieved through individual effort alone, but rather by leaning on the expertise of those around me for guidance. Utilizing everyone's strengths through teamwork and collaboration is the key ingredient to successful technology development.

Future Work

Future work stemming from the TPV Visualizer program should prioritize using the tool to produce meta-analyses of various TPV publications and new concepts. Analyses can be performed which examine previously published TPV systems or cells and how well they performed relative to their calculated peak efficiency. Other analyses include examining how various semiconductors with similar or overlapping bandgaps perform in head-to-head comparisons for various applications. Building a comprehensive data base for material JSON files can be easily completed. In addition to using the tool, upgrades to the code should be considered. Code modifications which increase the user's design freedom of the TPV system would be welcomed. A more complicated, but worthwhile effort, would include code modifications to analyze multijunction cells.

For the iridium metasurface project, future work can take many forms. One could redesign the SE, or another type of optical metasurface, and *successfully* fabricate it with the processing knowledge already learned. Utilizing the HiTemps testbed to collect data on the fabricated device would lead to an assured publication of significant impact. Alternatively, one could continue to explore alternative fabrication techniques for the current SE design, moving away from etching. There are many other materials that could be explored for use as a hard mask which may yield more favorable results. Also worth researching, would be to perform the same experiments but with all other available refractory metals. The fabrication challenges faced when using iridium may be very different for other metals, such as rhenium or tungsten.

There were several follow-on efforts planned for the monolithically integrated photodetector. First, intensive modelling should be done to understand the impact from all variety of fabrication imperfections. These include misaligned layers from lithography, off target etch depths, minimum feature size inclusion/exclusion, and others. In addition to better understanding what was previously made, looking to what could be made next was discussed. Moving to a metasurface lens was the next major step planned. This metasurface could provide additional capabilities such as polarization selection or wavelength filtering. This fabrication effort should also be preceded by a thorough modelling effort.

Appendices

List of Acronyms

AC	Alternative current
ACV	Alternating current voltage
AFM	Atomic force microscopy
APD	Avalanche photodiode
BFL	Back focal length
CMOS	Complementary metal-oxide semiconductor
CNS	Center for Nanoscale Systems (at Harvard University)
COTS	Commercial off-the-shelf
COVID-19	Coronavirus Disease, 2019 strand
CVD	Chemical vapor deposition
DC	Direct current
ECE	Electrical and Computer Engineering
FDTD	Finite-difference time-domain
FIB	Focused ion beam
FOV	Field of view
GDS	Graphic Data System (a file format)
HiTemps	High Temperature Emission Spectroscopy (a REAP Labs testbed)
HMDS	hexamethyldisilazane
IBE	Ion beam etching
ICP	Inductively coupled plasma
IR	Infrared
JPG	Joint Photographic Experts Group (a file format)
JSON	JavaScript Object Notation (a file format)
LED	Light emitting diode
LWIR	Long-wave infrared

MBE	Molecular beam epitaxy
MDL	Multilayer diffractive lens
MITLL	Massachusetts Institute of Technology Lincoln Laboratory
MLA	Microlens array
MOCVD	Metal-oxide chemical vapor deposition
MORTI	Mobile Optics Room Testing Instrumentation (a Matlab application)
MSE	Materials Science Engineering
MWIR	Mid-wave infrared
NIR	Near infrared
OAP	Off-axis parabolic mirror
PECVD	Plasma-enhanced chemical vapor deposition
PhD	Doctorate of Philosophy
PR	Photoresist
PV	Photovoltaic
PVD	Physical vapor deposition
RF	Radio frequency
RIE	Reactive ion etching
sccm	Standard cubic centimeters per minute
SE	Selective emitter
SEM	Scanning electron microscopy
SWIR	Short-wave infrared
TIFF	Tagged Image File Format (a file format)
TPV	Thermophotovoltaic
VASE	Variable angle spectroscopic ellipsometry
X-SEM	Cross-sectional scanning electron microscopy
XYR	a stage that moves linearly and rotates in the XY plane
ZED	Zeon Corp. e-beam developer
ZEP	Zeon Corp. e-beam photoresist

SOPs and Fabrication Notes

Iridium Metasurface Fabrication:

1. Book SP3 at CNS, or another sputter tool, for a minimum of 8 hours. Upon booking, request that the shutters be cleaned with glass bead polish. Prepare and clean two 4-inch silicon wafers. Vent the SP3 tool and retrieve the sample mounting plate. Adhere the wafer to the plate using Kapton tape, not clips (will introduce warping with stressed films). Change the targets to Iridium on a DC gun, Titanium on another DC gun, and the desired mask material on the RF gun. Insert the wafer and pump down the SP3 tool. Wait until chamber pressure has reached 5E-6 Torr or lower (this may take 2-3 hours).

2. Make sure the rotation is on. Flow argon at 15sccm and set the chamber pressure to the required value to light a plasma with the RF gun. Ramp up the RF target to 150W and set the chamber pressure to 4mTorr. Open the shutter for 2 hours. Do not walk away, check that the plasma remains lit the entire time. Record the total time the plasma remained lit. If less than 60 minutes, restart the plasma and continue counting. Ramp down RF gun.

3. Vent the chamber and retrieve the coated sample. Place the other cleaned wafer on the chuck and begin pumping down (another 2-3 hours). While waiting for chamber pumping, read ahead and follow whichever steps you can in the available time.

4. Make sure the stage rotation is on. Flow argon a 15sccm and set chamber pressure to 4mTorr. Follow tool use instructions to ramp up Ti target to 200W. Open shutter for 90 seconds (assume this film is 6-10 nm thick). Ramp down Ti and ramp up Ir target to 160W. Open shutter for 1 hour. Do not walk away, check that the plasma remains lit the entire time. Long metal depositions have the tendency to produce flakes which will short the DC gun and stop the plasma. Record the total time the plasma remained lit. If less than 30 minutes, restart the plasma and continue counting. Ramp down Ir target.

5. Vent the chamber and retrieve the Ir coated sample. Restore the tool to idle.

6. Measure the thickness of the films to check the deposition rate. If the mask film is a dielectric, it is recommended to use VASE. However, only use if confident in the material properties to determine the thickness very accurately. For the Ir, X-SEM will provide the most accurate result. If using X-SEM, remember to convert for the foreshortened angle.
7. Once the film thicknesses are accurately known, move on to determining etch rates. The etch rate should be determined using the same technique used for determining the original material thickness. In this case, it is not necessary to use a PR mask and pattern the samples, however, that would be the traditional method for this step. Dice or cleave the samples into chips, roughly 20-25mm squares.
8. Place one chip of each film together on a carrier wafer and process the etch recipe on both chips. Repeat for each recipe variation with new chips. Retrieve the chips and determine the etch rates for each recipe.
9. With this information (deposition rate and etch rate of both Ir and mask material), calculate the selectivity and determine the correct mask thickness (add extra mask thickness to be safe). Book the SP3 tool for the appropriate amount of time to deposit a full film stack of Ti, Ir, and mask material all in series.
10. Using previously described parameters, deposit the full thickness film stack on SP3. It is recommended to make two of these samples. You will also need to produce another sample from step 2, which will be called “mask dummy”.
11. Spin ZEP520A PR on the mask dummy wafer. From the ZEP data sheet, determine the RPM and bake time/temp to produce a sufficiently thick film. After the PR mask is baked, dice/cleave the sample into chips (same size as before). You can strip the PR off of some of these chips using Remover PG if you don’t have any remaining ones from the deposition rate sample. Only do this after the ZEP has been spun and baked on a full wafer, then diced. This will assure that each chip has a uniform ZEP layer for later processing steps.

12. Run RIE etch recipes on the mask material chips and ZEP chips as previously performed for Ir chips to determine the etch rates and selectivity required to pattern the hard mask.

13. With the ZEP selectivity calculated, you can spin and bake ZEP onto the full film stack wafers at the appropriate thickness.

14. Also in the ZEP data sheet, you will find recommended dosage settings. Expose the real metasurface pattern on the mask dummy chips with ZEP. The area of pattern writing should be a minimum of $4mm^2$. On EL6 at CNS, a dose of $90uC/cm^2$ was used for 1uA of beam current. If using EL7, triple this value. EL6 = 50keV and EL7 = 150keV beam.

15. Develop the pattern in ZED-N50. Develop time will change depending on the volume of developer, orientation of chip, agitation, age of developer, and what you ate for breakfast that day. Confirm the PR is fully developed with AFM. Follow the AFM scanning procedure outline in the appendix.

16. After the PR is fully developed, run a descum plasma clean on RIE14 at CNS, or another equivalent tool, for 1 minute. Process at least one of these mask dummy chips to transfer the metasurface pattern into the hard mask. Remove the residual ZEP in Remover PG.

17. Characterize the patterned hard mask using AFM, X-SEM, or any other technique to precisely determine the pattern opening dimensions. If the hard mask pattern is not slightly undersized for the desired final pattern in iridium, then the GDS mask features must be edited before exposing the real samples.

18. Now using the finalized metasurface GDS mask, expose the real sample wafers. The pattern should now be a minimum of $25mm^2$ and each patterned area should be centered at +/- 25mm from the wafer center in each quadrant. This will center the patterns in segment after the wafer is quartered. Do not quarter the wafer at this step. Do this for both real sample wafers.

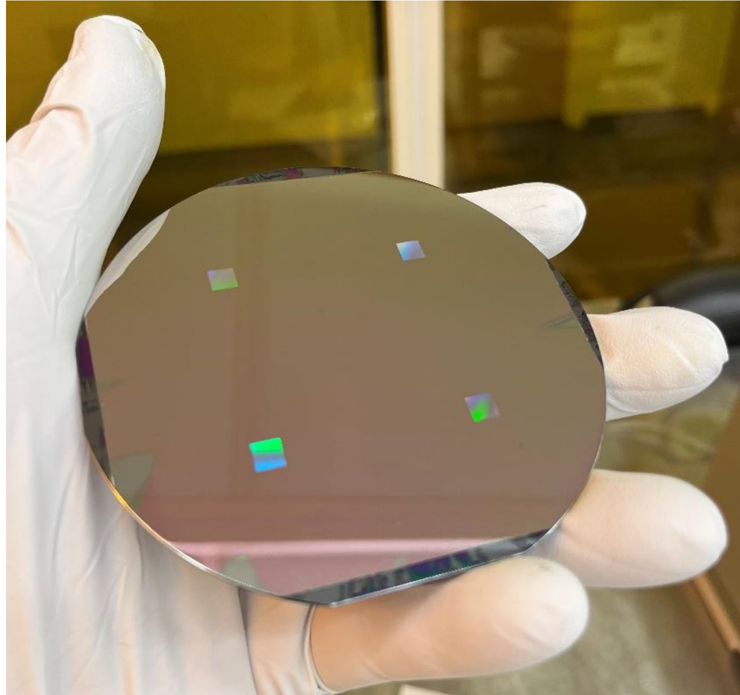

19. Develop the wafer in ZED-N50. Confirm the patterns are fully developed with AFM. Descum after developing. Do this for both real sample wafers.

20. Run the RIE recipe to pattern the hard mask. Remove the residual ZEP with Remover PG. Do this for both real sample wafers.

21. Run the etch process to pattern the iridium. Remove the residual hard mask using the RIE recipe used to pattern it, or another sufficient process such as wet etching. Do this for only one of the real sample wafers. The second will remain at this step for now. It can be performed after future characterization steps confirm the process accuracy for the first sample.

22. Quarter the wafer. Use these quarters to characterize with any destructive processes, such as X-SEM. Once the final metasurface structure is characterized physically, determine if minor process adjustments are needed before completing step 21 on the second sample.

23. Take a quarter wafer and place the 3D printed dicing stencil over the sample. Trace the 40mm octagon lines on the sample with permanent marker. Dice, do not cleave, the sample into a 40mm regular octagon with the metasurface in the center.

24. The octagonal samples can now be optically characterized by the HiTemps (High Temperature Emission Spectroscopy) testbed. You can also optically characterize these samples using VASE, but being octagonal is not a requirement for VASE.

AFM Scanning Procedure:

1. This procedure is for the Jupiter XR from Asylum Research, SPM12 at CNS, in tapping mode. Begin with AR10-NCLR tips. This is high aspect ratio, 10:1. Load the tip and secure tightly with the screw. Replace the tip chuck into the tool. Enter the length, width, and frequency from the package for the corresponding tip when prompted.

2. Load sample onto the stage and secure with vacuum. (green button centered above stage)

3. Move stage to roughly align the sample under the microscope.

4. Lower the tip to about 2mm.

5. Focus on the tip, adjust zoom of microscope and set focus position once optimally focused on edge of the cantilever.

6. Position the laser in the center of the triangular section using the "spot on" control. Right click and set the tip position as the center of the base of the triangular section of the cantilever.

7. Calibrate the tip using the get real thermal button. Once the thermal samples are collected, right click and select send frequency and phase to tune.

8. In the new window, click the auto tune button. This will set the drive amplitude once completed.
9. Move the focus (DO NOT MOVE TIP) to the sample surface. Ensure that you are looking at the sample substrate and not the stage below. Move around until you discover the metasurface pattern; it should appear as a darker colored area with sharp square edges.
10. Adjust focus until the sharpness of the edge of the metasurface pattern is optimized. Set the focus position for the sample.
11. Return to focus on tip. Lower the tip to the pre-engage height.
12. Change the gain to 50. The other default values of 800mV set point and approach speed should be fine to leave as is.
13. Change scanning parameters to 45 degrees (relative to metasurface lines), scan rate 1Hz, and scan size 2 microns. Change save directory to desired personal folder and prepare a file name for scans.
14. Click start tip approach. After contact is made, begin scanning with frame up (or down). Only while scanning is active, click the arrows to increase the drive amplitude until the trace and retrace lines are very well overlapped. You may notice that one is straighter and one is sloped when going down into the trenches, which may alternate. This will not improve by increasing drive amplitude. This can only be improved by scanning slower.
15. Do not increase the drive amplitude more than 8 clicks from the calibrated value. If trace and retrace lines have not improved by this point, then the Z-voltage is likely pinned meaning the piezo is maxed out of its range. If this happens, reduce the drive amplitude by several clicks. Stop scanning and return to pre-engage. Increase the gain to 60 and repeat step 14.

HiTemps Testbed Operation:

1. Before beginning work at this testbed, make sure all safety precautions are in place. You should be wearing polycarbonate safety glasses to protect your eyes from UV light. Identify the location of the insulated furnace mitts and fire blanket. Identify the location of the fire extinguisher. Confirm all the electrical wiring is firmly connected and there is no evidence of melting on any portion of the wiring. Locate and position the temporary barrier to prevent unwelcomed foot traffic near the testbed.

2. Post signs on the outside of the doors leading to the optics room alerting others that the testbed will be in use.

3. Place the sample over the furnace opening. Place the second thermocouple between the center and the edge of the sample.

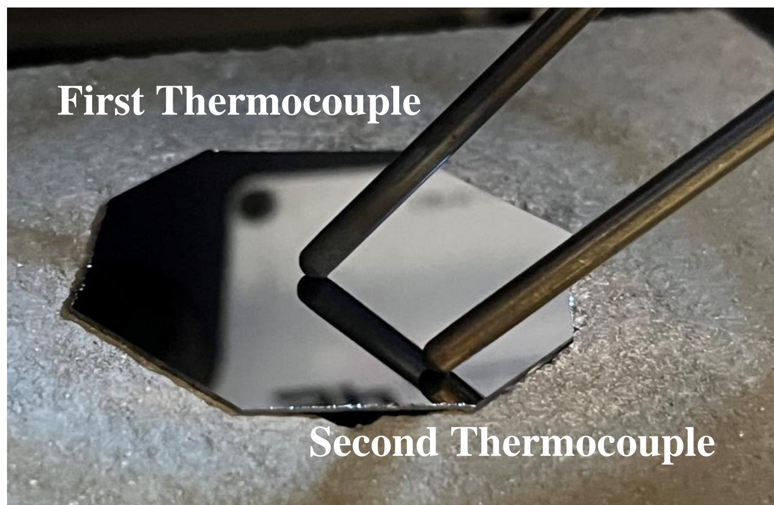

4. Insert the red LED magnetic base in place of the monochromator and plug the USB cord into power. Adjust the sample position so that the red dot is focused sharply in the center of the metasurface pattern. Disconnect the USB and carefully remove the LED base from the system.

5. Connect the monochromator and detector to the computer and power. Make sure they are turned on and functioning properly before returning them to the magnetic base. Return

the monochromator to the base inside the enclosure. Close the door. Turn on the interior light and confirm that everything looks correct through the view port before continuing.

6. Reset the Raspberry Pi and wait 30 seconds. Turn on the digital thermometer. Open a web browser and go to "thermo.larrys.tech". Adjust the sample collection rate to 10 seconds. Update the plot and confirm that temperature readings are being recorded.
7. Confirm that the Keithely source meters are connected to each variac output and are measuring ACV. Turn on the power strip for the variacs. Note that the case fan inside the enclosure will also turn on. Flip the switch to on for the first variac. Adjust the rheostat until the output is measured at 55V.
8. Make sure the rheostat of the second variac is at zero. Flip the switch to on for the second variac. Increase the rheostat slowly to the voltage target. The target should be determined based on the previous calibration look-up table for voltage vs temperature. Note that there is a significant delay after adjusting the rheostat. The voltage will continue to climb after the adjustment is completed. It may take several minutes to get the correct value set properly.
9. Watch the thermometer plot to confirm the sample has stabilized at the desired temperature. Thermal equilibrium in the sample typically takes 20 minutes after the temperature is adjusted. Note that the temperature being probed is the outer location on the sample and the metasurface temperature is at a higher temperature than the measured value. Use the calibration look-up table to confirm the measurement for the desired temperature at the center of the sample.
10. Throughout the remainder of the experiment, you must be mindful that the enclosure could act like an oven. Observe the glass rod thermometer sticking through the right-side enclosure wall. Pull it out and check the enclosure temperature. The temperature should not exceed 60°C or some plastics inside the enclosure will become damaged. Return the thermometer to the designated depth indicated in permanent marker on the enclosure wall after readings.

11. While wearing safety glasses, look into the view port to confirm that the sample is in-tact, the thermocouple or sample has not shifted, and the sample temperature is radially distributed from the metasurface. Power off and cool down before making adjustments if needed.

12. Open MORTI, the Matlab app. Setup the spectroscopic scan parameters in the app. Note that the optical chopper must be enabled manually. Run the spectroscopic scan. Save your data before running a new scan.

13. Adjust the rheostat of the second variac to zero and switch the power off. Switch the power off for the first variac after the second. Power off the source meters.

14. Leave the main power strip on and the thermometer recording. Observe the cool down for the sample on the temperature plot. Once the sample temperature has reached less than 30°C, it is safe to turn off the thermometer and flip the power off on the main power strip. Open the door and retrieve your sample.

Calibrating HiTemps Testbed:

1. Before beginning work at this testbed, make sure all safety precautions are in place. You should be wearing polycarbonate safety glasses to protect your eyes from UV light. Identify the location of the insulated furnace mitts and fire blanket. Identify the location of the fire extinguisher. Confirm all the electrical wiring is firmly connected and there is no evidence of melting on any portion of the wiring. Locate and position the temporary barrier to prevent unwelcomed foot traffic near the testbed.

2. Post signs on the outside of the doors leading to the optics room alerting others that the testbed will be in use.

3. Place the first thermocouple directly in contact with the heating element coil. Leave the second thermocouple hanging or place it out of the way for now. Close the door of the experiment enclosure.

4. Reset the Raspberry Pi and wait 30 seconds. Turn on the digital thermometer. Open a web browser and go to "thermo.larrys.tech". Adjust the sample collection rate to 10 seconds. Update the plot and confirm that temperature readings are being recorded.

5. Confirm that the Keithely source meters are connected to each variac output and are measuring ACV. Turn on the power strip for the variacs. Note that the case fan inside the enclosure will also turn on. Flip the switch to on for the first variac. Adjust the rheostat until the output is measured at 55V.

6. Make sure the rheostat of the second variac is at zero. Flip the switch to on for the second variac. Increase the rheostat slowly to the voltage target. The target should be determined based on the previous calibration look-up table for voltage vs temperature. Note that there is a significant delay after adjusting the rheostat. The voltage will continue to climb after the adjustment is completed. It may take several minutes to get the correct value set properly.

7. Watch the thermometer plot to confirm the sample has stabilized at the desired temperature. Thermal equilibrium typically takes 20 minutes after the temperature is adjusted. DO NOT EXCEED 1000°C – this is the operational limit of the thermocouples.

8. Generate a data set that correlates the variac voltage settings with the coil temperature. Plot this data and fit a linear trendline to it. Extend this trendline to the voltage settings that would produce 1400°C on the coil. DO NOT GO THIS HIGH – this is the melting point of the resistive wire coil. Be aware that the maximum allowable voltage is less than the last point of this trendline.

9. Reduce the voltage to zero on the second variac and allow the coil to cool down before proceeding to the next step.

10. Place a test sample (octagonal wafer, preferably with the correct film) over the furnace opening and place the two thermocouples as shown below.

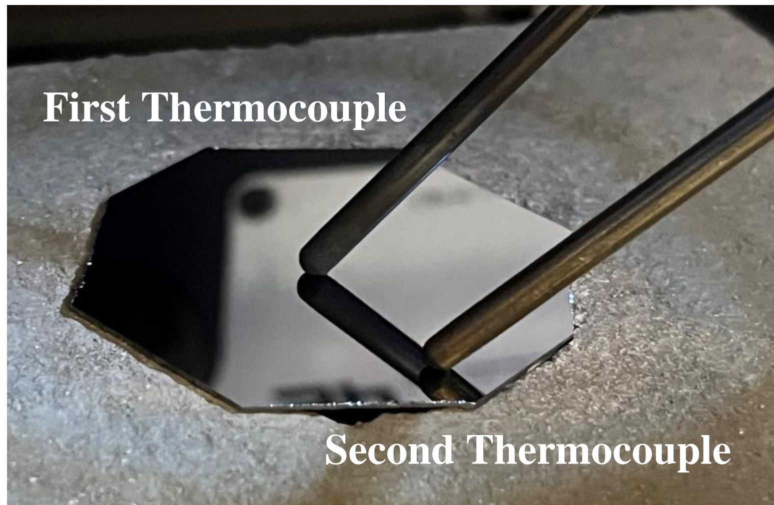

11. Repeat the heating stages previously measured for the coil. Produce a data set which correlates both surface temperatures to the variac voltage settings. You may approach the upper limit of the coil temperature with caution.

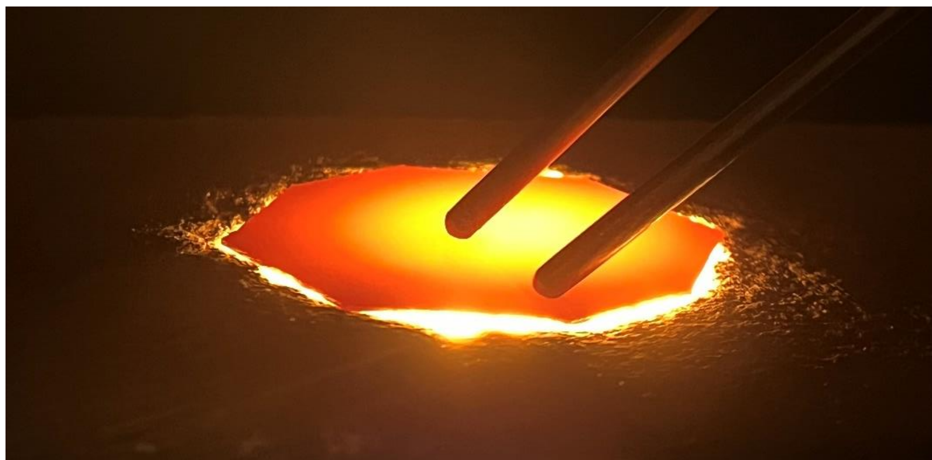

12. While wearing safety glasses, look into the view port to confirm that the sample is in-tact, the thermocouples or sample have not shifted. Power off and cool down before making adjustments if needed. You should observe the image below.

13. Produce two trendlines for each sample temperature. Use the best fit, this may or may not be linear. This will serve as your calibration look-up table when measuring real samples.

MLA Microscope Operation:

1. Carefully mount the MLA sample on the appropriate holder over the opening. Remember that the first optical interface is the bottom surface when mounted.
2. Attach the sample holder to the hexapod chuck and secure gently.
3. Open the software to move the hexapod, PI MikroMove. Communication with the hexapod should automatically begin from memory settings.
4. Open the software to view the camera, IDS Cockpit. Position these windows side-by-side on screen.
5. Open MATLAB, leave in the background for now.
6. In MikroMove, Reference-move the hexapod (homing procedure). Confirm all axes values are zero. Set the system velocity to 0.05 mm per second.
7. In Cockpit, flip the horizontal and vertical image axes. Set the frame rate to 33fps, the exposure time to 25.00ms and the digital and analog gain factors to 1.0.
8. Rotate the 50x objective into place and turn on the white light source. Adjust the brightness as required with sample reflectivity.
9. Move the hexapod Z-axis to get the sample in focus. It is recommended to use the edge of the sample if it can be reached with reasonable X and Y axis motions.

10. Move X and Y to the bottom left corner, or noteworthy feature. Adjust Z-axis to maintain focus. Note the X_0, Y_0, and Z_0 position for best focus.

11. Move in only X to the bottom right corner, or noteworthy feature. Adjust Z-axis to return to best focus. Note the X_3 and Z_3 position for best focus.

12. Return to position (X_0, Y_0, Z_0).

13. Move in only Y to the top left corner, or noteworthy feature. Adjust Z-axis to return to best focus. Note the Y_1 and Z_1 position for best focus.

14. Using the graphic below, calculate the sample tip and tilt angles and subtract them with U and V axis adjustments. Use MATLAB to assist you. All motions from here on out should be absolute, not relative.

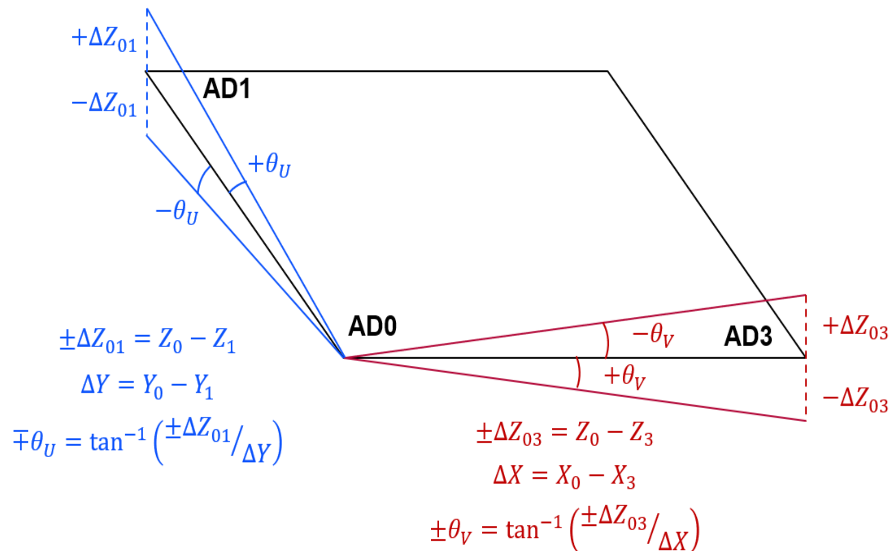

15. Return to position (X_0, Y_0) and adjust Z-axis to find best focus. Confirm the sample is planarized by moving to X_3 and Y_1 without adjusting Z. The sample should remain in focus the entire time.

16. Move in X and Y to the target lens. Center it within the FOV. Record this location as BFL = 0.

17. In MikroMove, set the system velocity between 1 and 5 microns per second.

18. Turn off the white light and turn on the laser to half-power. If the laser light cannot be seen, first increase the digital gain in Cockpit, then increase analog gain if needed, then increase laser power if still needed. After these adjustments if the laser light cannot be seen, you may need to move closer to the beam's waist.

19. As you approach the beam waist. Ensure that the camera gain values are minimized and the laser power is low enough such that it does the image brightness is just below saturation. This may take several adjustments before reaching the waist.

20. Capture images as you see fit. Save them as TIF files with the BFL, laser power, and gain settings listed in the file name.

21. Analyze images in MALAB using the Microlens Focus Analyzer program provided.

MDL Fabrication:

1. Document the handoff and inspect the starting condition of the wafer.
2. Clean the wafer with soapy water spray, DI water rinse, nitrogen blow dry. Spray/rinse with acetone, spray/rinse with IPA, nitrogen blow dry.
3. Plasma ash for 3-minutes at 100W in 3% oxygen/helium.
4. HMDS vapor prime on hot plate under bell jar for 10 minutes.
5. Spin AZ1529 PR at 4k RPM for 30 sec.
6. Bake on hot plate at 115C for 90 sec.
7. Locate the appropriate GDS file and expose layer-0 on Heidelberg Direct Writer with dosage 350 mJ/cm^2 and defocus 0. Perform front-to-back alignment if necessary.
8. Run the YES oven ammonia program (1:45 hrs).
9. Load wafer into the MA6 aligner with no mask. Flood expose with dosage 1215 mJ/cm^2 for 85 sec.
10. Develop PR in (1:9) 303A:DI water for 20 seconds.
11. Inspect wafer and return to developer for 5 seconds intervals as necessary.
12. Plasma ash for 3-minutes at 100W in 3% oxygen/helium.
13. Load titanium and gold sources in the Temescal evaporator. Load sample.

14. Pump chamber to 5E-7 Torr. Deposit Ti (250A), Au (1000A), Ti (500A) onto the sample.
15. Lift-off in beaker of acetone for 45-minute soak.
16. Inspect under microscope. Return to acetone soak/spray if needed. Photograph alignment marks, serial numbers, and process tracking fields.
17. Clean the wafer with soapy water spray, DI water rinse, nitrogen blow dry. Spray/rinse with acetone, spray/rinse with IPA, nitrogen blow dry.
18. Load into PECVD system and load recipe DNIT400 to deposit silicon nitride (7-hr).
19. Map film thickness across the wafer with VASE or alternative ellipsometer.
20. Plasma ash for 5-minutes at 100W in 3% oxygen/helium.
21. HMDS vapor prime on hot plate under bell jar for 10 minutes.
22. Spin *AZ1518* PR at 4k RPM for 30 sec.
23. Soft bake PR
    a. If whole wafer: Bake on hot plate at 115C for 60 seconds.
    b. If on carrier: Bake in oven at 70C for 25 minutes.
24. Locate the appropriate GDS file and expose layer-*51* on Heidelberg Direct Writer with dosage *150* mJ/cm^2 and defocus -4. Perform front-to-back alignment if necessary.
25. Post-exposure bake PR
    a. If whole wafer: Bake on hot plate at 115C for 30 seconds.
    b. If on carrier: Bake in oven at 110C for 8-10 minutes.
26. Develop PR in (1:12) 303A:DI water for 60 seconds.
27. Inspect wafer and return to developer for 15 seconds intervals as necessary.
28. Plasma ash for 3-minutes at 100W in 3% oxygen/helium.
29. Hard bake PR
    a. If whole wafer: Bake on hot plate at 115C for 90 seconds.
    b. If on carrier: Bake in oven at 110C for 30 minutes.
30. Etch in SAMCO RIE to remove *2125* angstroms on silicon nitride.
31. Plasma ash for 5-minutes at 100W in 3% oxygen/helium.
32. Soak in Remover PG on hot plate at 70C for 30-40 minutes.
33. Spray/rinse with acetone, spray/rinse with IPA, nitrogen blow dry.

34. Plasma ash for 3-minutes at 100W in 3% oxygen/helium.
35. Measure the etch depth with Zygo optical profilometer. Photograph and document results of process step.
36. Clean the wafer with soapy water spray, DI water rinse, nitrogen blow dry. Spray/rinse with acetone, spray/rinse with IPA, nitrogen blow dry.
37. Repeat steps 21 through 36 for 5 total loops with the following changes (*italic above*).

Loop #	PR	Dosage	Layer-#	Etch Depth
1	AZ1518	150	51	2125
2	AZ1529	275	52	4250
3	AZ1529	275	53	8500
4	AZ1529	275	54	17000
5	AZ1529	275	55	15 mins

Code

TPV Design Toolbox and Visualizer

```
%% TPV Design Toolbox and Visualizer
% Created by: Zachary E. Kranefeld
% Copyleft: DSL (Design Science License)
% Published in August 2025

%% Hard-coded parameters
%Unviersal Constants
Defaults.Const.h1 = 4.13567E-15; %(eV*s) Plank const
Defaults.Const.k1 = 8.6173E-5; %(eV/K) Boltzmann cont
Defaults.Const.c = 2.99792E8; %(m/s) speed of light in vac
Defaults.Const.h2 = 6.626E-34; %(J*s) Plank const
Defaults.Const.k2 = 1.38065E-23; %(J/K) Boltzmann cont
Defaults.Const.hbar1 = Defaults.Const.h1/(2*pi); %(eV*s)
Defaults.Const.hbar2 = Defaults.Const.h2/(2*pi); %(J*s)
Defaults.Const.eps0 = 8.854188E-12; %vacuum permittivity (C^2*s^2/kg*m^3)
Defaults.Const.q = 1.602177E-19; %elemental charge (C)
Defaults.Const.Me = 9.109E-31; %electron mass (kg)

%Default Parameters
Defaults.ST_res = 100; %total number of steps for temperature range resolution
Defaults.Spect_res = 10; %def units nm
Defaults.STmin = 1000; %Source Temp min/max (def units C)
Defaults.STmax = 2000;
Defaults.SPmin = 400; %Spectrum min/max (def units nm)
Defaults.SPmax = 3000;
Defaults.ARC = 0.95;
Defaults.BSR = 0.95;
Defaults.thick_res = 20; %number of slices for depth into each material
Defaults.movie = false;
Defaults.SR = [1000,1000]; %surface recombination velocity (um/s) [front,back]
Defaults.FF = 0.9; %electrical fill factor

%%%%%%%%%%%%%%%%%%%%%%%%%%%%%%%%%%%%%%%%%%%
%AUTHOR WARNING
%changing the number of cell temps will create an error during the ABS vs
%Depth visualization because the number of buttons are predefined, not
%dependent upon this variable
Defaults.CT_res = 5; %number of cell temperatures
```

```
%%%%%%%%%%%%%%%%%%%%%%%%%%%%%%%%%%%%%%%%%%%

%Efficiency Color Map
gradients = 20;
%add as many sections to Colors struct as you like
Colors.c1 = [0.4,0,0.5]; %dark purple
Colors.c2 = [0.8,0,0.5]; %magenta darkened
Colors.c3 = [1,0,0]; %red
Colors.c4 = [1,0.5,0]; %orange
Colors.c5 = [1,1,0]; %yellow
Colors.c6 = [0.5,1,0.5]; %light green
EffMap = makeColorMap(Colors,gradients); %colormap for efficiency plot


%% User Defines the Source
[PhotonUnit,PhotonRange] = DefineSpectrum(Defaults);
[TempUnit,STRange] = DefineSource(Defaults);

switch TempUnit
    case 'C'
        Defaults.CTmin = 20;
        Defaults.CTmax = 40;
        Defaults.CTlims = [-273,inf];
    case 'K'
        Defaults.CTmin = 290;
        Defaults.CTmax = 330;
        Defaults.CTlims = [0,inf];
    case 'F'
        Defaults.CTmin = 65;
        Defaults.CTmax = 110;
        Defaults.CTlims = [-459,inf];
end

% Author Comments
% We have now defined the range and units for how we wish to visualize the
% rest of our TPV system. Some math is done using temperature in Kelvin or
% wavelengths in microns, explicilty, but those conversions are taken care
% of by the code. The next section provides a visual of the parameter space
% defined here.

%% Produce Source Visualization
SOURCE.E = zeros(length(PhotonRange),length(STRange));
SOURCE.Q = zeros(length(PhotonRange),length(STRange));
for temp = 1:length(STRange)
    [SOURCE.E(:,temp),SOURCE.Q(:,temp)] = generateBB(TempUnit,STRange(temp),PhotonUnit,PhotonRange,Defaults);
end

makeThermal(SOURCE.E,PhotonRange,PhotonUnit,STRange,TempUnit)
hold on
title('Temperature Spectrum Plot (E_i_n Source1)');
c = colorbar;
c.Ruler.TickLabelFormat = '%.1f W/m^2';
hold off
makeThermal(SOURCE.Q,PhotonRange,PhotonUnit,STRange,TempUnit)
hold on
title('Temperature Spectrum Plot (Q_i_n Source1)');
c = colorbar;
c.Ruler.TickLabelFormat = '%.1f pt/sm^2';
hold off
progCheck;

%% User Defines Source Filtering
m = msgbox('You will now be prompted to apply a filter to the Blackbody Source. This filtering will be applied BEFORE the spectrum is
incident on the TPV device.');
uiwait(m);
SOURCE2 = FilterSource(SOURCE,PhotonUnit,PhotonRange,STRange,TempUnit);

% Author Comments
% The first stage of filtering is done to the blackbody curve. Most real
% sources are not perfect blackbodies. The user is meant to scale down to
% a gray body or apply a known emission profile to the blackbody spectrum
% which more accurately represents the fuel soucre of this TPV system.
% Additional filtering will be available when define the selective emitter.

%% Produce Filtered Source Visualization
makeThermal(SOURCE2.E,PhotonRange,PhotonUnit,STRange,TempUnit)
hold on
title('Temperature Spectrum Plot (E_i_n Source2)');
c = colorbar;
c.Ruler.TickLabelFormat = '%.1f W/m^2';
hold off
makeThermal(SOURCE2.Q,PhotonRange,PhotonUnit,STRange,TempUnit)
hold on
title('Temperature Spectrum Plot (Q_i_n Source2)');
c = colorbar;
```

```
c.Ruler.TickLabelFormat = '%.1f pt/sm^2';
hold off
progCheck;

%% User Defines CELL
CELL = DefineCell(TempUnit,Defaults);

indexVtemp.TOP = zeros(length(PhotonRange),3,Defaults.CT_res);
indexVtemp.MID = zeros(length(PhotonRange),3,Defaults.CT_res);
indexVtemp.BOT = zeros(length(PhotonRange),3,Defaults.CT_res);
for CT = 1:length(CELL.CellTempK)
    indexVtemp.TOP(:,:,CT) = findIndex(CELL.TOP,PhotonRange,PhotonUnit,CELL.CellTempK(CT),Defaults);
    indexVtemp.MID(:,:,CT) = findIndex(CELL.MID,PhotonRange,PhotonUnit,CELL.CellTempK(CT),Defaults);
    indexVtemp.BOT(:,:,CT) = findIndex(CELL.BOT,PhotonRange,PhotonUnit,CELL.CellTempK(CT),Defaults);
    indexVtemp.SUB(:,:,CT) = findIndex(CELL.SUB,PhotonRange,PhotonUnit,CELL.CellTempK(CT),Defaults);
end
[ABS,Atot,T] = generateABS(indexVtemp,CELL,TempUnit,Defaults);
[CELL,EmArea] = DefineGeom(CELL,Defaults);

% Author Comments
% Now we have imported the material properties file for the semiconductor
% you've chosen to build the PV cell from. Because refractive index is
% tabulated as a lookup table for a given temperature, we had to fit linear
% segments between the two nearest existing points to the target, both in
% temperature and wavelength.
% The matrix "indexVtemp" has an N by 3 by M size where N are the
% wavelengths previously defined. The 3 columns are wavelength (um), n, and k.
% The M pages are the temperatures defined by the cell temp prompt.
% The ABS data provides a 3D matrix of absorption: rows=wvl, columns=depth
% into material, pages=cell temperature. The total absorption vs wvl graph is
% generated during the function callback. This info is provided to the user
% to verify the absorption behavior around the bandgap.

%% Produce CELL Visualization
ExamineCell(ABS,Atot,T,CELL,PhotonRange,PhotonUnit,TempUnit);

%% User Defines Selective Emitter
m = msgbox('You will now be prompted to create the Selective Emitter Profile. This filtering will be applied BEFORE the spectrum is absorbed
by the PV cell.');
uiwait(m);
%scale down sourcce spectrum to emitter area
SOURCEi.E = (SOURCE2.E/1E6)*EmArea; %convert from m^2 to mm^2 then multiply by Emitter Area
SOURCEi.Q = (SOURCE2.Q/1E6)*EmArea;
SOURCE3 = FilterSource(SOURCEi,PhotonUnit,PhotonRange,STRange,TempUnit);

% Author Comments
% The second stage of filtering defines the selective emitter behavior.
% This filter is applied to the result of the previous filter. This prompt
% comes after the "Define Cell" prompts so that the user can
% carefully match the SE cutoff to the sharp absorption edge of the cell
% material.

%% Produce Emitter Visualization
makeThermal(SOURCE3.E,PhotonRange,PhotonUnit,STRange,TempUnit)
hold on
title('Selective Emitter Spectrum Plot (E_i_n Source3)');
c = colorbar;
c.Ruler.TickLabelFormat = '%.1f W';
hold off
makeThermal(SOURCE3.Q,PhotonRange,PhotonUnit,STRange,TempUnit)
hold on
title('Selective Emitter Spectrum Plot (Q_i_n Source3)');
c = colorbar;
c.Ruler.TickLabelFormat = '%.1f pt/s';
hold off
progCheck;

%% Electrical Calculations
[G] = generateCarriers(SOURCE3,ABS,Atot,CELL);
[ExProb,I_sc] = extractCarriers(CELL,G,[],Defaults);

%plot carrier extraction probability
figure; hold on
plot(CELL.TOP.thick,ExProb.TOP(:,1,1),'Color',[1,0,0]);
plot(CELL.TOP.thick(end)+CELL.MID.thick,ExProb.MID(:,1,1),'Color',[1,0,0]);
plot(CELL.TOP.thick(end)+CELL.MID.thick(end)+CELL.BOT.thick,ExProb.BOT(:,1,1),'Color',[1,0,0]);
plot(CELL.TOP.thick,ExProb.TOP(:,end,1),'Color',[0,0,1]);
plot(CELL.TOP.thick(end)+CELL.MID.thick,ExProb.MID(:,end,1),'Color',[0,0,1]);
plot(CELL.TOP.thick(end)+CELL.MID.thick(end)+CELL.BOT.thick,ExProb.BOT(:,end,1),'Color',[0,0,1]);
ylim([0,1]);
xlim([0,CELL.TOP.thick(end)+CELL.MID.thick(end)+CELL.BOT.thick(end)])
title('Extraction Probability vs Depth (at min cell temp)')
legend({['Source Temp = ',num2str(STRange(1)),char(176),TempUnit],'','',['Source Temp =
',num2str(STRange(end)),char(176),TempUnit]},'Box','off','Location','south')
hold off
```

```
CELL.P_el = zeros(Defaults.ST_res,Defaults.CT_res);
for CT = 1:Defaults.CT_res
    for ST = 1:Defaults.ST_res
        CELL.P_el(ST,CT) = CELL.FF*(CELL.MID.Eg(CT)/2)*I_sc.Total(ST,CT); %Voc estimated as Eg/2
    end
end

%% Produce Efficiency Visualization
EFFIC = ExamineEff(SOURCE2,SOURCE3,CELL,STRange,TempUnit,EffMap);

%% Supporting Functions
%%%%%%%%%%%%%%%%%%%%%%%%%%%%%%%%%%%%%%%%%%%%%%%%%%%%%%%%%%%%%%%%%%%%%%%%%%%%%%%%%%%%%%%%
%%%%%%%%%%%%%%%%%%%%%%%%%%%%%%%%%%%%%%%%%%%%%%%%%%%%%%%%%%%%%%%%%%%%%%%%%%%%%%%%%%%%%%%%
function progCheck
    m = msgbox(['Take a moment to rearrange the plots generated so their information will be accessible later.',newline,'Close this window
when you are ready to proceed.'],'Organize Figure Windows');
    waitfor(m);
end

function [BB_E,BB_Q] = generateBB(TempUnit,TempVal,PhotonUnit,PhotonRange,Defaults)
    switch TempUnit %differentiate between input and K units
        case "K"
            TempK = TempVal;
        case "C"
            TempK = TempVal + 273.15; %convert to K
        case "F"
            TempK = (TempVal-32)*(5/9) + 273.15; %convert to K
    end
    E_bb=@(wvl)
(2*pi*Defaults.Const.h2*Defaults.Const.c^2/(wvl^5))*(1/(exp((Defaults.Const.h2*Defaults.Const.c)/(wvl*Defaults.Const.k2*TempK))-1));
%Watts/(area*wvl)
    Q_bb=@(wvl) (2*pi*Defaults.Const.c/(wvl^4))*(1/(exp((Defaults.Const.h2*Defaults.Const.c)/(wvl*Defaults.Const.k2*TempK))-1));
%(#photons/sec)/(area*wvl)
    switch PhotonUnit %convert wvl to meters
        case "eV"
            %wvl = hc/E
            lambda = (Defaults.Const.h1*Defaults.Const.c)./PhotonRange;
        case "nm"
            lambda = PhotonRange*1E-9;
    end
    BB_E = zeros(length(lambda),1);
    BB_Q = zeros(length(lambda),1);
    for wvl = 1:length(lambda)
        BB_E(wvl) = E_bb(lambda(wvl));
        BB_Q(wvl) = Q_bb(lambda(wvl))/1E9; %convert back to wvl=(1/nm)
    end
end

function [NewIndex] = findIndex(Matl,PhotonRange,PhotonUnit,TargetTempK,Defaults)
    if strcmp(PhotonUnit,'eV')
        lambda = ((Defaults.Const.h1*Defaults.Const.c)./PhotonRange)*1E6; %wavelength in microns
    else
        lambda = PhotonRange/1E3; %wavelength in microns
    end
    NewIndex(:,1) = lambda;
    %check how many temps exist in material data
    Temps = fieldnames(Matl.index);
    if length(Temps)>1
        [diff,tempNum] = mink(abs(Matl.indexTemps-TargetTempK),2); %finds 2 closest temperatures
        if min(diff)>100
            w = warndlg('The index data loaded for this material is listed at a temperature greater than 100 Kelvin away from target
temperature. The available data was used but this may effect the accuracy of the results.');
            waitfor(w);
        end
        Nset(:,1) = interp1(Matl.index.(Temps{tempNum(1)}).wvl,Matl.index.(Temps{tempNum(1)}).n,lambda,'linear','extrap');
        Nset(:,2) = interp1(Matl.index.(Temps{tempNum(2)}).wvl,Matl.index.(Temps{tempNum(2)}).n,lambda,'linear','extrap');
        Kset(:,1) = interp1(Matl.index.(Temps{tempNum(1)}).wvl,Matl.index.(Temps{tempNum(1)}).k,lambda,'linear','extrap');
        Kset(:,2) = interp1(Matl.index.(Temps{tempNum(2)}).wvl,Matl.index.(Temps{tempNum(2)}).k,lambda,'linear','extrap');
        TempVect = ones(1,length(lambda))*TargetTempK;
        %Improved loop speed method
        if length(lambda)==1 %single wvl value will break interp2
            NewIndex(:,2) = interp1([Matl.indexTemps(tempNum(1)),Matl.indexTemps(tempNum(2))],Nset,TargetTempK,'linear','extrap');
            NewIndex(:,3) = abs(interp1([Matl.indexTemps(tempNum(1)),Matl.indexTemps(tempNum(2))],Kset,TargetTempK,'linear','extrap'));
        else
            NewIndex(:,2) = interp2(lambda,[Matl.indexTemps(tempNum(1)),Matl.indexTemps(tempNum(2))],Nset',lambda,TempVect,'spline'); %spline
covers extrapolation
            NewIndex(:,3) = abs(interp2(lambda,[Matl.indexTemps(tempNum(1)),Matl.indexTemps(tempNum(2))],Kset',lambda,TempVect,'spline'));
%with only 2 points, spline should be linear
        end
    else
        %check how close temp data is to target
        OffTemp = abs(Matl.indexTemps-TargetTempK);
        if OffTemp>100
```

```
            w = warndlg('The index data loaded for this material is listed at a temperature greater than 100 Kelvin away from target
temperature. The available data was used but this may effect the accuracy of the results.');
            waitfor(w);
        end
        %Improved loop speed method
        NewIndex(:,2) = interp1(Matl.index.(Temps{1}).wvl,Matl.index.(Temps{1}).n,lambda,'linear','extrap');
        NewIndex(:,3) = abs(interp1(Matl.index.(Temps{1}).wvl,Matl.index.(Temps{1}).k,lambda,'linear','extrap'));
    end
end

function [ABS,Atot,T] = generateABS(IndexData,CELL,TempUnit,Defaults)
    %double pass through material (air/vacuum front interface)
    air = 1;
    temps = Defaults.CT_res;
    wvls = length(IndexData.TOP(:,1,1));
    depth = Defaults.thick_res;
    tTOP = CELL.TOP.thick;
    tMID = CELL.MID.thick;
    tBOT = CELL.BOT.thick;
    alpha=@(k,wvl) 4*pi*k/wvl;
    tao=@(a,d) exp(-a*d);
    rho=@(n_1,n_2) ((n_1-n_2)/(n_1+n_2))^2;
    %pre-allocate for speed
    T.T1 = zeros(wvls,depth,temps);
    T.T2 = zeros(wvls,depth,temps);
    T.T3 = zeros(wvls,depth,temps);
    T.T4 = zeros(wvls,depth,temps);
    T.T5 = zeros(wvls,depth,temps);
    T.T6 = zeros(wvls,depth,temps);
    T.T_1 = zeros(wvls,depth,temps);
    T.T_2 = zeros(wvls,depth,temps);
    T.T_3 = zeros(wvls,depth,temps);
    T.Tlost = zeros(wvls,temps);
    T.Trecy = zeros(wvls,temps);
    A1TOP = zeros(1,depth);
    A1MID = zeros(1,depth);
    A1BOT = zeros(1,depth);
    A2BOT = zeros(1,depth);
    A2MID = zeros(1,depth);
    A2TOP = zeros(1,depth);
    A_1TOP = zeros(1,depth);
    A_1MID = zeros(1,depth);
    A_2TOP = zeros(1,depth);
    Atot.max = zeros(wvls,temps);
    Atot.TOP = zeros(wvls,depth,temps);
    Atot.MID = zeros(wvls,depth,temps);
    Atot.BOT = zeros(wvls,depth,temps);
    ABS.TOP = zeros(wvls,depth,temps);
    ABS.MID = zeros(wvls,depth,temps);
    ABS.BOT = zeros(wvls,depth,temps);
    %figure movie
    if Defaults.movie
        figure; hold on
        ylim([0,1]);xlim([0,tTOP(end)+tMID(end)+tBOT(end)]);
        anno1 = annotation('textbox',[.7 .7 .1 .1],'String','you never see this','FitBoxToText','on');
        anno2 = annotation('textbox',[.7 .8 .1 .1],'String',['Cell Temp = ',CELL.CellTemp(1),char(176),TempUnit],'FitBoxToText','on');
        xlabel('PV Cell thickness (microns)');
        ylabel('Normalized Transmission');
        pause(0.001);
    end
    for Zdim = 1:temps
        %each "page" of the array is a different temperature
        if Defaults.movie
            anno2.String = ['Cell Temp = ',num2str(round(CELL.CellTemp(Zdim),2)),char(176),TempUnit];
        end
        for Ydim = 1:wvls
            %each row of the array is a different wavelength
            if Defaults.movie
                anno1.String = ['Wavelength(um) = ',num2str(round(IndexData.TOP(Ydim,1),3))];
            end
            for Xdim = 1:depth
                %each column is a different depth in the material
                if CELL.ARC
                    R1 = 1-CELL.ARCprct;
                else
                    R1 = rho(air,IndexData.TOP(Ydim,2,Zdim)); %value for n at current wvl and temp
                end
                if CELL.BSR
                    R4 = CELL.BSRprct;
                else
                    R4 = rho(IndexData.BOT(Ydim,2,Zdim),IndexData.SUB(Ydim,2,Zdim)); %value for n at current wvl and temp
                end
                R2 = rho(IndexData.TOP(Ydim,2,Zdim),IndexData.MID(Ydim,2,Zdim)); %interface betwen top and mid
                R3 = rho(IndexData.MID(Ydim,2,Zdim),IndexData.BOT(Ydim,2,Zdim)); %interface betwen mid and bot
                aTOP = alpha(IndexData.TOP(Ydim,3,Zdim),IndexData.TOP(Ydim,1,Zdim));
```

```
                aMID = alpha(IndexData.MID(Ydim,3,Zdim),IndexData.MID(Ydim,1,Zdim));
                aBOT = alpha(IndexData.BOT(Ydim,3,Zdim),IndexData.BOT(Ydim,1,Zdim));
                T.T1(Ydim,Xdim,Zdim) = (1-R1)*tao(aTOP,tTOP(Xdim)); %first pass top layer
                T.T_1(Ydim,Xdim,Zdim) = (1-R1)*tao(aTOP,tTOP(end))*R2*tao(aTOP,tTOP(Xdim)); %first interior reflection
                T.T2(Ydim,Xdim,Zdim) = (1-R1)*tao(aTOP,tTOP(end))*(1-R2)*tao(aMID,tMID(Xdim)); %first pass mid layer
                T.T_2(Ydim,Xdim,Zdim) = (1-R1)*tao(aTOP,tTOP(end))*(1-R2)*tao(aMID,tMID(end))*R3*tao(aMID,tMID(Xdim)); %second interior
reflection
                T.T_3(Ydim,Xdim,Zdim) = (1-R1)*tao(aTOP,tTOP(end))*(1-R2)*tao(aMID,tMID(end))^2*R3*tao(aTOP,tTOP(Xdim)); %follow second
reflection to top layer
                T.T3(Ydim,Xdim,Zdim) = (1-R1)*tao(aTOP,tTOP(end))*(1-R2)*tao(aMID,tMID(end))*(1-R3)*tao(aBOT,tBOT(Xdim)); %first pass bot
layer
                T.Tlost(Ydim,Zdim) = (1-R1)*tao(aTOP,tTOP(end))*(1-R2)*tao(aMID,tMID(end))*(1-R3)*tao(aBOT,tBOT(end))*(1-R4); %will be lost
completely
                T.T4(Ydim,Xdim,Zdim) = (1-R1)*tao(aTOP,tTOP(end))*(1-R2)*tao(aMID,tMID(end))*(1-
R3)*tao(aBOT,tBOT(end))*R4*tao(aBOT,tBOT(Xdim)); %second pass bot layer
                T.T5(Ydim,Xdim,Zdim) = (1-R1)*tao(aTOP,tTOP(end))*(1-R2)*tao(aMID,tMID(end))*(1-
R3)^2*tao(aBOT,tBOT(end))^2*R4*tao(aMID,tMID(Xdim)); %second pass mid layer
                T.T6(Ydim,Xdim,Zdim) = (1-R1)*tao(aTOP,tTOP(end))*(1-R2)^2*tao(aMID,tMID(end))^2*(1-
R3)^2*tao(aBOT,tBOT(end))^2*R4*tao(aTOP,tTOP(Xdim)); %second pass top layer
                T.Trecy(Ydim,Zdim) = (1-R1)^2*(1-R2)^2*(1-R3)^2*R4*tao(aTOP,tTOP(end))^2*tao(aMID,tMID(end))^2*tao(aBOT,tBOT(end))^2; %sent
back to emitter
                T.ThirdPass(Ydim,Zdim) = (1-R1)*R1*(1-R2)^2*(1-R3)^2*R4*tao(aTOP,tTOP(end))^2*tao(aMID,tMID(end))^2*tao(aBOT,tBOT(end))^2;
%anything reflected back from front face
            end
            Atot.max(Ydim,Zdim) = abs(1-R1-T.Tlost(Ydim,Zdim)-T.Trecy(Ydim,Zdim)-T.ThirdPass(Ydim,Zdim));
            %Asum = A1+A2
            %A1 = (1-R1-Tfirst)
            %A2 = (1-R1-A1(end)-Tlost-Tsecond)
            A1TOP(Ydim,:,Zdim) = 1-R1-T.T1(Ydim,:,Zdim);
            A1MID(Ydim,:,Zdim) = 1-R1-T.T2(Ydim,:,Zdim);
            A1BOT(Ydim,:,Zdim) = 1-R1-T.T3(Ydim,:,Zdim);
            A2BOT(Ydim,:,Zdim) = 1-R1-A1BOT(Ydim,end,Zdim)-T.Tlost(Ydim,Zdim)-flip(T.T4(Ydim,:,Zdim));
            A2MID(Ydim,:,Zdim) = 1-R1-A1BOT(Ydim,end,Zdim)-T.Tlost(Ydim,Zdim)-flip(T.T5(Ydim,:,Zdim));
            A2TOP(Ydim,:,Zdim) = 1-R1-A1BOT(Ydim,end,Zdim)-T.Tlost(Ydim,Zdim)-flip(T.T6(Ydim,:,Zdim));
            A_1TOP(Ydim,:,Zdim) = 1-R1-A1TOP(Ydim,end,Zdim)-T.T2(Ydim,1,Zdim)-flip(T.T_1(Ydim,:,Zdim));
            A_1MID(Ydim,:,Zdim) = 1-R1-A1MID(Ydim,end,Zdim)-T.T3(Ydim,1,Zdim)-flip(T.T_2(Ydim,:,Zdim));
            A_2TOP(Ydim,:,Zdim) = 1-R1-A1MID(Ydim,end,Zdim)-T.T3(Ydim,1,Zdim)-flip(T.T_2(Ydim,end,Zdim))-(T.T_2(Ydim,end,Zdim)*R1)-
flip(T.T_3(Ydim,:,Zdim));
            %combine slices for each layer
            Atot.TOP(Ydim,:,Zdim) = abs(A1TOP(Ydim,:,Zdim)+A2TOP(Ydim,:,Zdim)+A_1TOP(Ydim,:,Zdim)+A_2TOP(Ydim,:,Zdim));
            Atot.MID(Ydim,:,Zdim) = abs(A1MID(Ydim,:,Zdim)+A2MID(Ydim,:,Zdim)+A_1MID(Ydim,:,Zdim));
            Atot.BOT(Ydim,:,Zdim) = abs(A1BOT(Ydim,:,Zdim)+A2BOT(Ydim,:,Zdim));
            %differentiate Atot to get position of photons absorbed
            ABS.TOP(Ydim,1,Zdim) = 0;
            ABS.MID(Ydim,1,Zdim) = (Atot.TOP(Ydim,end,Zdim)-Atot.TOP(Ydim,end-1,Zdim));
            ABS.BOT(Ydim,1,Zdim) = (Atot.MID(Ydim,end,Zdim)-Atot.MID(Ydim,end-1,Zdim));
            %ABS.MID(Ydim,1,Zdim) = (Atot.TOP(Ydim,end,Zdim)-Atot.TOP(Ydim,end-1,Zdim))/(tTOP(end)-tTOP(end-1));
            %ABS.BOT(Ydim,1,Zdim) = (Atot.MID(Ydim,end,Zdim)-Atot.MID(Ydim,end-1,Zdim))/(tMID(end)-tMID(end-1));
            for Xdim = 2:depth
                ABS.TOP(Ydim,Xdim,Zdim) = (Atot.TOP(Ydim,Xdim,Zdim)-Atot.TOP(Ydim,Xdim-1,Zdim));
                ABS.MID(Ydim,Xdim,Zdim) = (Atot.MID(Ydim,Xdim,Zdim)-Atot.MID(Ydim,Xdim-1,Zdim));
                ABS.BOT(Ydim,Xdim,Zdim) = (Atot.BOT(Ydim,Xdim,Zdim)-Atot.BOT(Ydim,Xdim-1,Zdim));
                % ABS.TOP(Ydim,Xdim,Zdim) = (Atot.TOP(Ydim,Xdim,Zdim)-Atot.TOP(Ydim,Xdim-1,Zdim))/(tTOP(Xdim)-tTOP(Xdim-1));
                % ABS.MID(Ydim,Xdim,Zdim) = (Atot.MID(Ydim,Xdim,Zdim)-Atot.MID(Ydim,Xdim-1,Zdim))/(tMID(Xdim)-tMID(Xdim-1));
                % ABS.BOT(Ydim,Xdim,Zdim) = (Atot.BOT(Ydim,Xdim,Zdim)-Atot.BOT(Ydim,Xdim-1,Zdim))/(tBOT(Xdim)-tBOT(Xdim-1));
            end
            %show plot of light transmission
            if Defaults.movie
                cla;
                xline(tTOP(end),'--k');
                xline(tTOP(end)+tMID(end),'--k');
                plot(tTOP,T.T1(Ydim,:,Zdim),'Color',[0,0,1]);
                plot(tTOP(end)+tMID,T.T2(Ydim,:,Zdim),'Color',[0,0,1]);
                plot(tTOP(end)+tMID(end)+tBOT,T.T3(Ydim,:,Zdim),'Color',[0,0,1]);
                plot(tTOP(end)+tMID(end)+tBOT,flip(T.T4(Ydim,:,Zdim)),'Color',[1,0,0]);
                plot(tTOP(end)+tMID,flip(T.T5(Ydim,:,Zdim)),'Color',[1,0,0]);
                plot(tTOP,flip(T.T6(Ydim,:,Zdim)),'Color',[1,0,0]);
                legend({'Material Interface','','First Pass','','','Second Pass'},"Location",'southeast','Box','off');
                pause(0.001);
            end
        end
    end
end

function [G] = generateCarriers(Source,ABS,Atot,CELL)
    CTs = length(CELL.CellTemp);
    STs = length(Source.E(1,:));
    depths = length(ABS.TOP(1,:,1));
    G.TOP = zeros(depths,STs,CTs);
    G.MID = zeros(depths,STs,CTs);
    G.BOT = zeros(depths,STs,CTs);
    G.max = zeros(STs,CTs);
    for CT = 1:CTs %each cell temp
        for ST = 1:STs %each temp in source data
            for depth = 1:depths
```

```
                G.TOP(depth,ST,CT) = sum(2*ABS.TOP(:,depth,CT).*(Source.Q(:,ST)*CELL.F12));
                G.MID(depth,ST,CT) = sum(2*ABS.MID(:,depth,CT).*(Source.Q(:,ST)*CELL.F12));
                G.BOT(depth,ST,CT) = sum(2*ABS.BOT(:,depth,CT).*(Source.Q(:,ST)*CELL.F12));
            end
            G.max(ST,CT) = sum(2*Atot.max(:,CT).*Source.Q(:,ST));
        end
    end
    %fix first value of G.TOP
    G.TOP(1,:,:) = G.TOP(2,:,:);
end

function [ExProb,I_sc] = extractCarriers(CELL,G,SRH,Defaults)
    if ~exist('SRH','var')||isempty(SRH)
        switch CELL.TOP.minCarr
            case 'hole'
                topType = ' n-doped';
                botType = ' p-doped';
            case 'elec'
                topType = ' p-doped';
                botType = ' n-doped';
        end
        srhRec = str2double(inputdlg({['What is the Shockley-Reed-Hall recombination lifetime (sec)?',newline,newline,'Top Layer:
',num2str(CELL.TOP.N),topType],...
            'Intrinsic Layer',['Bottom Layer: ',num2str(CELL.BOT.N),botType]},"SRH Recomb Rate",[1 50; 1 50; 1 50]));
        SRH.TOP = srhRec(1);
        SRH.MID = srhRec(2);
        SRH.BOT = srhRec(3);
    end
    M = 1; %photon recycle factor (re-absorb radiative recombination) (values 1-10)
    STs = Defaults.ST_res;
    CTs = Defaults.CT_res;
    depths = Defaults.thick_res;
    ExProb.TOP = zeros(depths,STs,CTs);
    ExProb.MID = ones(depths,STs,CTs); %will be 100% extraction everywhere
    ExProb.BOT = zeros(depths,STs,CTs);
    %equations repeated
    B=@(Eg,T,eps,M_hole,M_elec)  (0.58E-12)*sqrt(eps)*(1/(M_elec+M_hole))^3*(1+(1/M_elec)+(1/M_hole))*(300/T)^(3/2)*Eg^2;
    n_intr=@(Eg,T,M_hole,M_elec)
sqrt(0.5*(Defaults.Const.k1*T/(pi*Defaults.Const.hbar1^2))^3*(M_elec*M_hole)^(3/2))*exp(Eg/(2*Defaults.Const.k1*T));
    CP=@(S,L,D,W,x) cosh(x/L)-(sinh(x/L))*(((S*L/D)*cosh(W/L)+(sinh(W/L)))/((S*L/D)*sinh(W/L)+cosh(W/L)));
    % mu=@(NA,ND)
    for CT = 1:CTs
        temp = CELL.CellTempK(CT);
        Eg.TOP = CELL.TOP.Eg(CT);
        Eg.MID = CELL.MID.Eg(CT);
        Eg.BOT = CELL.BOT.Eg(CT);
        index.TOP = findIndex(CELL.TOP,Eg.TOP,'eV',temp,Defaults);
        index.MID = findIndex(CELL.MID,Eg.MID,'eV',temp,Defaults);
        index.BOT = findIndex(CELL.BOT,Eg.BOT,'eV',temp,Defaults);
        eps.TOP = Defaults.Const.eps0*index.TOP(2)^2;
        eps.MID = Defaults.Const.eps0*index.MID(2)^2;
        eps.BOT = Defaults.Const.eps0*index.BOT(2)^2;
        muE.TOP = CELL.TOP.electons(2)*10000^2; %scale from cm^2 to um^2
        muE.MID = CELL.MID.electons(2)*10000^2;
        muE.BOT = CELL.BOT.electons(2)*10000^2;
        muH.TOP = CELL.TOP.holes(2)*10000^2;
        muH.MID = CELL.MID.holes(2)*10000^2;
        muH.BOT = CELL.BOT.holes(2)*10000^2;
        for ST = 1:STs
            for depth = 1:depths
                N.TOP =
n_intr(Eg.TOP,temp,CELL.TOP.holes(1)*Defaults.Const.Me,CELL.TOP.electons(1)*Defaults.Const.Me)+G.TOP(depth,ST,CT)+CELL.TOP.N;
                N.MID =
n_intr(Eg.MID,temp,CELL.MID.holes(1)*Defaults.Const.Me,CELL.MID.electons(1)*Defaults.Const.Me)+G.MID(depth,ST,CT)+CELL.MID.N;
                N.BOT =
n_intr(Eg.BOT,temp,CELL.BOT.holes(1)*Defaults.Const.Me,CELL.BOT.electons(1)*Defaults.Const.Me)+G.BOT(depth,ST,CT)+CELL.BOT.N;
                lifetime.Rad.TOP = 1/(B(Eg.TOP,temp,eps.TOP,CELL.TOP.holes(1),CELL.TOP.electons(1))*N.TOP);
                lifetime.Rad.MID = 1/(B(Eg.MID,temp,eps.MID,CELL.MID.holes(1),CELL.MID.electons(1))*N.MID);
                lifetime.Rad.BOT = 1/(B(Eg.BOT,temp,eps.BOT,CELL.BOT.holes(1),CELL.BOT.electons(1))*N.BOT);
                lifetime.srh.TOP = SRH.TOP;
                lifetime.srh.MID = SRH.MID;
                lifetime.srh.BOT = SRH.BOT;
                lifetime.eff.TOP = 1/(((1/(M*lifetime.Rad.TOP))+(1/(CELL.TOP.Auger(CT)*N.TOP^2))+(1/lifetime.srh.TOP)));
                lifetime.eff.MID = 1/(((1/(M*lifetime.Rad.MID))+(1/(CELL.MID.Auger(CT)*N.MID^2))+(1/lifetime.srh.MID)));
                lifetime.eff.BOT = 1/(((1/(M*lifetime.Rad.BOT))+(1/(CELL.BOT.Auger(CT)*N.BOT^2))+(1/lifetime.srh.BOT)));
                Delec.TOP = muE.TOP*Defaults.Const.k2*temp/Defaults.Const.q;
                Delec.MID = muE.MID*Defaults.Const.k2*temp/Defaults.Const.q;
                Delec.BOT = muE.BOT*Defaults.Const.k2*temp/Defaults.Const.q;
                Dhole.TOP = muH.TOP*Defaults.Const.k2*temp/Defaults.Const.q;
                Dhole.MID = muH.MID*Defaults.Const.k2*temp/Defaults.Const.q;
                Dhole.BOT = muH.BOT*Defaults.Const.k2*temp/Defaults.Const.q;
                difLenE.TOP = sqrt(Delec.TOP*lifetime.eff.TOP);
                difLenE.MID = sqrt(Delec.MID*lifetime.eff.MID);
                difLenE.BOT = sqrt(Delec.BOT*lifetime.eff.BOT);
                difLenH.TOP = sqrt(Dhole.TOP*lifetime.eff.TOP);
```

```
                difLenH.MID = sqrt(Dhole.MID*lifetime.eff.MID);
                difLenH.BOT = sqrt(Dhole.BOT*lifetime.eff.BOT);
                switch CELL.TOP.minCarr
                    case 'hole'
                        ExProb.TOP(depth,ST,CT) = CP(Defaults.SR(1),difLenH.TOP,Dhole.TOP,CELL.TOP.thick(end),CELL.TOP.thick(end+1-depth));
                        ExProb.BOT(depth,ST,CT) = CP(Defaults.SR(2),difLenE.BOT,Delec.BOT,CELL.BOT.thick(end),CELL.BOT.thick(depth));
                        if
isnan(ExProb.TOP(depth,ST,CT))||isnan(ExProb.BOT(depth,ST,CT))||isinf(ExProb.TOP(depth,ST,CT))||isinf(ExProb.BOT(depth,ST,CT))
                            %large number rounding issue
                            ExProb.TOP(depth,ST,CT) = exp(-CELL.TOP.thick(end+1-depth)/difLenH.TOP);
                            ExProb.BOT(depth,ST,CT) = exp(-CELL.BOT.thick(depth)/difLenE.BOT);
                        end
                    case 'elec'
                        ExProb.TOP(depth,ST,CT) = CP(Defaults.SR(1),difLenE.TOP,Delec.TOP,CELL.TOP.thick(end),CELL.TOP.thick(end+1-depth));
                        ExProb.BOT(depth,ST,CT) = CP(Defaults.SR(2),difLenH.BOT,Dhole.BOT,CELL.BOT.thick(end),CELL.BOT.thick(depth));
                        if
isnan(ExProb.TOP(depth,ST,CT))||isnan(ExProb.BOT(depth,ST,CT))||isinf(ExProb.TOP(depth,ST,CT))||isinf(ExProb.BOT(depth,ST,CT))
                            %large number rounding issue
                            ExProb.TOP(depth,ST,CT) = exp(-CELL.TOP.thick(end+1-depth)/difLenE.TOP);
                            ExProb.BOT(depth,ST,CT) = exp(-CELL.BOT.thick(depth)/difLenH.BOT);
                        end
                end
            end
        end
    end
    I_sc.TOP = G.TOP.*ExProb.TOP*Defaults.Const.q;
    I_sc.MID = G.MID.*ExProb.MID*Defaults.Const.q;
    I_sc.BOT = G.BOT.*ExProb.BOT*Defaults.Const.q;
    I_sc.TOP = sum(I_sc.TOP,1);
    I_sc.MID = sum(I_sc.MID(2:end,:,:),1); %omit the first point to avoid double counting
    I_sc.BOT = sum(I_sc.BOT(2:end,:,:),1);
    I_sc.Total = zeros(STs,CTs);
    for CT = 1:CTs
        for ST = 1:STs
            I_sc.Total(ST,CT) = I_sc.TOP(1,ST,CT)+I_sc.MID(1,ST,CT)+I_sc.BOT(1,ST,CT);
        end
    end

end

function MyMap = makeColorMap(colorStruct,gradients)
    colors = array2table(cell2mat(struct2cell(colorStruct)),'VariableNames',{'R','G','B'});
    MyMap = [colors.R(1),colors.G(1),colors.B(1)];
    mapIndex = 2;
    for color = 2:height(colors)
        start = colors(color-1,:);
        stop = colors(color,:);
        reds = linspace(start.R,stop.R,gradients);
        greens = linspace(start.G,stop.G,gradients);
        blues = linspace(start.B,stop.B,gradients);
        for newcolor = 1:gradients
            MyMap(mapIndex,:) = [reds(newcolor),greens(newcolor),blues(newcolor)];
            mapIndex = mapIndex + 1;
        end
    end
end

function CellParams = loadCellMatl(filename)
if ~exist("filename",'var')
    [filename,~] = uigetfile('*.matl.json','Choose the Material Properties Database File for the PV Cell');
end
    loadedfile = jsondecode(fileread(filename));
    CellParams.Name = filename(1:end-10);
    %check fieldnames to prevent errors
    fnames = fieldnames(loadedfile);
    if ~any(strcmp('Varshni',fnames))
        %prompt user for info
        w = warndlg('Some critical data is missing from your material file. You will be prompted to enter the values next. Please refer to
the user manual for more information if needed.','Matl Data Missing');
        uiwait(w);
        VarshInput = str2double(inputdlg({'Varshni: E_0 (eV)','Varshni: alpha (eV/K)','Varshni: beta (K)'},'Enter Varshni Coefficients',[1
50; 1 50; 1 50]));
        CellParams.Varshni = [VarshInput(1),VarshInput(2),VarshInput(3)];
    else
        CellParams.Varshni = [loadedfile.Varshni(1),loadedfile.Varshni(2),loadedfile.Varshni(3)];
    end
    if ~any(strcmp('Electrons',fnames))
        %prompt user for info
        w = warndlg('Some critical data is missing from your material file. You will be prompted to enter the values next. Please refer to
the user manual for more information if needed.','Matl Data Missing');
        uiwait(w);
        ElecInput = str2double(inputdlg({'Electron effective mass (unitless)','Electron mobility lead coeff.','Electron mobility
intercept'},'Enter Electron Parameters',[1 50; 1 50; 1 50]));
        CellParams.electons = [ElecInput(1),ElecInput(2)];
    else
```

```
        CellParams.electons = loadedfile.Electrons;
    end
    if ~any(strcmp('Holes',fnames))
        %prompt user for info
        w = warndlg('Some critical data is missing from your material file. You will be prompted to enter the values next. Please refer to 
the user manual for more information if needed.','Matl Data Missing');
        uiwait(w);
        HoleInput = str2double(inputdlg({'Hole effective mass (unitless)','Hole mobility lead coeff.','Hole mobility intercept'},'Enter Hole 
Parameters',[1 50; 1 50; 1 50]));
        CellParams.holes = [HoleInput(1),HoleInput(2)];
    else
        CellParams.holes = loadedfile.Holes;
    end
    if ~any(strcmp('Auger',fnames))
        %prompt user for info
        w = warndlg('Some critical data is missing from your material file. You will be prompted to enter the values next. Please refer to 
the user manual for more information if needed.','Matl Data Missing');
        uiwait(w);
        CellParams.Auger = str2double(inputdlg({'Auger lead coeff. (cm^6/s)','Auger exponential'},'Enter Auger Coefficent',[1 50; 1 50]));
    else
        CellParams.Auger = loadedfile.Auger;
    end
    %go through index data
    IndexData = contains(fnames,'Index_');
    if ~any(IndexData)
        w = warndlg('This file does not contain any refractive index data. Program will abort.');
        uiwait(w);
        return
    else
        %strip var names from file to create structure fields
        loopCount = 1;
        for var = 1:length(fnames)
            if IndexData(var)
                VarName = fnames{var};
                CellParams.index.(['K',VarName(7:end)]) = 
table(loadedfile.(fnames{var})(:,1),loadedfile.(fnames{var})(:,2),loadedfile.(fnames{var})(:,3),'VariableNames',{'wvl','n','k'});
                CellParams.indexTemps(loopCount) = str2double(VarName(7:end));
                loopCount = loopCount+1;
            end
        end
    end
end

function makeThermal(SOURCE,PhotonRange,PhotonUnit,STRange,TempUnit)
    figure;
    [maxVals,idx] = max(SOURCE);
    hold on
    mesh(STRange,PhotonRange,SOURCE,'FaceColor','flat');
    scatter3(STRange,PhotonRange(idx),maxVals,10,'green','filled');
    switch PhotonUnit
        case 'nm'
            ylabel(['Photon Wavelength (',PhotonUnit,')']);
        case 'eV'
            ylabel(['Photon Energy (',PhotonUnit,')']);
    end
    xlabel(['Source Temperature (',char(176),TempUnit,')']);
    colormap(hot)
    colorbar
    ylim([min(PhotonRange),max(PhotonRange)]);
    xlim([min(STRange),max(STRange)]);
    switch PhotonUnit
        case 'eV'
            vertPos = min(PhotonRange)+((max(PhotonRange)-min(PhotonRange))*0.95); % 5% from the top
            text(STRange(5),vertPos,max(max(SOURCE)),'Peak Value','Color','green');
        case 'nm'
            vertPos = min(PhotonRange)+((max(PhotonRange)-min(PhotonRange))*0.05); % 5% from the bottom
            text(STRange(5),vertPos,max(max(SOURCE)),'Peak Value','Color','green');
    end
    view(0,90);
    hold off
end

function [TempUnit,TempRange] = DefineSource(Defaults)
SourceDef = uifigure('Name','Define Blackbody Source','WindowStyle','normal','Position',[500 500 300 150]);
UnitBtns = uibuttongroup(SourceDef,'Position',[25 20 50 100],'Title','Units');
b1 = uitogglebutton(UnitBtns,"Text","C","Position",[10 54 30 20]);
b2 = uitogglebutton(UnitBtns,"Text","K","Position",[10 32 30 20]);
b3 = uitogglebutton(UnitBtns,"Text","F","Position",[10 10 30 20]);
btn = uicontrol('Parent',SourceDef,'Position',[200 25 50 30],'String','DONE','Callback',@DoneSource,'BackgroundColor',[0,1,1]);
minLabel = uicontrol('Parent',SourceDef,'Style','text','Position',[90 95 90 20],'HorizontalAlignment','left','String','Min Temperature');
Tmin = uieditfield(SourceDef,'numeric','Position',[90 75 50 20],'Limits',[-inf,inf],'Value',Defaults.STmin);
maxLabel = uicontrol('Parent',SourceDef,'Style','text','Position',[90 45 90 20],'HorizontalAlignment','left','String','Max Temperature');
Tmax = uieditfield(SourceDef,'numeric','Position',[90 25 50 20],'Limits',[-inf,inf],'Value',Defaults.STmax);
uiwait(SourceDef);
    function DoneSource(~,event)
```

```
        TempUnit = UnitBtns.SelectedObject.Text;
        TempRange = linspace(Tmin.Value,Tmax.Value,Defaults.ST_res);
        delete(SourceDef);
    end
end

function [PhotonUnit,PhotonRange] = DefineSpectrum(Defaults)
SpectDef = uifigure('Name','Define Optical Spectrum','WindowStyle','normal','Position',[500 500 300 150]);
UnitBtns = uibuttongroup(SpectDef,'Position',[25 20 50 100],'Title','Units','SelectionChangedFcn',@updateUnits);
b1 = uitogglebutton(UnitBtns,"Text","nm","Position",[10 54 30 20]);
b2 = uitogglebutton(UnitBtns,"Text","eV","Position",[10 32 30 20]);
btn = uicontrol('Parent',SpectDef,'Position',[210 25 50 30],'String','DONE','Callback',@DoneSpect,'BackgroundColor',[0,1,1]);
minLabel = uicontrol('Parent',SpectDef,'Style','text','Position',[90 95 90 20],'HorizontalAlignment','left','String','Minimum Value');
Smin = uieditfield(SpectDef,'numeric','Position',[90 75 50 20],'Limits',[0,inf],'Value',Defaults.SPmin);
maxLabel = uicontrol('Parent',SpectDef,'Style','text','Position',[90 45 90 20],'HorizontalAlignment','left','String','Maximum Value');
Smax = uieditfield(SpectDef,'numeric','Position',[90 25 50 20],'Limits',[0,inf],'Value',Defaults.SPmax);
resLabel = uicontrol('Parent',SpectDef,'Style','text','Position',[180 95 110 20],'HorizontalAlignment','left','String','Specturm
Resolution');
Sres = uieditfield(SpectDef,'numeric','Position',[180 75 50 20],'Limits',[0,inf],'Value',Defaults.Spect_res);
unitLabel = uicontrol('Parent',SpectDef,'Style','text','Position',[232 75 20 20],'HorizontalAlignment','left','String','nm');
uiwait(SpectDef);
    function DoneSpect(~,event)
        PhotonUnit = UnitBtns.SelectedObject.Text;
        PhotonRange = [Smin.Value:Sres.Value:Smax.Value];
        delete(SpectDef);
    end
    function updateUnits(~,event)
        unitLabel.String = event.NewValue.Text;
        if strcmp(event.NewValue.Text,'eV')
            Sres.Limits = [0,0.2];
            Smin.Limits = [0,6.2];
            Smax.Limits = [0,6.2];
        end
        if strcmp(event.NewValue.Text,'nm')
            Sres.Limits = [1,inf];
            Smin.Limits = [200,inf];
            Smax.Limits = [200,inf];
        end
    end
end

function SOURCE2 = FilterSource(SOURCE,PhotonUnit,PhotonRange,TempRange,TempUnit)
FiltDef = uifigure('Name','Define Optical Filter','WindowStyle','normal','Position',[500 500 600 300]);
btn = uicontrol('Parent',FiltDef,'Position',[530 30 50 30],'String','DONE','Callback',@DoneFilt,'BackgroundColor',[0,1,1]);
btn2 = uicontrol('Parent',FiltDef,'Position',[530 70 50 30],'String','APPLY','Callback',@ApplyFilt,'BackgroundColor',[0,1,0]);
btn3 = uicontrol('Parent',FiltDef,'Position',[530 110 50 30],'String','CHECK','Callback',@checkProfile,'BackgroundColor',[1,0,1]);
inputLabel = uicontrol('Parent',FiltDef,'Style','text','Position',[10 275 200 20],'HorizontalAlignment','left','String','Select Input Source
to Filter');
dd1 = uidropdown(FiltDef,'Position',[10 260 210 20],'Items',["Start from Original Source","Continue from Last Filter
Applied"],'BackgroundColor',[1,1,1]);
typeLabel = uicontrol('Parent',FiltDef,'Style','text','Position',[240 275 200 20],'HorizontalAlignment','left','String','Select Filter
Type');
dd2 = uidropdown(FiltDef,'Position',[240 260 190 20],'Items',["Database Option","Uniform Scaling","File
Upload"],'ValueChangedFcn',@FiltType,'BackgroundColor',[1,1,1]);
scaleLabel = uicontrol('Parent',FiltDef,'Style','text','Position',[450 275 100 20],'HorizontalAlignment','left','String','Scaling Percent');
scale = uieditfield(FiltDef,'numeric','Position',[450 260 50 20],'Limits',[0,100],'Value',90);
prcntLabel = uicontrol('Parent',FiltDef,'Style','text','Position',[503 257 30 20],'HorizontalAlignment','left','String','%');
switch PhotonUnit
    case 'eV'
        lims = [0,6.2];
        defVal = 0;
    case 'nm'
        lims = [200,inf];
        defVal = 200;
end
%database filter options
DBopt = uipanel(FiltDef,'Position',[10 10 500 240],'Title','Database Filter Construction Options');
BGLabel = uicontrol('Parent',DBopt,'Style','text','Position',[10 185 80 20],'HorizontalAlignment','left','String','Bandgap Cutoff');
BGap = uieditfield(DBopt,'numeric','Position',[100 190 50 20],'Limits',lims,'Value',defVal);
unitLabel1 = uicontrol('Parent',DBopt,'Style','text','Position',[155 185 30 20],'HorizontalAlignment','left','String',PhotonUnit);
Shape = uibuttongroup(DBopt,'Position',[10 120 480 60],'Title','Emissivity Profile Shape','SelectionChangedFcn',@NewOpts);
b1 = uitogglebutton(Shape,"Text","Square","Position",[10 10 100 20]);
b2 = uitogglebutton(Shape,"Text","Gaussian","Position",[120 10 100 20]);
b3 = uitogglebutton(Shape,"Text","Decaying","Position",[230 10 100 20]);
wLabel = uicontrol('Parent',DBopt,'Style','text','Position',[20 90 90 20],'HorizontalAlignment','left','String','Width');
width = uieditfield(DBopt,'numeric','Position',[20 75 50 20],'Limits',[0,inf],'Value',0);
unitLabel2 = uicontrol('Parent',DBopt,'Style','text','Position',[75 70 30 20],'HorizontalAlignment','left','String',PhotonUnit);
sigLabel = uicontrol('Parent',DBopt,'Style','text','Position',[150 90 90 20],'HorizontalAlignment','left','String','Sigma');
sigma = uieditfield(DBopt,'numeric','Position',[150 75 50 20],'Limits',[0,inf],'Value',0);
unitLabel3 = uicontrol('Parent',DBopt,'Style','text','Position',[205 70 30 20],'HorizontalAlignment','left','String',PhotonUnit);
zLabel = uicontrol('Parent',DBopt,'Style','text','Position',[150 45 90 20],'HorizontalAlignment','left','String','Z-score');
Zscore = uieditfield(DBopt,'numeric','Position',[150 30 50 20],'Limits',[0,4],'Value',2);
DecayBtn = uibuttongroup(DBopt,"Title",'Decay Profile','Position',[240 10 120 100],'SelectionChangedFcn',@NewOpts);
bb1 = uitogglebutton(DecayBtn,"Text","Linear","Position",[10 52 100 20]);
bb2 = uitogglebutton(DecayBtn,"Text","Exponential","Position",[10 30 100 20]);
```

```
bb3 = uitogglebutton(DecayBtn,"Text","Hyperbolic","Position",[10 8 100 20]);
magLabel = uicontrol('Parent',DBopt,'Style','text','Position',[380 80 90 30],'HorizontalAlignment','left','String','Magnitude of Curvature');
magnitude = uieditfield(DBopt,'numeric','Position',[380 60 50 20],'Limits',[1,inf],'Value',1);
FiltType;
uiwait(FiltDef);
    function FiltType(~,event)
        switch dd2.Value
            case 'Database Option'
                DBopt.Enable = 'on';
                scale.Enable = 'off';
                NewOpts
            case "Uniform Scaling"
                DBopt.Enable = 'off';
                scale.Enable = 'on';
            case 'File Upload'
                m = msgbox('This feature is not yet supported. Please choose another option.','Missing Source Code');
                uiwait(m);
                dd2.Value = "Uniform Scaling";
                FiltType;
        end
    end

    function NewOpts(~,event)
        switch Shape.SelectedObject.Text
            case 'Square'
                width.Enable = 'on';
                sigma.Enable = 'off';
                Zscore.Enable = 'off';
                DecayBtn.Enable = 'off';
                magnitude.Enable = 'off';
            case 'Gaussian'
                width.Enable = 'off';
                sigma.Enable = 'on';
                Zscore.Enable = 'on';
                DecayBtn.Enable = 'off';
                magnitude.Enable = 'off';
            case 'Decaying'
                width.Enable = 'off';
                sigma.Enable = 'off';
                Zscore.Enable = 'off';
                DecayBtn.Enable = 'on';
                magnitude.Enable = 'off';
                switch DecayBtn.SelectedObject.Text
                    case 'Linear'
                        %do nothing else
                    case 'Exponential'
                        magnitude.Enable = 'on';
                    case 'Hyperbolic'
                        width.Enable = 'on';
                        magnitude.Enable = 'on';
                end
        end
    end

    function profile = MakeProfile(~,event)
        if strcmp(dd2.Value,"Uniform Scaling")
            profile = ones(1,length(PhotonRange))*(scale.Value/100);
        else
            switch Shape.SelectedObject.Text
                case 'Square'
                    switch PhotonUnit
                        case 'nm'
                            profile = PhotonRange<=BGap.Value;
                            fix = PhotonRange<(BGap.Value-width.Value);
                            profile = profile-fix;
                        case 'eV'
                            profile = PhotonRange>=BGap.Value;
                            fix = PhotonRange>(BGap.Value+width.Value);
                            profile = profile-fix;
                    end
                case 'Gaussian'
                    %f(x) = ae^(-(x-mu)^2)/2*sigma^2), a=1, mu=center, sigma=std dev
                    Gauss = @(x,mu) exp(-(((x-mu).^2)/(2*sigma.Value^2)));
                    switch PhotonUnit
                        case 'nm'
                            mu = BGap.Value-(Zscore.Value*sigma.Value);
                            profile = Gauss(PhotonRange,mu);
                        case 'eV'
                            mu = BGap.Value+(Zscore.Value*sigma.Value);
                            profile = Gauss(PhotonRange,mu);
                    end
                case 'Decaying'
                    switch DecayBtn.SelectedObject.Text
                        case 'Linear'
                            switch PhotonUnit
```

```
                            case 'nm'
                                profile = double(PhotonRange<=BGap.Value);
                                slope = 1/(BGap.Value-PhotonRange(1));
                                for a = 1:length(profile)
                                    if profile(a)==1
                                        profile(a) = profile(a)-(BGap.Value-PhotonRange(a))*slope;
                                    end
                                end
                            case 'eV'
                                profile = double(PhotonRange>=BGap.Value);
                                slope = 1/(PhotonRange(end)-BGap.Value);
                                for a = 1:length(profile)
                                    if profile(a)==1
                                        profile(a) = profile(a)-(PhotonRange(a)-BGap.Value)*slope;
                                    end
                                end
                        end
                    case 'Exponential'
                        switch PhotonUnit
                            case 'nm'
                                profile = double(PhotonRange<=BGap.Value);
                                for a = 1:length(profile)
                                    if profile(a)==1
                                        profile(a) = exp(-magnitude.Value*(BGap.Value-PhotonRange(a)));
                                    end
                                end
                            case 'eV'
                                profile = double(PhotonRange>=BGap.Value);
                                for a = 1:length(profile)
                                    if profile(a)==1
                                        profile(a) = exp(-magnitude.Value*(PhotonRange(a)-BGap.Value));
                                    end
                                end
                        end
                    case 'Hyperbolic'
                        switch PhotonUnit
                            case 'nm'
                                cutoff = BGap.Value-width.Value;
                                profile = double(PhotonRange<=BGap.Value);
                                for a = 1:length(profile)
                                    if profile(a)==1
                                        if PhotonRange(a)>=cutoff
                                            profile(a) = ((PhotonRange(a)^magnitude.Value-
cutoff^magnitude.Value)^(1/magnitude.Value))/cutoff;
                                        else
                                            profile(a) = 0;
                                        end
                                    end
                                end
                            case 'eV'
                                cutoff = BGap.Value+width.Value;
                                profile = double(PhotonRange>=BGap.Value);
                                for a = 1:length(profile)
                                    if profile(a)==1
                                        if PhotonRange(a)<=cutoff
                                            profile(a) = ((cutoff^magnitude.Value-
PhotonRange(a)^magnitude.Value)^(1/magnitude.Value))/cutoff;
                                        else
                                            profile(a) = 0;
                                        end
                                    end
                                end
                        end
                end
            end
        end
    end

    function checkProfile(~,event)
        profile = MakeProfile;
        figure;
        plot(PhotonRange,profile);
        hold on
        ylim([0,1]);
        xlim([min(PhotonRange),max(PhotonRange)]);
        xlabel(['Photon Range (',PhotonUnit,')']);
        ylabel('Emissivity of Filter');
        hold off
    end

    function ApplyFilt(~,event)
        profile = MakeProfile;
        switch dd1.Value
            case "Start from Original Source" %use input Source
                SOURCE2.E = SOURCE.E.*profile';
```

```
                SOURCE2.Q = SOURCE.Q.*profile';
            case "Continue from Last Filter Applied" %use recent Source
                if ~exist("SOURCE2",'var')
                    SOURCE2.E = SOURCE.E;
                    SOURCE2.Q = SOURCE.Q;
                end
                SOURCE2.E = SOURCE2.E.*profile';
                SOURCE2.Q = SOURCE2.Q.*profile';
        end
        makeThermal(SOURCE2.E,PhotonRange,PhotonUnit,TempRange,TempUnit);
        makeThermal(SOURCE2.Q,PhotonRange,PhotonUnit,TempRange,TempUnit);
    end

    function DoneFilt(~,event)
        if ~exist("SOURCE2",'var')
            profile = MakeProfile;
            SOURCE2.E = SOURCE.E.*profile';
            SOURCE2.Q = SOURCE.Q.*profile';
        end
        delete(FiltDef);
    end
end

function CELL = DefineCell(TempUnit,Defaults)
CellDef = uifigure('Name','Define PV Cell','WindowStyle','normal','Position',[500 500 600 240]);
btn = uicontrol('Parent',CellDef,'Position',[530 170 50 30],'String','DONE','Callback',@DoneCell,'BackgroundColor',[0,1,1]);
NA_Label = uicontrol('Parent',CellDef,'Style','text','Position',[390 132 50 20],'HorizontalAlignment','center','String','NA');
NA_top = uieditfield(CellDef,'numeric','Position',[390 110 50 20],'Limits',[0,inf],'Value',0);
NA_mid = uieditfield(CellDef,'numeric','Position',[390 85 50 20],'Limits',[0,inf],'Value',0);
NA_bot = uieditfield(CellDef,'numeric','Position',[390 60 50 20],'Limits',[0,inf],'Value',0);
ND_Label = uicontrol('Parent',CellDef,'Style','text','Position',[460 132 50 20],'HorizontalAlignment','center','String','ND');
ND_top = uieditfield(CellDef,'numeric','Position',[460 110 50 20],'Limits',[0,inf],'Value',0);
ND_mid = uieditfield(CellDef,'numeric','Position',[460 85 50 20],'Limits',[0,inf],'Value',0);
ND_bot = uieditfield(CellDef,'numeric','Position',[460 60 50 20],'Limits',[0,inf],'Value',0);
t_Label = uicontrol('Parent',CellDef,'Style','text','Position',[530 132 60 20],'HorizontalAlignment','left','String','Thick (um)');
t_top = uieditfield(CellDef,'numeric','Position',[530 110 50 20],'Limits',[0,inf],'Value',1);
t_mid = uieditfield(CellDef,'numeric','Position',[530 85 50 20],'Limits',[0,inf],'Value',1);
t_bot = uieditfield(CellDef,'numeric','Position',[530 60 50 20],'Limits',[0,inf],'Value',1);
Matl_files = dir('*.matl.json');
Materials = {Matl_files.name};
dd_Label = uicontrol('Parent',CellDef,'Style','text','Position',[120 132 250 20],'HorizontalAlignment','center','String','Material Selection
(light incident on this side)');
dd_top = uidropdown(CellDef,'Position',[120 110 250 20],'Items',Materials,'BackgroundColor',[1,1,1]);
dd_mid = uidropdown(CellDef,'Position',[120 85 250 20],'Items',Materials,'BackgroundColor',[1,1,1]);
dd_bot = uidropdown(CellDef,'Position',[120 60 250 20],'Items',Materials,'BackgroundColor',[1,1,1]);
dd_sub = uidropdown(CellDef,'Position',[120 20 250 20],'Items',Materials,'BackgroundColor',[1,1,1]);
top_Label = uicontrol('Parent',CellDef,'Style','text','Position',[105 100 10 20],'HorizontalAlignment','right','String','n');
mid_Label = uicontrol('Parent',CellDef,'Style','text','Position',[105 85 10 20],'HorizontalAlignment','right','String','i');
bot_Label = uicontrol('Parent',CellDef,'Style','text','Position',[105 60 10 20],'HorizontalAlignment','right','String','p');
sub_Label = uicontrol('Parent',CellDef,'Style','text','Position',[15 20 100 20],'HorizontalAlignment','right','String','substrate');
StackBtn = uibuttongroup(CellDef,"Title",'Junction','Position',[10 60 80 80],'SelectionChangedFcn',@labelChange);
b1 = uitogglebutton(StackBtn,"Text","n / i / p","Position",[10 32 60 20]);
b2 = uitogglebutton(StackBtn,"Text","p / i / n","Position",[10 10 60 20]);
Tmax_Label = uicontrol('Parent',CellDef,'Style','text','Position',[20 200 80 20],'HorizontalAlignment','right','String','Max Cell Temp');
Tmax = uieditfield(CellDef,'numeric','Position',[110 200 50 20],'Limits',Defaults.CTlims,'Value',Defaults.CTmax);
tempLabel1 = uicontrol('Parent',CellDef,'Style','text','Position',[165 200 20
20],'HorizontalAlignment','left','String',[char(176),TempUnit]);
Tmin_Label = uicontrol('Parent',CellDef,'Style','text','Position',[20 170 80 20],'HorizontalAlignment','right','String','Min Cell Temp');
Tmin = uieditfield(CellDef,'numeric','Position',[110 170 50 20],'Limits',Defaults.CTlims,'Value',Defaults.CTmin);
tempLabel2 = uicontrol('Parent',CellDef,'Style','text','Position',[165 170 20
20],'HorizontalAlignment','left','String',[char(176),TempUnit]);
ARC_Label = uicontrol('Parent',CellDef,'Style','text','Position',[200 190 80 20],'HorizontalAlignment','left','String','ARC Trans.');
ARC = uieditfield(CellDef,'numeric','Position',[200 170 50 20],'Limits',[0,1],'Value',Defaults.ARC);
BSR_Label = uicontrol('Parent',CellDef,'Style','text','Position',[270 190 80 20],'HorizontalAlignment','left','String','BRS Refle.');
BSR = uieditfield(CellDef,'numeric','Position',[270 170 50 20],'Limits',[0,1],'Value',Defaults.BSR);
ARC_check = uicheckbox(CellDef,'Text','Has Anti-Reflective Coating?','Position',[340 190 170 20]);
BSR_check = uicheckbox(CellDef,'Text','Has Backside Reflector?','Position',[340 170 170 20]);
labelChange;
uiwait(CellDef);
    function labelChange(~,event)
        switch StackBtn.SelectedObject.Text
            case 'n / i / p'
                top_Label.String = 'n';
                bot_Label.String = 'p';
                % remove confusion
                NA_top.Editable = 'off';
                NA_top.Value = 0;
                ND_bot.Editable = 'off';
                ND_bot.Value = 0;
                % allow changes
                ND_top.Editable = 'on';
                NA_bot.Editable = 'on';
            case 'p / i / n'
                top_Label.String = 'p';
                bot_Label.String = 'n';
```

```
                % remove confusion
                ND_top.Editable = 'off';
                ND_top.Value = 0;
                NA_bot.Editable = 'off';
                NA_bot.Value = 0;
                % allow changes
                NA_top.Editable = 'on';
                ND_bot.Editable = 'on';
            end
        end
        function DoneCell(~,event)
            CELL.top = {dd_top.Value,NA_top.Value+ND_top.Value,t_top.Value};
            CELL.TOP = loadCellMatl(CELL.top{1});
            CELL.mid = {dd_mid.Value,NA_mid.Value+ND_mid.Value,t_mid.Value};
            CELL.MID = loadCellMatl(CELL.mid{1});
            CELL.bot = {dd_bot.Value,NA_bot.Value+ND_bot.Value,t_bot.Value};
            CELL.BOT = loadCellMatl(CELL.bot{1});
            CELL.SUB = loadCellMatl(dd_sub.Value);
            CELL.CellTemp = linspace(Tmin.Value,Tmax.Value,Defaults.CT_res);
            CELL.TOP.thick = linspace(0,CELL.top{3},Defaults.thick_res);
            CELL.MID.thick = linspace(0,CELL.mid{3},Defaults.thick_res);
            CELL.BOT.thick = linspace(0,CELL.bot{3},Defaults.thick_res);
            switch TempUnit
                case 'K'
                    CELL.CellTempK = CELL.CellTemp;
                case 'C'
                    CELL.CellTempK = CELL.CellTemp+273.15;
                case 'F'
                    CELL.CellTempK = (CELL.CellTemp-32)*(5/9) + 273.15;
            end
            switch StackBtn.SelectedObject.Text
                case 'n / i / p'
                    CELL.TOP.minCarr = 'hole';
                    CELL.BOT.minCarr = 'elec';
                case 'p / i / n'
                    CELL.TOP.minCarr = 'elec';
                    CELL.BOT.minCarr = 'hole';
            end
            CELL.TOP.N = ND_top.Value+NA_top.Value;
            CELL.MID.N = ND_mid.Value+NA_mid.Value;
            CELL.BOT.N = ND_bot.Value+NA_bot.Value;
            CELL.TOP.Eg = CELL.TOP.Varshni(1) - ((CELL.TOP.Varshni(2)*CELL.CellTempK.^2)./(CELL.CellTempK+CELL.TOP.Varshni(3)));
            CELL.MID.Eg = CELL.MID.Varshni(1) - ((CELL.MID.Varshni(2)*CELL.CellTempK.^2)./(CELL.CellTempK+CELL.MID.Varshni(3)));
            CELL.BOT.Eg = CELL.BOT.Varshni(1) - ((CELL.BOT.Varshni(2)*CELL.CellTempK.^2)./(CELL.CellTempK+CELL.BOT.Varshni(3)));
            CELL.TOP.Auger = CELL.TOP.Auger(1)*exp(CELL.TOP.Auger(2).*CELL.TOP.Eg);
            CELL.MID.Auger = CELL.MID.Auger(1)*exp(CELL.MID.Auger(2).*CELL.MID.Eg);
            CELL.BOT.Auger = CELL.BOT.Auger(1)*exp(CELL.BOT.Auger(2).*CELL.BOT.Eg);
            CELL.TOP.electons = [CELL.TOP.electons(1),CELL.TOP.electons(2)*log(CELL.TOP.N)+CELL.TOP.electons(3)];
            CELL.MID.electons = [CELL.MID.electons(1),CELL.MID.electons(2)*log(CELL.MID.N)+CELL.MID.electons(3)];
            CELL.BOT.electons = [CELL.BOT.electons(1),CELL.BOT.electons(2)*log(CELL.BOT.N)+CELL.BOT.electons(3)];
            CELL.TOP.holes = [CELL.TOP.holes(1),CELL.TOP.holes(2)*log(CELL.TOP.N)+CELL.TOP.holes(3)];
            CELL.MID.holes = [CELL.MID.holes(1),CELL.MID.holes(2)*log(CELL.MID.N)+CELL.MID.holes(3)];
            CELL.BOT.holes = [CELL.BOT.holes(1),CELL.BOT.holes(2)*log(CELL.BOT.N)+CELL.BOT.holes(3)];
            if ARC_check.Value
                CELL.ARC = true;
                CELL.ARCprct = ARC.Value;
            else
                CELL.ARC = false;
                CELL.ARCprct = [];
            end
            if BSR_check.Value
                CELL.BSR = true;
                CELL.BSRprct = BSR.Value;
            else
                CELL.BSR = false;
                CELL.BSRprct = [];
            end
            delete(CellDef);
        end
    end

    function ExamineCell(ABS,Atot,T,CELL,PhotonRange,PhotonUnit,TempUnit)
    AvD = uifigure('Name','Examine Cell','WindowStyle','normal','Position',[500 500 1100 900]);
    ax1 = uiaxes(AvD,'Position',[40,120,450,350]); %abs v depth
    hold(ax1,'on');
    title(ax1,'Absorption vs Cell Depth');
    ylim(ax1,'auto');
    xlim(ax1,[0,CELL.TOP.thick(end)+CELL.MID.thick(end)+CELL.BOT.thick(end)]);
    xlabel(ax1,'Depth of Cell (microns)');
    ylabel(ax1,'Total Absorbed Photons (%)');
    ax2 = uiaxes(AvD,'Position',[600,120,450,350]); %transmission plot
    hold(ax2,'on');
    title(ax2,'Transmission vs Cell Depth');
    ylim(ax2,[0,1]);
    xlim(ax2,[0,CELL.TOP.thick(end)+CELL.MID.thick(end)+CELL.BOT.thick(end)]);
```

```
xlabel(ax2,'Depth of Cell (microns)');
ylabel(ax2,'Normalized Transmission');
ax3 = uiaxes(AvD,'Position',[40,500,450,350]); %abs v wvl
hold(ax3,'on');
grid(ax3,'on');
title(ax3,'Absorption vs Wavelength');
ylim(ax3,'auto');
xlim(ax3,[PhotonRange(1),PhotonRange(end)]);
switch PhotonUnit
    case 'nm'
        xlabel(ax3,['Wavelength (',PhotonUnit,')']);
    case 'eV'
        xlabel(ax3,['Photon Energy (',PhotonUnit,')']);
end
ylabel(ax3,'Total Absorbed Photons (%)');
ax4 = uiaxes(AvD,'Position',[600,500,450,350]); %Eg v CT
hold(ax4,'on');
grid(ax4,'on');
title(ax4,'Bandgap vs Cell Temp');
ylim(ax4,'auto');
xlim(ax4,[CELL.CellTemp(1),CELL.CellTemp(end)]);
xlabel(ax4,['Cell Temperature (',TempUnit,')']);
ylabel(ax4,'Bandgap Energy (eV)');
CTBtn = uibuttongroup(AvD,"Title",'Cell Temp','Position',[500 600 90 140],'SelectionChangedFcn',@updatePlot,'TitlePosition','centertop');
b1 = uitogglebutton(CTBtn,"Text",[num2str(CELL.CellTemp(1)),char(176),TempUnit],"Position",[10 93 70 20]);
b2 = uitogglebutton(CTBtn,"Text",[num2str(CELL.CellTemp(2)),char(176),TempUnit],"Position",[10 71 70 20]);
b3 = uitogglebutton(CTBtn,"Text",[num2str(CELL.CellTemp(3)),char(176),TempUnit],"Position",[10 49 70 20]);
b4 = uitogglebutton(CTBtn,"Text",[num2str(CELL.CellTemp(4)),char(176),TempUnit],"Position",[10 27 70 20]);
b5 = uitogglebutton(CTBtn,"Text",[num2str(CELL.CellTemp(5)),char(176),TempUnit],"Position",[10 5 70 20]);
ALabel = uicontrol('Parent',AvD,'Style','text','Position',[500 230 90 20],'HorizontalAlignment','center','String','ABS Total');
A = uieditfield(AvD,'numeric','Position',[520 210 50
20],'Limits',[0,1],'Value',Atot.max(1,1),'Editable','off','HorizontalAlignment','center','ValueDisplayFormat','%1.4f');
btn = uicontrol('Parent',AvD,'Position',[520 470 50 30],'String','DONE','Callback',@DoneABS,'BackgroundColor',[0,1,1]);
sld = uislider(AvD,'Position',[60 50 1000
3],'Limits',[PhotonRange(1),PhotonRange(end)],'ValueChangingFcn',@updateBox,'ValueChangedFcn',@updateSlide);
AplBtn = uibuttongroup(AvD,"Title",'ABS Plot','Position',[500 265 90 70],'SelectionChangedFcn',@updatePlot,'TitlePosition','centertop');
bb1 = uitogglebutton(AplBtn,"Text",'Cumulative',"Position",[10 27 70 20]);
bb2 = uitogglebutton(AplBtn,"Text",'Positional',"Position",[10 5 70 20]);
switch PhotonUnit
    case 'nm'
        wvlWords = 'Photon Wavelength';
    case 'eV'
        wvlWords = 'Photon Energy';
end
wvlLabel1 = uicontrol('Parent',AvD,'Style','text','Position',[365 80 150 20],'HorizontalAlignment','right','String',wvlWords);
B = uieditfield(AvD,'numeric','Position',[520 80 50
20],'Limits',[PhotonRange(1),PhotonRange(end)],'Value',PhotonRange(1),'HorizontalAlignment','center','ValueChangedFcn',@updateSlide);
wvlLabel1 = uicontrol('Parent',AvD,'Style','text','Position',[575 80 50 20],'HorizontalAlignment','left','String',PhotonUnit);
updatePlot;
uiwait(AvD);
    function updatePlot(~,event)
        %determine temp button pushed (must be a better way)
        switch CTBtn.SelectedObject.Text
            case [num2str(CELL.CellTemp(1)),char(176),TempUnit]
                CT = 1;
            case [num2str(CELL.CellTemp(2)),char(176),TempUnit]
                CT = 2;
            case [num2str(CELL.CellTemp(3)),char(176),TempUnit]
                CT = 3;
            case [num2str(CELL.CellTemp(4)),char(176),TempUnit]
                CT = 4;
            case [num2str(CELL.CellTemp(5)),char(176),TempUnit]
                CT = 5;
        end
        [~,wvl] = min(abs(PhotonRange-B.Value)); %determine wvl selected
        A.Value = Atot.max(wvl,CT);
        %make ABS v Depth plot
        cla(ax1);
        xline(ax1,CELL.TOP.thick(end),'--k');
        xline(ax1,CELL.TOP.thick(end)+CELL.MID.thick(end),'--k');
        switch AplBtn.SelectedObject.Text
            case 'Cumulative'
        plot(ax1,CELL.TOP.thick,Atot.TOP(wvl,:,CT)*100,'LineWidth',2,'Color',[0.5,0.5,0]);
        plot(ax1,CELL.TOP.thick(end)+CELL.MID.thick,Atot.MID(wvl,:,CT)*100,'LineWidth',2,'Color',[0.5,0.5,0]);
        plot(ax1,CELL.TOP.thick(end)+CELL.MID.thick(end)+CELL.BOT.thick,Atot.BOT(wvl,:,CT)*100,'LineWidth',2,'Color',[0.5,0.5,0]);
            case 'Positional'
        plot(ax1,CELL.TOP.thick,ABS.TOP(wvl,:,CT)*100,'LineWidth',2,'Color',[0,0.7,0],'Marker','o','MarkerSize',4);
        plot(ax1,CELL.TOP.thick(end)+CELL.MID.thick,ABS.MID(wvl,:,CT)*100,'LineWidth',2,'Color',[0,0.7,0],'Marker','o','MarkerSize',4);

plot(ax1,CELL.TOP.thick(end)+CELL.MID.thick(end)+CELL.BOT.thick,ABS.BOT(wvl,:,CT)*100,'LineWidth',2,'Color',[0,0.7,0],'Marker','o','MarkerSiz
e',4);
        end

        %make Transmission plot
        cla(ax2);
```

```
        xline(ax2,CELL.TOP.thick(end),'--k');
        xline(ax2,CELL.TOP.thick(end)+CELL.MID.thick(end),'--k');
        plot(ax2,CELL.TOP.thick,T.T1(wvl,:,CT),'Color',[1,0,0],'LineWidth',2);
        plot(ax2,CELL.TOP.thick(end)+CELL.MID.thick,T.T2(wvl,:,CT),'Color',[1,0,0],'LineWidth',2);
        plot(ax2,CELL.TOP.thick(end)+CELL.MID.thick(end)+CELL.BOT.thick,T.T3(wvl,:,CT),'Color',[1,0,0],'LineWidth',2);
        plot(ax2,CELL.TOP.thick,flip(T.T6(wvl,:,CT)),'Color',[0,0,1],'LineWidth',2);
        plot(ax2,CELL.TOP.thick(end)+CELL.MID.thick,flip(T.T5(wvl,:,CT)),'Color',[0,0,1],'LineWidth',2);
        plot(ax2,CELL.TOP.thick(end)+CELL.MID.thick(end)+CELL.BOT.thick,flip(T.T4(wvl,:,CT)),'Color',[0,0,1],'LineWidth',2);
        plot(ax2,CELL.TOP.thick,flip(T.T_1(wvl,:,CT)),'-.','Color',[0.5,0,0.5],'LineWidth',2);
        plot(ax2,CELL.TOP.thick(end)+CELL.MID.thick,flip(T.T_2(wvl,:,CT)),'-.','Color',[0.3,0,0.3],'LineWidth',2);
        plot(ax2,CELL.TOP.thick,flip(T.T_3(wvl,:,CT)),'-.','Color',[0.3,0,0.3],'LineWidth',2);
        legend(ax2,{'','','1st Pass (in)','','','2nd Pass (out)','','','1st Refletion (out)','2nd Reflection (out)'},"Box",'off');

        %make ABS v Wvl plot
        cla(ax3);
        plot(ax3,PhotonRange,Atot.max(:,CT)*100,'LineWidth',2)
        legend(ax3,[num2str(CELL.CellTemp(CT)),char(176),TempUnit],"Box",'off')

        %make Eg plot
        cla(ax4);
        plot(ax4,CELL.CellTemp,CELL.TOP.Eg,'LineWidth',2);
        plot(ax4,CELL.CellTemp,CELL.MID.Eg,'LineWidth',2);
        plot(ax4,CELL.CellTemp,CELL.BOT.Eg,'LineWidth',2);
        switch CELL.TOP.minCarr
            case 'hole'
                toplayer = 'n-layer';
                botlayer = 'p-layer';
            case 'elec'
                toplayer = 'p-layer';
                botlayer = 'n-layer';
        end
        legend(ax4,{toplayer,'intrinsic',botlayer},"Box",'off')
    end

    function updateBox(~,event)
        B.Value = event.Value;
    end

    function updateSlide(~,event)
        %find nearest accepted value
        [~,wvl] = min(abs(PhotonRange-event.Value));
        B.Value = PhotonRange(wvl);
        sld.Value = PhotonRange(wvl);
        updatePlot;
    end

    function DoneABS(~,event)
        delete(AvD);
    end
end

function [CELL,EmArea] = DefineGeom(CELL,Defaults)
GeoDef = uifigure('Name','Define Cell Geometry','WindowStyle','normal','Position',[500 500 320 200]);
ShapeBtn = uibuttongroup(GeoDef,"Title",'SHAPE','Position',[20 90 90 100],'SelectionChangedFcn',@changeLabels);
b1 = uitogglebutton(ShapeBtn,"Text",'Squares',"Position",[10 55 70 20]);
b2 = uitogglebutton(ShapeBtn,"Text",'Cylinder',"Position",[10 30 70 20]);
b3 = uitogglebutton(ShapeBtn,"Text",'Custom',"Position",[10 5 70 20]);
emLabel = uicontrol('Parent',GeoDef,'Style','text','Position',[120 170 100 20],'HorizontalAlignment','right','String','Emitter Width');
ceLabel = uicontrol('Parent',GeoDef,'Style','text','Position',[120 145 100 20],'HorizontalAlignment','right','String','Cell Width');
spLabel = uicontrol('Parent',GeoDef,'Style','text','Position',[120 120 100 20],'HorizontalAlignment','right','String','Spacing');
F12Label = uicontrol('Parent',GeoDef,'Style','text','Position',[120 95 100 20],'HorizontalAlignment','right','String','View Factor (F_12)');
F12 = uieditfield(GeoDef,'numeric','Position',[225 95 50 20],'Limits',[0,1],'Value',0,'Editable','off','ValueChangedFcn',@calcF12);
Em = uieditfield(GeoDef,'numeric','Position',[225 170 50 20],'Limits',[0,inf],'Value',1,'ValueChangedFcn',@calcF12);
Ce = uieditfield(GeoDef,'numeric','Position',[225 145 50 20],'Limits',[0,inf],'Value',1,'ValueChangedFcn',@calcF12);
Sp = uieditfield(GeoDef,'numeric','Position',[225 120 50 20],'Limits',[0,inf],'Value',1,'ValueChangedFcn',@calcF12);
emUnitLabel = uicontrol('Parent',GeoDef,'Style','text','Position',[280 170 30 20],'HorizontalAlignment','left','String','mm');
ceUnitLabel = uicontrol('Parent',GeoDef,'Style','text','Position',[280 145 30 20],'HorizontalAlignment','left','String','mm');
spUnitLabel = uicontrol('Parent',GeoDef,'Style','text','Position',[280 120 30 20],'HorizontalAlignment','left','String','mm');
FF = uieditfield(GeoDef,'numeric','Position',[225 70 50 20],'Limits',[0,1],'Value',Defaults.FF);
FFLabel = uicontrol('Parent',GeoDef,'Style','text','Position',[120 60 100 30],'HorizontalAlignment','right','String','Electrical Fill Factor
(from I-V curve)');
ShapeLabel = uicontrol('Parent',GeoDef,'Style','text','Position',[20 25 150 20],'HorizontalAlignment','left','String','Description of
SHAPE:');
ShapeDesc = uicontrol('Parent',GeoDef,'Style','text','Position',[20 10 280 20],'HorizontalAlignment','left','String','unequal parallel
coaxial squares');
btn = uicontrol('Parent',GeoDef,'Position',[230 30 50 30],'String','DONE','Callback',@DoneGeo,'BackgroundColor',[0,1,1]);
calcF12;
uiwait(GeoDef);
    function changeLabels(~,event)
        switch ShapeBtn.SelectedObject.Text
            case 'Squares'
                emLabel.String = 'Emitter Width';
                emUnitLabel.String = 'mm';
                ceLabel.String = 'Cell Width';
                ceUnitLabel.String = 'mm';
```

```
                spLabel.String = 'Spacing';
                ShapeDesc.String = 'unequal parallel coaxial squares';
                F12.Editable = 'off';
            case 'Cylinder'
                emLabel.String = 'Emitter Radius';
                emUnitLabel.String = 'mm';
                ceLabel.String = 'Cell Radius';
                ceUnitLabel.String = 'mm';
                spLabel.String = 'Cylinder Length';
                ShapeDesc.String = 'coaxial cylinders of equal length';
                F12.Editable = 'off';
            case 'Custom'
                emLabel.String = 'Emitter Area';
                emUnitLabel.String = 'mm^2';
                ceLabel.String = 'Cell Area';
                ceUnitLabel.String = 'mm^2';
                spLabel.String = 'Not Used';
                ShapeDesc.String = 'manual view factor and device area entry';
                F12.Editable = 'on';
        end
        calcF12;
    end

    function calcF12(~,event)
        switch ShapeBtn.SelectedObject.Text
            case 'Squares'
                %%%%%%%%%%%%%%%%%%%%%%%%%%%%%%%%%%%%%%%%%%%%%%%%%%%%%%%
                w1 = Em.Value/Sp.Value;     w2 = Ce.Value/Sp.Value;
                x = w2-w1;                      y = w2+w1;
                u = sqrt(x^2+4);                v = sqrt(y^2+4);
                p = (w1^2+w2^2+2)^2;            q = (x^2+2)*(y^2+2);
                s = u*(x*atan(x/u)-y*atan(y/u));
                t = v*(x*atan(x/v)-y*atan(y/v));
                %%%%%%%%%%%%%%%%%%%%%%%%%%%%%%%%%%%%%%%%%%%%%%%%%%%%%%%
                F12.Value = (1/(pi*w1^2))*(log(p/q)+s-t);
                CELL.Area = Ce.Value^2;
                EmArea = Em.Value^2;
            case 'Cylinder'
                %%%%%%%%%%%%%%%%%%%%%%%%%%%%%%%%%%%%%%%%%%%%%%%%%%%%%%%%%%%%%%%
                r1 = Em.Value;                r2 = Ce.Value;
                h = Sp.Value/r1;              R = r2/r1;
                f1 = h^2+R^2-1;               f2 = h^2-R^2+1;
                f3 = sqrt((f1+2)^2-4*R^2);    f4 = f3*acos(f2/(f1*R))+f2*asin(1/R)-(pi*f1/2);
                %%%%%%%%%%%%%%%%%%%%%%%%%%%%%%%%%%%%%%%%%%%%%%%%%%%%%%%%%%%%%%%
                F12.Value = 1-(1/pi)*(acos(f2/f1)-(f4/(2*h)));
                CELL.Area = 2*pi*Ce.Value*Sp.Value;
                EmArea = 2*pi*Em.Value*Sp.Value;
            case 'Custom'
                CELL.Area = Ce.Value;
                EmArea = Em.Value;
        end
    end

    function DoneGeo(~,event)
        CELL.F12 = F12.Value;
        CELL.FF = FF.Value;
        delete(GeoDef);
    end
end

function EFFIC = ExamineEff(SOURCE2,SOURCE3,CELL,STRange,TempUnit,EffMap)
ExEff = uifigure('Name','Examine Efficiency','WindowStyle','normal','Position',[500 500 700 600]);
btn = uicontrol('Parent',ExEff,'Position',[550 20 100 30],'String','Terminate Program','Callback',@DoneEff,'BackgroundColor',[0,1,1]);
ax1 = uiaxes(ExEff,'Position',[20,80,650,500]); %abs v depth
hold(ax1,'on');
title(ax1,'System Efficiency');
xlim(ax1,[STRange(1),STRange(end)]);
ylim(ax1,[CELL.CellTemp(1),CELL.CellTemp(end)]);
ylabel(ax1,['Cell Temperature (',char(176),TempUnit,')']);
xlabel(ax1,['Source Temperature (',char(176),TempUnit,')']);
colormap(ax1,EffMap)
clim(ax1,'auto');
c = colorbar(ax1);
c.Ruler.TickLabelFormat = '%0.1f%%';
Sin = uibuttongroup(ExEff,"Title",'Efficiency Denominator','Position',[245 15 150
50],'SelectionChangedFcn',@updateEff,'TitlePosition','centertop');
b1 = uitogglebutton(Sin,"Text",'Source2',"Position",[10 5 60 20]);
b2 = uitogglebutton(Sin,"Text",'Source3',"Position",[80 5 60 20]);
STs = length(STRange);
CTs = length(CELL.CellTemp);
EffData = zeros(STs,CTs);
plotres = 500;
updateEff;
uiwait(ExEff);
    function updateEff(~,event)
```

```
        switch Sin.SelectedObject.Text
            case 'Source2'
                S_in = SOURCE2.E;
                ax1.Title.String = 'System Efficiency';
            case 'Source3'
                S_in = SOURCE3.E;
                ax1.Title.String = 'Conversion Efficiency';
        end
        for CT = 1:CTs
            for ST = 1:STs
                EffData(ST,CT) = (CELL.P_el(ST,CT)/sum(S_in(:,ST)))*100;
            end
        end
        %improve plot color resolution
        newX = linspace(STRange(1),STRange(end),plotres);
        newY = linspace(CELL.CellTemp(1),CELL.CellTemp(end),plotres);
        [Xq,Yq] = meshgrid(newX,newY);
        EffFinal = interp2(STRange,CELL.CellTemp,EffData',Xq,Yq,'spline');
        EFFIC.X = newX;
        EFFIC.Y = newY;
        EFFIC.V = EffFinal';
        %generate plot
        cla(ax1);
        mesh(ax1,EFFIC.X,EFFIC.Y,EFFIC.V,'FaceColor','flat');
        view(0,90);
    end

    function DoneEff(~,event)
        delete(ExEff);
    end
end
```

JSON File Generator

```
function ConfigJSON(Struct,defaultPath)
if exist("defaultPath","var")
    filename = uiputfile('*.*','Select the Filename and Path for this Material File',[defaultPath,'_replaceText_.matl.json']);
    path = defaultPath;
else
    [filename,path] = uiputfile('*.*','Select the Filename and Path for this Material File','_replaceText_.matl.json');
end
json = jsonencode(Struct,"PrettyPrint",true);
writelines(json,[path,filename]);
end
```

Microlens Focus Analyzer

Not approved for public release.

Bibliography

1. Andrews, Jonathan R., Sergio R. Restaino, Thomas E. Vandervelde, et al. "Comparison of Long-Wave Infrared Quantum-Dots-in-a-Well and Quantum-Well Focal Plane Arrays." *IEEE Transactions on Electron Devices*, vol. 56, no. 3, Mar. 2009, pp. 512–16.
2. Andrews, Jonathan R., Sergio R. Restaino, Scott W. Teare, et al. "Comparison of Quantum Dots-in-a-Double-Well and Quantum Dots-in-a-Well Focal Plane Arrays in the Long-Wave Infrared." *IEEE Transactions on Electron Devices*, vol. 58, no. 7, July 2011, pp. 2022–27.
3. Aull, Brian F., et al. "Large-Format Geiger-Mode Avalanche Photodiode Arrays and Readout Circuits." *IEEE Journal of Selected Topics in Quantum Electronics*, vol. 24, no. 2, Mar. 2018, pp. 1–10.
4. Aull, Brian F., et al. "Large-Format Image Sensors Based on Custom Geiger-Mode Avalanche Photodiode Arrays." *Optical Sensing, Imaging, and Photon Counting: From X-Rays to THz*, vol. 10729, SPIE, 2018, pp. 20–32.
5. Aull, Brian F., et al. "Mitigation of Optical Crosstalk in Geiger-Mode Avalanche Photodiode Arrays for Lidar." *Advanced Photon Counting Techniques XVI*, vol. 12089, SPIE, 2022, pp. 98–104.
6. Bronzi, Danilo, et al. "SPAD Figures of Merit for Photon-Counting, Photon-Timing, and Imaging Applications: A Review." *IEEE Sensors Journal*, vol. 16, no. 1, Jan. 2016, pp. 3–12.
7. Charbon, Edoardo, et al. "SPAD-Based Sensors." *TOF Range-Imaging Cameras*, edited by Fabio Remondino and David Stoppa, Springer, 2013, pp. 11–38.
8. Chubb, Donald. *Fundamentals of Thermophotovoltaic Energy Conversion*. First Edition, Elsevier, 2007.
9. Chung, Chee Won, et al. "High-Density Plasma Etching of Iridium Thin Films in a $Cl_2/O_2/Ar$ Plasma." *Journal of The Electrochemical Society*.
10. Chung, Chee Won, and Chang Jung Kim. "Effect of Etch Gases on Iridium Etching Using a Hard Mask." *Integrated Ferroelectrics*, vol. 39, no. 1–4, Jan. 2001, pp. 119–26.
11. Cicchi, R., et al. "Multidimensional Custom-Made Non-Linear Microscope: From Ex-Vivo to in-Vivo Imaging." *Applied Physics B*, vol. 92, no. 3, Sep. 2008, pp. 359–65.

12. Fan, Qingbin, et al. “A High Numerical Aperture, Polarization-Insensitive Metalens for Long-Wavelength Infrared Imaging.” *Applied Physics Letters*, vol. 113, no. 20, Nov. 2018, p. 201104.
13. Gramuglia, Francesco, et. al. “A Low-Noise CMOS SPAD Pixel with 12.1 Ps SPTR and 3Ns Dead Time.” *IEEE Journal of Selected Topics in Quantum Electronics*, vol. 28, no. 2. Mar. 2022.
14. Li, Fangzhe, et al. “HgCdTe Mid-Infrared Photo Response Enhanced by Monolithically Integrated Meta-Lenses.” *Scientific Reports*, vol. 10, no. 1, 1, Apr. 2020, p. 6372.
15. Majewska, Ania, et al. “A Custom-Made Two-Photon Microscope and Deconvolution System.” *Pflügers Archiv*, vol. 441, no. 2, Dec. 2000, pp. 398–408.
16. Nussbaum, Ph, et al. “Design, Fabrication and Testing of Microlens Arrays for Sensors and Microsystems.” *Pure and Applied Optics: Journal of the European Optical Society Part A*, vol. 6, no. 6, Nov. 1997, pp. 617–36.
17. Oh, Minsu, and Thomas E. Vandervelde. “Wafer-Area Selective Emitters Based on Optical Interference.” *MRS Advances*, vol. 6, no. 12, Jun. 2021, pp. 327–33.
18. Pfiester, Nicole A., et al. “Effect of Microstructure on the Optical Properties of Sputtered Iridium Thin Films.” *Optical Materials Express*, vol. 10, no. 4, Apr. 2020, p. 1120.
19. Pestana, N., et al. “Evaluation of Asynchronous Geiger-Mode Avalanche Photodiode Arrays for Deep-Space Optical Communications.” *Advanced Photon Counting Techniques XV*, vol. 11721, SPIE, 2021, pp. 56–64.
20. Punjiya, Meera, et al. “A Direct-Detection LIDAR Detector for the Europa Lander Concept.” *Advanced Photon Counting Techniques XVI*, vol. 12089, SPIE, 2022, pp. 8–17.
21. Ryu, Kevin, et. al. “Geiger-Mode Avalanche Photodiode Arrays Fabricated on SOI Engineered-Substrates.” *Advanced Photon Counting Techniques XVI*, vol. 12089, SPIE, 2022.
22. Tudisco, Salvatore, et al. “A New Generation of SPAD—Single-Photon Avalanche Diodes.” *IEEE Sensors Journal*, vol. 8, no. 7, July 2008, pp. 1324–29.
23. Vandervelde, Thomas E., et al. “Quantum Dots-in-a-Well Focal Plane Arrays.” *IEEE Journal of Selected Topics in Quantum Electronics*, vol. 14, no. 4, July 2008, pp. 1150–61.

24. Vandervelde, Thomas E., and Sanjay Krishna. “Progress and Prospects for Quantum Dots in a Well Infrared Photodetectors.” *Journal of Nanoscience and Nanotechnology*, vol. 10, no. 3, Mar. 2010, pp. 1450–60.
25. Verghese, S., et al. “Arrays of 128x32 InP-Based Geiger-Mode Avalanche Photodiodes.” *Advanced Photon Counting Techniques III*, vol. 7320, SPIE, 2009, pp. 122–29.
26. Walker, Perrin, and William H. Tarn, editors. *CRC Handbook of Metal Etchants*. CRC Press, 1991.
27. Wu, Wang-ping, and Zhao-feng Chen. “Iridium Coating: Processes, Properties and Application. Part I: Processes for Protection in High-Temperature Environments against Oxidation and Corrosion.” *Johnson Matthey Technology Review*, vol. 61, no. 1, Jan. 2017, pp. 16–28.
28. Wu, Wang-ping, and Zhao-feng Chen. “Iridium Coating: Processes, Properties and Application. Part II: Analysis of the Coatings against High-Temperature Oxidation and Corrosion.” *Johnson Matthey Technology Review*, vol. 61, no. 2, Apr. 2017, pp. 93–110.
29. Yan, Li, and John A. Woollam. “Optical Constants and Roughness Study of Dc Magnetron Sputtered Iridium Films.” *Journal of Applied Physics*, vol. 92, no. 8, Oct. 2002, pp. 4386–92.
30. Yeh, Chia-Pin, et al. “High Temperature Reactive Ion Etching of Iridium Thin Films with Aluminum Mask in CF4/O2/Ar Plasma.” *AIP Advances*, vol. 6, no. 8, Aug. 2016, p. 085111.
31. Yu, Yinchuan, et al. “Confocal Microscopy with a Microlens Array.” *Applied Optics*, vol. 59, no. 10, Apr. 2020, pp. 3058–63.
32. Zappa, Franco, et al. “InGaAs SPAD and Electronics for Low Time Jitter and Low Noise.” *Photon Counting Applications, Quantum Optics, and Quantum Cryptography*, vol. 6583, SPIE, 2007, pp. 131–42.